REMOVAL OF HYDROGEN SULFIDE FROM NATURAL GAS USING ZEOLITES

Mirzokhid Abdirakhimov Ibrokhimjon ugli

MSc

Submitted in fulfilment of the requirements for the degree of

Doctor of Philosophy

The Faculty of Chemistry

Department of Chemical Engineering and Process Design

Silesian University of Technology

Supervisor:

dr hab. inż., Janusz Wójcik Prof. PŚ.

Gliwice, 2024

Abstract

Despite the advancement of time, natural gas still plays a crucial role as a fuel and raw material for many productions. The rise of alternative energy sources has not diminished the demand for natural gas, because it is one of the most economically efficient fuel options.

Natural gas requires removing to extract harmful constituents before it is suitable for consumption. Hydrogen sulfide (H_2S), a component of "sour" gas, causes corrosion in equipment and poses a health hazard. It is also a primary precursor of SO_2, which is the main contributor to acid rain. Various methods exist for purifying natural gas from hydrogen sulfide, and finding more efficient one could substantially reduce costs and protect the environment.

Due to their unique characteristics, zeolites serve as both adsorbents and catalysts in numerous fields. They are essential in the natural gas purification process, effectively eliminating sour elements.

The objective of this work is to modify the commercially available zeolites such as 4A, 5A and 13X and synthesis of zeolites from kaolin for the removal of H_2S from natural gas and nitrogen.

A literature review on various hydrogen sulfide elimination technologies from natural gas mixture is presented. Adsorption processes have shown promising performance for gas separation due to design flexibility, high separation efficiency, low operational costs, and high-purity product. Therefore, for the removal of H_2S from natural gas, adsorption processes utilizing zeolites, and their modified forms were chosen in this work

Initially, Faujasite type zeolite (13X) and Linde type zeolite (5A) underwent treatment with a silver nitrate solution to enhance their capacity for adsorbing H_2S. The process of removing H_2S from natural gas took place in a lab-scale adsorption unit. The studies involved employing binary mixtures of H_2S/CH_4 and H_2S/N_2. The adsorber was packed with zeolite samples, and a mixture of natural gas with varying amounts of H_2S was passed through the adsorber column. The adsorption capacity of zeolite samples was determined based on the results of adsorption experiments. The

results revealed that the alteration of 13X zeolite with silver presents a viable option for adsorbing and eliminating H_2S from natural gas.

Then, zeolite samples were synthesized from Angren Kaolin (Uzbekistan) to purify natural gas from H_2S. The synthesis process involved alkali-fusion following by hydrothermal and traditional hydrothermal procedures. Moreover, sodium silicate was added as a source of sodium to the kaolin to adjust Si/Al ratio. Effects of the aging and crystallization time as well as addition of sodium silicate were evaluated.

The adsorption performance of synthesized samples was assessed by separating H_2S from methane, and the results were compared with those of commercial zeolites. The findings indicated that the synthesized samples exhibited a high adsorption capacity relative to commercial zeolites.

KEY WORDS: hydrogen sulfide, natural gas, zeolites, adsorption, silver modification, halloysite, kaolin, zeolite synthesis, LTA type zeolites, FAU type zeolites.

Streszczenie

Mimo upływu czasu gaz ziemny nadal odgrywa kluczową rolę jako paliwo i surowiec dla wielu produkcji. Rozwój alternatywnych źródeł energii nie zmniejszył popytu na gaz ziemny, ponieważ jest to jedna z najbardziej efektywnych ekonomicznie opcji paliwowych.

Gaz ziemny wymaga usunięcia szkodliwych składników, zanim będzie nadawał się do zużycia. Siarkowodór (H_2S), składnik "kwaśnego" gazu, powoduje korozję sprzętu i stanowi zagrożenie dla zdrowia. Jest również prekursorem SO_2, który jest głównym czynnikiem przyczyniającym się do powstawania kwaśnych deszczy. Istnieją różne metody oczyszczania gazu ziemnego z siarkowodoru, a znalezienie bardziej wydajnej metody może znacznie obniżyć koszty i chronić środowisko.

Ze względu na swoje unikalne właściwości zeolity służą zarówno jako adsorbenty, jak i katalizatory w wielu dziedzinach. Są one pomocne w procesie oczyszczania gazu ziemnego, skutecznie eliminując pierwiastki kwaśne.

Celem niniejszej pracy jest modyfikacja dostępnych na rynku zeolitów takich jak 4A, 5A i 13X oraz ich synteza z kaolinu w celu usunięcia H_2S z gazu ziemnego i azotu.

Przedstawiono przegląd piśmiennictwa na temat różnych technologii eliminacji siarkowodoru z mieszaniny gazów ziemnych. Procesy adsorpcji wykazały obiecującą wydajność separacji gazów dzięki elastyczności projektowania, wysokiej wydajności separacji, niskim kosztom operacyjnym i produktowi o wysokiej czystości. W związku z tym w niniejszej pracy wybrano procesy adsorpcji z wykorzystaniem zeolitów i ich zmodyfikowanych form

Początkowo zeolit typu Faujasite (13X) i zeolit typu Linde A (5A) poddano działaniu roztworu azotanu srebra w celu zwiększenia ich zdolności do adsorpcji H_2S. Proces usuwania H_2S z gazu ziemnego odbywał się w laboratoryjnej instalacji adsorpcyjnej. W badaniach wykorzystano mieszaniny H_2S/CH_4 i H_2S/N_2. Adsorber wypełniono próbkami zeolitu, i przepuszczono mieszaninę gazu ziemnego z różnymi ilościami H_2S. Zdolność adsorpcyjną próbek zeolitu określono na podstawie

rezultatów eksperymentów adsorpcyjnych. Wyniki pokazały, że modyfikacje zeolitu 13X srebrem stanowi realną opcję adsorpcji i eliminacji H_2S z gazu ziemnego.

Następnie zsyntetyzowano próbki zeolitu z Angren Kaolin (Uzbekistan). Proces syntezy obejmował fuzję alkaliczną i tradycyjne procedury hydrotermalne. Ponadto krzemian sodu został dodany jako źródło sodu do kaolinu w celu dostosowania stosunku Si/Al. Oceniono wpływ czasu starzenia i krystalizacji oraz dodatku krzemianu sodu.

Wydajność adsorpcji zsyntetyzowanych próbek oceniono, przeprowadzając separację H_2S od metanu, a wyniki porównano z wydajnością komercyjnych zeolitów. Wskazują one że zsyntetyzowane próbki mają wysoką zdolność adsorpcji w porównaniu z komercyjnymi zeolitami.

SŁOWA KLUCZOWE: siarkowodór, gaz ziemny, zeolity, adsorpcja, modyfikacja srebra, haloizyt, kaolin, synteza zeolitu, zeolity typu LTA, zeolity typu FAU.

Table of Contents

List of Figures

List of Tables

List of Abbreviations

AFM – atomic force microscopy
ASTM – American Society for Testing and Materials
BEA – Beta
BET – Brunauer-Emmett-Teller
CHA – Chabazite
DEA – diethanolamine
DGA – diglycerol amine
DIPA – di isopropyl amine
EDS – energy dispersive spectroscopy
EG – ethylene glycol
FAU – Faujasite
GC – gas chromatography
HFM – hollow fibre membrane
HS – hydroxy sodalite
IUPAC – International Union of Pure and Applied Chemistry
LTA – Linde Type A
MDEA – methyl diethanolamine
MEA – monoethanolamine
MOFs – metal organic frameworks
MOR – Mordenite
NWs – nanowires
OSHA – Occupational Safety and Health Administration
PBU – primary building unit
PI – polyimide
PPO – poly (2,6-dimethyl-1,4-phenylene oxide)
PSA – pressure swing adsorption
PVP – polyvinylpyrrolidone
SBU – secondary building unit
SCD – sulfur chemiluminescence detector
SEM – scanning electron microscopy

SILMs – supported ionic liquid membranes

SOD – Sodalite

TDL – Tuneable diode lasers

TEM – transmission electron microscopy

TSA – temperature swing adsorption

XRD – X-ray diffraction

XRF – X-ray fluorescence

Statement of Original Authorship

The work contained in this thesis has not been previously submitted to meet requirements for an award at this or any other higher education institution. To the best of my knowledge and belief, the thesis contains no material previously published or written by another person except where due reference is made.

Signature: _____

Date: _____

Acknowledgements

In the Name of Allah (SWT) the Most Gracious, the Most Merciful.

First and foremost, I would like to express my deepest gratitude to my parents. They raised me and gave me the opportunity to pursue an education, which has been the foundation of my journey. Their unwavering support has been a constant source of motivation for me.

I am profoundly thankful to Prof. Janusz Wójcik, who has been a pillar of support throughout my doctoral studies. His invaluable guidance, mentorship, and extensive knowledge in the field of adsorption have consistently steered me in the right direction. I am deeply appreciative of his enthusiasm for research, which has greatly inspired my work.

I also wish to extend my thanks to Prof. Mohsen H. Al-Rashed for his continuous encouragement and invaluable advice. His support has been crucial throughout this process.

To my spouse, I owe a special debt of gratitude. Your support and motivation, especially during times of depression, have been my lifeline. The births of our daughter and son during my PhD journey have also been a source of immense inspiration, providing me with the strength to persevere.

I am deeply grateful to Mr. Pawel and Mrs. Katarzyna, the paternal grandparents, and the maternal grandmother of my children in Poland, for their invaluable assistance in numerous situations. Your support has been instrumental in helping me manage my responsibilities.

I would like to thank Mr. Marek for his work in building the adsorption experimental set-ups. I also acknowledge Dr. Jacek Kocurek for his assistance in constructing the data recording Arduino scheme. I am grateful to Prof. Roman Turczyn, Prof. Alicja Kazek-Kesik, and Dr. Wojciech Pudlo for their help with material characterization analyses. I would like to express my gratitude to Muhammad Omer Farooq for his efforts in preparing silver nanowires.

I also want to express my gratitude to all the educators who have taught me from my early years until now. Your tireless efforts have shaped my academic journey, and I am deeply appreciative of your guidance and support.

Finally, I want to thank everyone who has contributed to my personal and academic growth throughout my life. Your support, in countless forms, has been indispensable to my achievements.

Chapter 1: Introduction

The first chapter provided the context for the study. This chapter starts with an introduction to natural gas and its sweetening process applying various methods including absorption, adsorption, membrane separation. It aims to present a comprehensive solution to challenges by exploring various modification methods of zeolites and synthesizing zeolites from kaolin. The text then explains the objectives of the investigation and the extent to which they were pursued, addressing the study's limitations. Finally, the chapter concludes with an outline of the thesis's organizational structure.

This chapter offers an overview of the research background (section 1) and context (section 2), along with the research objectives (section 3). Section 4 highlights the importance and scope of this research and defines of the terminology employed. Section 5 presents a limitation. Section 6 describes summary of the forthcoming chapters in the thesis.

1.1 BACKGROUND

Prior to transportation and distribution to customers, it is necessary to process natural gas. Various techniques, such as dehydration, purification, and desulfurization, are employed to eliminate contaminants including water, sulfur compounds, and carbon dioxide to meet natural gas specifications. Removing sulfur compounds is critical due to their harmful effects, including pipeline corrosion and the release of sulfur dioxide, which contributes to acid rain formation. Exposure to hydrogen sulfide levels exceeding 10 ppm can have severe health consequences [1]. Zeolites play a key role in adsorbing various gases from natural gas. Furthermore, incorporating different metals into zeolites enhances their adsorption properties, reducing the cost and duration of the natural gas purification process. Furthermore, zeolites can be produced using cost-effective raw kaolin instead of sodium aluminate and silicate reagents, which are more expensive than kaolin. Utilising kaolin as the raw material for zeolite production decreases synthesis costs and provides environmental protection.

1.2 CONTEXT

As the demand for natural gas increases, so do the requirements for its quality. Although numerous techniques and materials are available for removing hydrogen sulfide from natural gas, there is potential to enhance the effectiveness of the adsorbents and absorbents employed in these procedures. Several studies have enhanced the quality of different zeolites by incorporating silver ions. However, these studies used different gas mixtures instead of natural gas, raising uncertainties regarding the effectiveness of silver-modified zeolites in removing hydrogen sulfide from natural gas.

The synthesis of zeolites utilizes various silica sources, such as sodium silicate, silica gel, colloidal sol, ethyl orthosilicate, and methyl orthosilicate. Similarly, aluminium sources including sodium aluminate, Boehmite (pseudo-boehmite), aluminium hydroxide, aluminium isopropoxide, aluminium nitrate, and metallic aluminium are used in the process [2]. Furthermore, cost-effective raw materials can be used as sources of aluminium and silica, reducing the overall cost of zeolite production. Kaolin is often chosen for zeolites synthesis because it contains both silicon (Si) and aluminium (Al). Currently, no research conducted on synthesizing zeolites using Angren kaolin from Uzbekistan.

1.3 PURPOSES

Given the lack of research regarding silver modification of zeolites toward H_2S removal from natural gas, this study aims to evaluate the efficacy of 13X zeolites that have been modified with silver ions of different concentrations in the separation of hydrogen sulfide from gas mixtures. The impact of the initial hydrogen sulfide concentration on adsorption will also be investigated. Additionally, we will explore the feasibility of synthesizing zeolites from Angren kaolin for the purpose of eliminating H_2S from natural gas.

1.4 SIGNIFICANCE, SCOPE AND DEFINITIONS

This study will contribute to natural gas treatment processes by modifying zeolites and synthesizing molecular sieves from kaolin. It will also possibly address the mechanism of adsorption of H_2S on silver modified zeolites.

In order to properly achieve this purpose, the following scopes are considered:

1. Modification of 13X zeolite with various concentration of silver nitrate in order to enhance adsorption performance
2. Conducting adsorption experiments to assess adsorption properties of modified 13X zeolites
3. Synthesizing 4A and 5A zeolites from Angren kaolin
4. Performing H_2S removal experiments with synthesized 4A and 5A zeolites
5. Silver modification of 5A with silver nanowires for enhancing affinity toward H_2S and carrying out adsorption experiments for comparison
6. Characterizing all the samples using scanning electron microscopy (SEM), X-ray diffraction (XRD), and Brunauer-Emmett-Teller (BET) techniques.

1.5 LIMITATION

The conclusions of this study must be viewed in the context of certain constraints. Initially, the investigation of regenerating the used adsorbent was not conducted due to shortage of time. Furthermore, the impact of other natural gas constituents, such as carbon dioxide, nitrogen, and other sulfur compounds, was not evaluated. Future research should explore the potential of silver-modified 13X molecular sieves under various conditions. Moreover, the study did not encompass the synthesis of other zeolites, such as NaX and NaY, which are commonly employed in natural gas processing.

1.6 THESIS OUTLINE

This thesis is composed of five chapters arranged in the following manner: Chapter 1: Introduction

The natural gas sweetening process and the use of zeolites as an adsorbent in the process are briefly explained in this chapter. It also discusses the synthesis and modification of zeolites aimed at H_2S removal. In accordance with the research conducted, this chapter presents a comprehensive solution for the purification of natural gas. Following this explanation, the chapter outlines the study's objectives, and the methodology employed to achieve them. The chapter concludes with a detailed account of the thesis's structure.

Chapter 2: Literature review

This chapter provides an in-depth review of methods for removing H_2S from various sources, along with a detailed examination of the properties of zeolites and the physical and chemical characteristics of H_2S. It covers the modification of zeolites for H_2S removal and the methods for determining and measuring H_2S. The chapter concludes with a comprehensive literature review of previous studies on H_2S adsorption.

Chapter 3: Research design and Methodology

This chapter thoroughly examines the process of adsorbing H_2S from nitrogen and methane utilizing commercially available molecular sieve zeolites, including 4A, 5A, 13X, and silver-modified 13X. It also explores the use of 4A and 5A zeolites manufactured from Angren Kaolin by fusion/hydrothermal and hydrothermal techniques and their adsorption capabilities. Characterisation techniques including X-ray diffraction (XRD), scanning electron microscopy (SEM), and Brunauer-Emmett-Teller (BET) method were utilized to investigate the physicochemical properties, structure, and elemental composition of zeolites. The chapter details the reagents and materials used in these experiments and delves into the techniques involved in synthesizing and modifying zeolites.

Chapter 4: Experimental results

This chapter presents the research results obtained through characterization techniques and adsorption experiments. Breakthrough curves generated based on the data collected from adsorption experiments were given in this chapter.

Chapter 5: Discussion

This chapter discusses the characterization results of materials and the effects of various parameters, such as the silver ion levels in zeolites and the concentration of H_2S in the initial mixture, on adsorption.

Chapter 6: Conclusion and Recommendation

This chapter presents the final findings and analysis of the research, confirming the achievement of the objectives and validating the results. This is accomplished by comparing the research findings with the previous results obtained from the literature review. The Chapter also examines the potential future tasks that can be derived from

the outcomes of this work. The research concludes with a comprehensive compilation of references used to support the conclusions.

Chapter 2: Literature Review

2.1 INTRODUCTON

Natural gas serves as an energy-efficient, clean fossil fuel and as a feedstock in petrochemical industry due to its role as a source of hydrocarbons. Natural gas currently comprises 23 percent of the world's primary energy demand, a figure that has increased significantly over the last two decades [3].

Natural gas is a complex mixture of components that are both hydrocarbon and nonhydrocarbon. It may contain a wide variety of chemicals in different proportions. Although methane (CH_4) makes up most of the natural gas, it can also contain sizable amounts of ethane (C_2H_6), propane (C_3H_8), butane (C_4H_{10}), and pentane (C_5H_{12}), along with traces of heavier hydrocarbons like hexane (C_6H_{14}). Nitrogen (N_2), carbon dioxide (CO_2), hydrogen sulfide (H_2S), and other sulfur components like mercaptans (ReSH), carbonyl sulfide (COS), and carbon disulfide (CS_2) are frequently found in a variety of natural gases. There may also be traces of helium, hydrogen, and argon. It is known that natural gases contain traces of certain metallic elements, such as uranium, selenium, mercury, and semi metal arsenic. The H_2S content is indicated by the phrases "sweet" and "sour." While the terms "sweet" and "sour" are applicable to acid gases such as H_2S and CO_2, they are predominantly used in the context of H_2S. Sour gas contains H_2S in concentrations that are deemed too high, in contrast, sweet gas has H_2S levels that are so low they are often undetectable. Although the terms are relative, sweet normally refers to a gas with fewer than 4 ppm of H_2S [4]. As long as the sales gas's heating value is adequate, carbon dioxide can be tolerated at much higher concentrations—roughly 3 mol % (3000 ppm) [4].

Natural gas composition varies across reservoirs, even within the same field [5]. Three kinds of wells provide raw natural gas: oil wells, gas wells, and condensate wells. Natural gas can be categorized into two types: associated (from oil and condensate wells) and non-associated (gas wells).

2.1.1 Chemical and physical properties of natural gas

Natural gas is colorless, odourless, and lighter than air. Since it is odourless, an odorant is introduced to ensure that any leaks can be easily detected. Mercaptan that

has odor of rotten egg with the general formula R-SH is added to natural gas in a trace amount that does not create any serious issue.

Understanding the physic-chemical properties of natural gas facilitates its efficient processing. In the Table 2-1 below, properties of natural gas are given [4]:

Table 2-1. Physical and chemical properties of natural gas

Properties	**Values**
Molar mass	17-20
Carbon content	73.3
Hydrogen content, weight%	23.9
Oxygen content, weight%	0.4
Hydrogen/carbon atomic ratio	3.0-4.0
Density, 15℃	0.72-0.81
Boiling point, ℃	-162
Autoignition temperature, ℃	540-560
Octane number	120-130
Methane number	69-99
Stoichiometric air/fuel ratio, weight	17.2
Vapor flammability limits, volume %	5-15
Flammability limits	0.7-2.1
Lower heating/calorific value, MJ/kg	38-50
Stoichiometric lower heating value, MJ/kg	2.75
Methane concentration, volume %	80-99
Ethane concentration, volume %	2.7-4.6
Nitrogen concentration, volume %	0.1-15
Carbon dioxide concentration, volume %	1-5
Sulfur concentration, weight% ppm	<5

Due to the presence of predominantly methane and other impurities with different molar masses, the molar mass of natural gas typically falls within the range of 16-20 g/mole. The presence of several sulfur compounds in natural gas necessitates the measurement of total sulfur concentrations rather than specific concentration of sulfur compounds.

2.2 HYDROGEN SULFIDE

Hydrogen sulfide (also known as hydrosulfuric acid, hydrogen sulfide, sewer gas, stink damp, dihydrogen monosulfide, dihydrogen sulfide, sulfane, sulfurated hydrogen, and sulfur hydride) is a colorless, flammable gas with a distinct odor reminiscent of rotten eggs. Being heavier than air, it tends to settle on the ground.

Table 2-2 shows some of the properties of hydrogen sulfide.

Naturally H_2S can be found in different concentrations in natural gas, syngas, biogas, petroleum refinery streams, etc.

Table 2-2. Physical properties of hydrogen sulfide

Properties	Value
Molar mass	34.081 g/mol
Specific gravity (relative to air)	1.19
Boiling point	-60.33 °C
Melting point	-85.49 °C
Smell	Rotten eggs
Colour	colorless

Despite the presence of traces of hydrogen sulfide in various sources, it may cause a variety of problems such as corrosion in refining facilities, pipeline, and storage vessel, poisoning of catalysts, pollution of the environment etc. As a result, hydrogen sulfide must be removed from the above-mentioned sources before it can be utilized.

2.2.1 H_2S sources

Hydrogen sulfide is present in many resources such as natural gas, biogas, refinery gas streams, coal gas, and volcanic gasses [6]. Natural gas is referred to as a "sour gas" when containing mainly H_2S and other sulfur compounds. The concentration of H_2S in natural gas can differ depending on the source. Although natural gas is mostly composed of hydrocarbons, it can also contain a significant amount of hydrogen sulfide [7]. Biogas is one of the renewable energy resources that contains a concentration of 1000-3000 ppm of H_2S [8] [9]. In refineries, processes like hydrodesulfurization, cracking, and pyrolysis emit hydrogen sulfide as a byproduct. This occurs because organic sulfur compounds undergo hydrogenation, resulting in the formation of hydrogen sulfide [10].

2.2.2 Corrosion caused by hydrogen sulfide.

Degradation caused by hydrogen sulfide represents a significant problem, costing the natural gas and petroleum industries billions of dollars annually. H_2S can lead to corrosion through both direct and indirect means [11]. It reacts with moisture to form weak sulfuric acid [12], which corrodes steel. Most metals react readily with H_2S as well. At a temperature of 20°C, the corrosion rate caused by H_2S is 0.1-1.0 mm/year [11]. Furthermore, the rate of H_2S-induced corrosion will reach 300 mm/year [13].

H_2S corrosion yields iron oxide as a product. The reaction mechanism is as follow [14]:

$$H_2S + H_2O \rightleftharpoons HS^- + H_3O^+ \quad (2.1)$$

$$HS^- + H_2O \rightleftharpoons S_2^- + H_3O^+ \quad (2.2)$$

$$Fe \rightarrow Fe^{2+} + 2e^- \quad (2.3)$$

$$xFe^{2+} + yS^{2-} \rightarrow Fe_xS_y \quad (2.4)$$

$$H_3O^= + e^- \rightarrow H^0 + H_2O \quad (2.5)$$

$$H^0 + H^0 \rightarrow H_2 \quad (2.6)$$

recombination reaction

2.2.3 Hydrogen sulfide hazards

The impact of hydrogen sulfide on the human body is highly detrimental. Hydrogen sulfide affects an individual via the respiratory system. The greater the concentration, the more severe the health effects. According to OSHA [15], H_2S concentration and its effects on human body was classified (Table 2-3).

Table 2-3. Hydrogen sulfide concentration and its effect on human body

Concentration (ppm)	**Symptoms/Effects**
0.00011-0.00033	Typical background concentrations
0.01-1.5	Odor threshold (when rotten egg smell is first noticeable to some). Odor becomes more offensive at 3-5 ppm. Above 30 ppm, odor described as sweet or sickeningly sweet.
2-5	Prolonged exposure may cause nausea, tearing of the eyes, headaches or loss of sleep. Airway problems (bronchial constriction) in some asthma patients.
20	Possible fatigue, loss of appetite, headache, irritability, poor memory, dizziness.
50-100	Slight conjunctivitis ("gas eye") and respiratory tract irritation after 1 hour. May cause digestive upset and loss of appetite.
100	Coughing, eye irritation, loss of smell after 2-15 minutes (olfactory fatigue). Altered breathing, drowsiness after 15-30 minutes. Throat irritation after 1 hour. Gradual increase in severity of symptoms over several hours. Death may occur after 48 hours.
100-150	Loss of smell (olfactory fatigue or paralysis).
200-300	Marked conjunctivitis and respiratory tract irritation after 1 hour. Pulmonary edema may occur from prolonged exposure.
500-700	Staggering, collapse in 5 minutes. Serious damage to the eyes in 30 minutes. Death after 30-60 minutes.
700-1000	Rapid unconsciousness, "knockdown" or immediate collapse within 1 to 2 breaths, breathing stops, death within minutes.
1000-2000	Nearly instant death

Hydrogen sulfide is an extremely combustible and explosive gas, which can lead to potentially fatal circumstances if not handled correctly. Furthermore, the combustion of hydrogen sulfide gas results in the emission sulfur dioxide.

2.3 THE STRUCTURE OF ZEOLITES

The first zeolite mineral was found by Cronstedt in 1756 [16]. He named this kind of mineral zeolite, from the Greek words "zeo" (to boil) and "lithos" (stone) because when mineral is heated it seems to boil. Zeolites are crystalline aluminosilicate minerals characterized by structures composed of four interconnected frameworks of SiO_4 and AlO_4 tetrahedra that are connected to one another by the sharing of oxygen atoms. AlO_4 is negatively charged with respect to SiO_4 due to the trivalent state of Al [17]. Group IA and group IIA elements are examples of extra-framework cations that counteract this negative charge. It is represented by the empirical formula as follows [18]:

$$M_{2/n}O \cdot Al_2O_3 \cdot xSiO_2 \cdot yH_2O$$

Zeolites are classified into groups such as "low," "intermediate," and "high" silica zeolites, along with "silica" molecular sieves, according to their increasing Si/Al ratio in the framework. This increase in the Si/Al ratio corresponds to enhanced thermal stability and hydrophobic properties in zeolites.

2.3.1 Building units for Zeolite Framework

Zeolites are formed by primary building unit (PBU) (Figure 2-1, a) that is TO_4 where the central T-atom is typically Si and Al and peripheral atoms are O. Each T atom is coordinated to four oxygen atoms and each oxygen atom bridges two T atoms. Secondary building units (SBUs) (Figure 2-1, b) are formed by many PBUs. SBUs contain up to 16 tetrahedrally coordinated atoms and there are 23 types of SBUs have been found to occur in tetrahedral framework [19] (Figure 2-2). A composite building unit is constructed by joining multiple PBUs together [20]. The final zeolite structure is composed of groupings of secondary units inside a consistent three-dimensional crystalline framework.

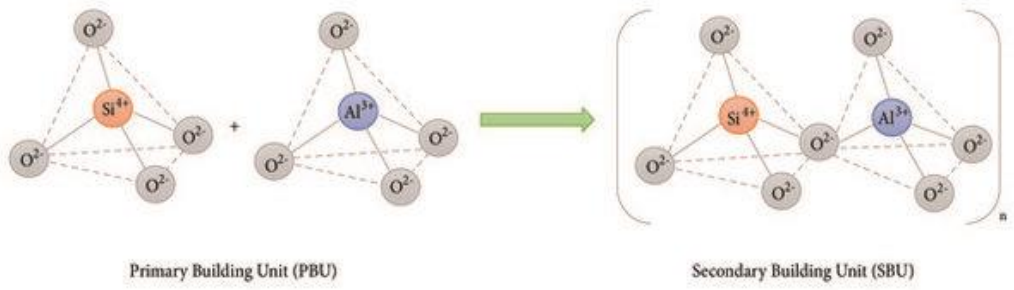

a) b)

Figure 2-1. a) Primary building unit and b) secondary building unit of zeolite.

Adapted from [21].

Zeolite frameworks feature unique cage-building units, which are typically characterized by the n-rings defining their surfaces. For example, the octahedra unit surface is formed by six 4 -rings and eight 6 rings. It can be designated [$4^6 6^8$] and called a sodalite cage.

3 (5)

4 (71)

6 (51)

8 (24)

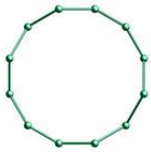

12 (5)

Spiro – 5 (2)

4-4 (4)

6-6 (10)

8-8 (3)

4-1 (13)

4-(1,1) (5)

1-4-1 (7)

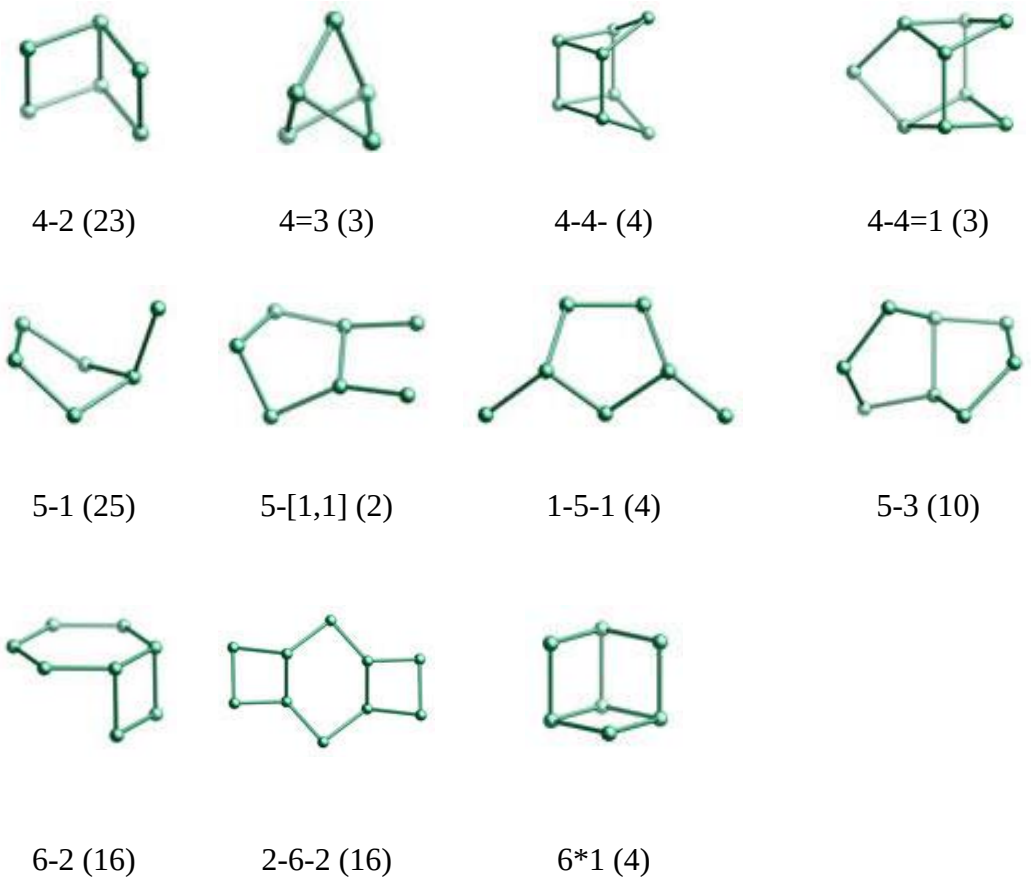

Figure 2-2. Secondary building unit patterns of zeolite frameworks.

Adapted from [21].

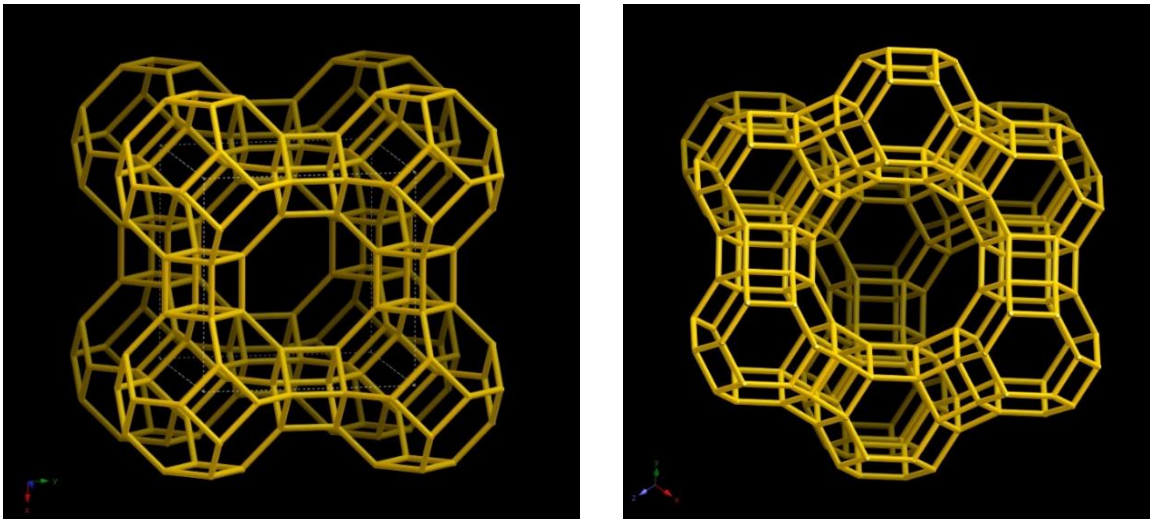

a) b)

Figure 2-3. Cages of a) Linde Type A (LTA) b) Faujasite (FAU)

Linde Type A (LTA) zeolite is built by linking sodalite cages through double four rings (Figure 2-3, a) while Faujasite (FAU) is built by linking sodalite cages through double six rings (Figure 2-3, b).

Table 2-4. Physical Properties of Zeolites Used Commercially

Adapted from [22]

Zeolite	Crystal framework Si/Al ratio	Crystal structure symmetry	Crystal density (g/cm^3)	Common ion exchanged forms	Pellet density (g/cm^3)	Bulk density (g/cm^3)	Nominal pore opening (A)
A	0.7- 1.2	Cubic	1.52	Na, K, Ag, Mg, Ca	1.20	0.72	3,4,5
X	1.0-1.5	Cubic	1.47	Na, Li, Ca, Ba	1.05	0.65	7.5 (NaX) 10.0 (CaX)
Mordenite (small port)	4.5 – 5.0	Orthorhombic	1.83	Na, H, Ca	1.39	0.88	4
Chabazite	1.6- 3.0	Trigonal	1.67	Na, Ca	1.16	0.73	4.9
Clinoptilolite	4.2-5.2	Monoclinic	1.85	K, Ca	-	-	3.5
Silicate	Very high	Orthorhombic	1.79	None	-	-	5.3

A wide array of zeolites has been discovered to date, finding utility in diverse roles including acting as catalyst [23], adsorbent [24] and ion-exchanger [25] in various applications. Zeolites are highly regarded for their effectiveness in purifying and separating gases [26]. Natural zeolite such as Mordenite, Chabazite, silicate and synthetic zeolites such as Linde Type A (3A, 4A, 5A) and Faujasite (X and Y) are commercially used for the purification and separation processes [22]. Some of the physical properties of zeolites used commercially are given in Table 2-4.

2.4 SELECTION OF THE BEST ZEOLITES FOR THE H_2S REMOVAL FROM NATURAL GAS

The success of the adsorption process heavily depends on the number of impurities that the adsorbent can capture. Adsorption capacity, selectivity, stability, regenerability, and cost are the main attributes of an adsorbent in selection [27]. It is uncommon for a single adsorbent to be ideal in all of these aspects. Enhancing the adsorbent's capacity to adsorb increases the efficiency of separating the target molecule from the mixture, thereby reducing the adsorption cycle time. The adsorption capacity is quantified as the ratio of the amount of the molecules adsorbed to the mass of the adsorbent.

2.4.1 Adsorption Capacity

The volume of impurities to be adsorbed by the adsorbent is crucial to the success of the operation. An increase in adsorption capacity enhances the separation of the targeted molecule from the mixture so decreases the adsorption cycle.

Adsorption capacity is measured by the ratio of the amount of the adsorbed molecule to the adsorbent mass.

2.4.2 Selectivity

The adsorbent's affinity for different species in the mixture varies, and this is a crucial aspect in evaluating its separation ability. The presence of different components in natural gas affects the selective absorption capacity differently, as they may have the ability to absorb different components at the same time. Therefore, the selectivity of adsorbents plays an important role in their suitability. In the selection and testing of zeolites capable of selectively absorbing hydrogen sulfide from natural gas, it is necessary to consider their ability to adsorb other impurities such as CO_2 and water. The selectivity of zeolites depends largely on their polarity, and the greater the polarity, the higher the selectivity. Since methane and its homologues found in natural gas are non-polar, while molecules like H_2S, CO_2, and water are polar, the latter group is effectively attracted to zeolites. As previously stated, choosing the proper zeolite is critical for reducing CO_2 and water adsorption while increasing H_2S absorption.

2.4.3 Stability

Adsorbent that has been filled with impurities should be cleaned of sorbed matter before reusing it in adsorption. This is known as desorption, and it takes place at a high temperature. Adsorbents need to maintain their original structure at high temperatures, a characteristic known as stability. This stability is a crucial attribute to consider when selecting an adsorbent, as it ensures the material's effectiveness over time and under various conditions.

2.4.4 Kinetic diameter of some molecules of natural gas

Understanding the kinetic diameter of molecules is a crucial aspect when studying adsorption. The kinetic diameter does not represent the actual physical size of a molecule; instead, it measures the distance between the centres of two molecules at their closest point during a collision. It is a crucial factor in understanding molecular interactions in gases, especially in processes such as diffusion and adsorption.

The kinetic diameter of molecules plays the main role in the separation. To adsorb a targeted molecule by zeolites, it should have a kinetic diameter smaller than zeolite pore. Thus, H_2S with a kinetic diameter of 0.36 nm is expected to be adsorbed by zeolite which has a aperture bigger than 0.36 nm. The approximation is subject to

variation as the apparent sizes of adsorbate molecules and the pores of the zeolite can change under different conditions.

Table 2-5. Kinetic diameter of some molecules of compound occurred in natural gas

Molecule	**Kinetic diameter (nm)**
CH_4	0.38
H_2O	0.27
H_2S	0.36
CO_2	0.33
CS_2	0.36
SO_2	0.36
N_2	0.36

2.4.5 Si/Al ratios

Zeolites are classified, based on the Si/Al ratio as low, medium, high, or silica [28], which is the most important factor in characterizing structures and the properties of zeolites. The Si/Al ratio affects thermal stability, acidity, and structure of the zeolites. For instance, as the Si/Al ratio increases, thermal stability enhances. Zeolites with low silica content are hydrophilic, whereas those with high silica content are hydrophobic. Additionally, the ion exchange capacity and concentration of cations, which are tied to the aluminium content, decline with an increase of Si/Al ratio. To effectively separate hydrogen sulfide from different streams, the use of zeolites that are both hydrophilic and possess high selectivity on their surface is recommended. Specifically, Type A and X zeolites, which have a low silica content and demonstrate strong adsorption qualities, stand out as particularly suitable options for this purpose.

2.4.6 Regenerability

After a few cycles of adsorption, the adsorbent will become incapable of adsorbing the specific molecules due to pore saturation. Hence, it is necessary to regenerate the used adsorbent for the next separation cycle. The adsorbate should exhibit poor adsorption characteristics, allowing for easy desorption of these molecules from the adsorbent in response to changes in temperature or pressure. The adsorbents utilized in the process can become poisoned by hazardous pollutants after a few cycles, as a result of aging and poisoning. Therefore, it is necessary to replace them with fresh ones. Following this procedure, the adsorbent is prepared for use in subsequent cycles. Regeneration becomes challenging if there is a strong interaction between the adsorbent and the adsorbate.

2.5 NATURAL GAS SWEETENING

The inclusion of acid gases adversely affects the quality of natural gas. Sweet gas refers to natural gas that solely contains CO_2, while sour gas is defined as natural gas that contains H_2S or other sulfur compounds. CO_2, being an inert gas, lowers the heating value of natural gas and is also regarded as a primary contributor to greenhouse gas emissions. H_2S and other sulfur compounds can cause corrosion to equipment and pipelines. In order to comply with emissions standards, pipeline gas specifications, and regulatory mandates, raw natural gas streams require treatment to remove acid gases. Gas sweetening is the technique of eliminating acid gases from natural gas. Table 2-6 provides typical pipeline gas specifications [29].

Table 2-6. Specifications for Pipeline Quality Gas

Characteristics	**Specification**
Water content	4-7 lb. H_2O/MMscf of gas (85-150 ppmv)
Hydrogen sulfide content	0.25-1.0 grain/100 scf (4-16 ppm)
Gross heating value	950-1200 Btu/scf (35-45 MJ)
Hydrocarbon dew point	14-40°F at specified pressure (3-23 °C)
Mercaptan content	0.25-1.0 grain/100 scf (4-16 ppm)
Total sulfur content	0.5-20 grain/100 scf (8-320 ppm)
Carbon dioxide content	2-4 mol%
Oxygen content	0.01 mol% (max)
Nitrogen content	4-5 mol%
Total inert content (N_2 + CO_2)	4-5 mol%
Sand, dust, gums, and free liquid	None
Typical delivery temperature	Ambient
Typical delivery pressure	400 to 1200 psig (27-82 ATM)

Different treatment techniques are employed depending on the intended use of the natural gas and the corresponding requirements for its quality. Various gas treatment techniques were illustrated grouping in several categories in Figure 2-4.

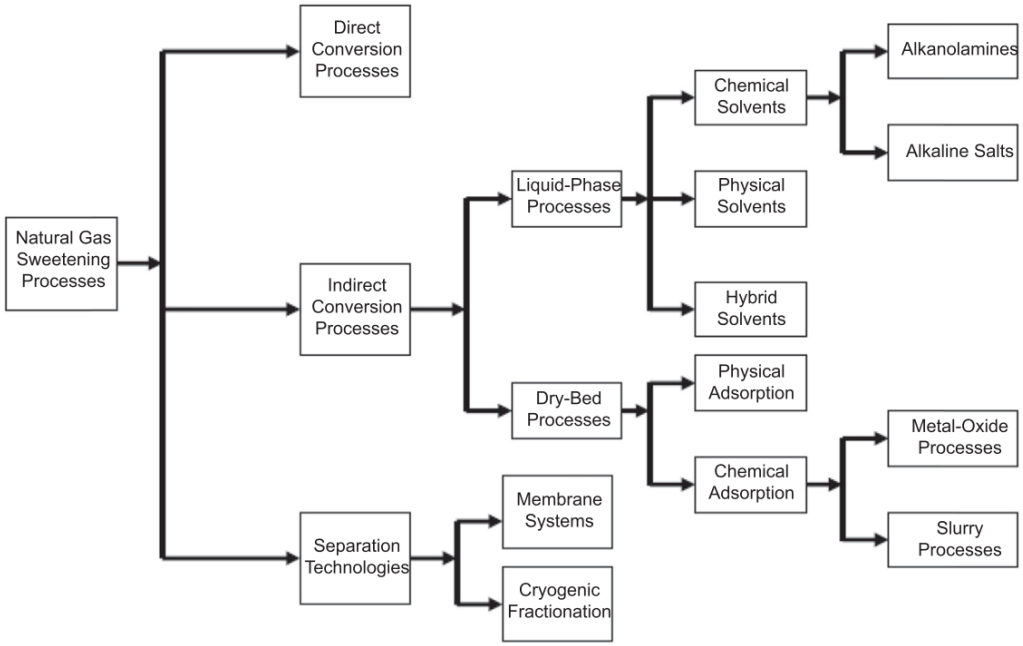

Figure 2-4. Various natural gas treating processes.

Adapted from [4].

Hydrogen sulfide is captured by the following methods: Absorption, adsorption, membrane separation, and cryogenic distillation. These methods are used depending on the amount of hydrogen sulfide in the natural gas. When the concentration of hydrogen sulfide is substantial, for instance, the absorption method is utilized [30] [31]. In the absorption, various liquid substances (amines, glycols, etc.) are used as sorbents, and this process is expensive as chemical reaction takes place between amine and acid components which makes the process irreversible. Adsorption is very cost-effective since physical phenomena takes place, and the adsorbent can be regenerated and used in the process for several years. Therefore, the development of effective adsorption methods of natural gas purification and the study of adsorbents used in this process is one of the tasks for scientists and technologists. Furthermore, the selection of the most suitable material and process design is influenced by the characteristics of the feed and the intended application of the natural gas. The integration of process engineering and material science is crucial for the effective operation of a process [32].

The methods for H_2S removal from natural gas will be thoroughly discussed below, along with their respective advantages and disadvantages.

2.5.1 Absorption

Absorption is widely used to remove acid gases from various streams. In absorption, liquid solvents serve as sorbents, and dissolution takes place. Alkanolamines, aqueous ammonia, alkaline salt solutions, and sodium and potassium carbonate solutions are frequently used as liquid solvents in absorption processes [33]. Although absorption has dominated natural gas purification for a century, some disadvantages, such as energy-intensive and high operating costs, are forcing engineers to find cost-effective alternatives. Amine technology is applied when H_2S concentration is above 200 ppm [34]. Amines such as MEA, DEA, DIPA, DGA, and MDEA are used to remove both H_2S and CO_2 from various streams. The application of alkanolamines as solvents for acid gas removal began in 1930 by Bottoms [12]. One characteristic of these chemical solvent procedures is the comparatively high heat of acid gas absorption. Solvent regeneration requires a significant quantity of heat. Amines can react in a variety of ways with CO_2, COS, and CS_2 and are thermally stable, but they are also susceptible to oxidation and high temperatures. As directed by the solvent providers, the degraded amine can be recovered thermally or by ion exchange [4].

Diethanolamine (DEA) and monoethanolamine (MEA) have the most widespread practical applications. Particularly when the source gas contains COS and CS_2, in addition to H_2S and CO_2, which react irreversibly with MEA and cause significant losses, DEA should be utilized. In order to achieve selective H_2S extraction in the presence of CO_2, methyl diethanolamine (MDEA), a tertiary amine, is employed.

Chemical reactions take place between amines and acid gases. The equilibrium reactions for H_2S, CO_2, primary amines, and secondary amines are as follows [12]. For hydrogen sulfide elimination:

$$RNH_2 + H_2S \leftrightarrow RNN_3^+ + HS^- \qquad \text{Fast} \qquad (2.7)$$

$$RNH_2 + HS^- \leftrightarrow RNN_3^+ + S^{--} \qquad \text{Fast} \qquad (2.8)$$

The reactions between H_2S and amines are straightforward as H_2S reacts quickly and directly with all amines to produce bisulfide according to Equation 2.1 and sulfide according to Equation 2.2. For carbon dioxide removal:

$$2RNH_2 + H_2S \leftrightarrow RNN_3^+ + RNHCOO^- \quad \text{Fast} \quad (2.9)$$

$$RNH_2 + HS^- + H_2O \leftrightarrow RNH_3^+ + HCO_3^- \quad \text{Slow} \quad (2.10)$$

$$RNH_2 + HCO_3^- \leftrightarrow RNH_3^+ + CO_3^{--} \quad \text{Slow} \quad (2.11)$$

Mandal et al. [35] studied simultaneous removal of CO_2 and H_2S with the blend of N-methyldiethanolamine and diethanolamine. The rate of CO_2 absorption increased until the gas flow rate reached 140×10^{-6} m^3/s, whereas the rate of H_2S absorption rose to 180×10^{-6} m^3/s.

Tian et al. [36] carried out a study on the absorption of low-partial-pressure H_2S using a monoethanolamine (MEA)-activated N-methyldiethanolamine (MDEA) aqueous solution. An analysis was conducted to examine the impact of MEA by applying different mass fractions of MDEA and MEA, ranging from 0.30 to 0.50 and from 0 to 0.075, respectively. A removal efficiency of 95% was attained while using ωMDEA = 0.5, ωMEA = 0.075, and T = 313.2 K. This indicates that the addition of MEA has a positive influence on the separation of H_2S. In their study, Lee et al. [37] investigated twelve absorbents for the simultaneous removal of CO_2 and H_2S from biogas. They used N-methyldiethanolamine (MDEA)-based additives for this purpose. Out of the several absorbents, the combination of MDEA/APA (bis(3-aminopropyl) amine) demonstrated better performance in terms of loading H_2S-rich gas, while MDEA/DETA (diethylenetriamine) exhibited better performance in terms of cyclic capacity for H_2S. Liu et al. [38] combined traditional MDEA absorption with hydrate-based separation of natural gas in order to eliminate acid gases. The proposed integrated approach can effectively decrease the concentration of sour components to meet the standards for commercial gas. The energy consumption was reduced to just 42% of the energy used in the MDEA approach.

2.5.2 Membrane separation.

The 1980s marked the era of industrialization of gas separation using membranes. In the industrial sector, membranes find widespread use primarily for hydrogen purification, nitrogen removal from air, carbon dioxide removal from natural gas, volatile organic compounds (VOCs) recovery and drying of gases [39].

In membrane separation, modified membranes allow only one species to pass through and can be used in a continuous mode. It is possible to separate and capture

certain species using modified membranes as an adsorbent. [40]. The membrane must be regenerated after a specific period of time if it is to be reused.

Membrane separation uses non-porous [41], thin films of various materials to separate impurities from gas mixtures. Due to the versatility of membrane techniques, they can be applied to numerous aspects of gas treatment.

Membranes can selectively absorb and diffuse certain components due to permeability or semi-permeability [42]. The single-stage membrane process (shown *Figure 2-5* [43]) is the simplest. The feed gas is separated into a permeating stream rich in H_2S and a hydrocarbon-rich retentate stream.

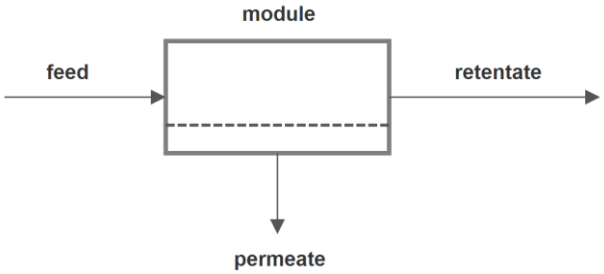

Figure 2-5. *Schematic representation of a membrane separation process.*

Maghsoudi and Soltanieh [44] [45] synthesized and studied a high silica CHA-type membrane in the simultaneous separation of CO_2 and H_2S from methane. H_2S permeance and H_2S/CH_4 selectivity were measured, $1.70x10^{-8}$ mol/ (m^2 s Pa) and 3.24, respectively. Iovane et al. [46] investigated the performance of polymeric membrane (made by Porogen Corporation) in the treatment of biogas in the presence of H_2S. They concluded that the presence of H_2S does not affect the performance of such membrane and has only 50% selectivity. Janocha and Wojtowicz [47] employed a polyamide membrane using hollow-fiber capillary membrane module to remove H_2S from natural gas and reached 90% performance. Chenar et al. [48] tested and compared poly (2,6-dimethyl-1,4-phenylene oxide) (PPO) and Cardo-type polyimide (PI) hollow fiber membranes that are available commercially. The concentration range of H_2S were 101 to 401 ppm in the mixture. The separation coefficients of hydrogen sulfide/methane were 6 and 4 for PI and PPO membranes, respectively. Increasing the temperature only improved whereas selectivity remained constant. Akhmetshina et al. [49] obtained permeability and ideal selectivity of CO_2/CH_4 and H_2S/CH_4 separation, 15 and 32, respectively, using supported ionic liquid membranes (SILMs) impregnated by 1-butyl-3-methylimidazolium acetate (bmim[OAc]). Yan Huang and Rui Wang [50]

designed core–shell-structured H_2S imprinted polymers (PMo12@UiO-66@H_2S-MIPs) in the removal of H_2S and CO_2 from gas streams. Despite the poor adsorption capacity of the PMo12@UiO-66@H_2S-MIPs, it exhibited excellent selectivity towards CO_2 and H_2S. The calculated adsorption capacities of PMo12@UiO-66@H_2S-MIPs for H_2S was 26 mg/g on average. SILMs were analysed on the selective separation of CO_2 and CH_4 and there were fewer attempts on H_2S and CH_4. Zhang et al. [51] studied permeability of CH_4, CO_2, and H_2S in SILMs and achieved the highest H_2S/CH_4 selectivity, 142, the permeability of H_2S was 5279 (units) barriers at 30 °C.

Liu et al. [52] investigates the simultaneous separation of CO_2 and H_2S from natural gas using fluorinated MOF-Based Membranes. [M1(M2Fx) (Ligand)2]n MOFs-based membranes were showed to have high performance of separation.

Hollow fiber membrane (HFM) modules offered several advantages as gas-liquid contactors but due to the high toxicity of H_2S, these modules were utilized in the removal of CO_2. The Marzouk et al. [53] adapted a hollow fibre membrane contactors module for the elimination of H_2S at percentile levels from a pressurized gas mixture of H_2S and CH_4. H_2S/CH_4 selectivity ratio was calculated at approximately 70 at 1 bar and about 51 at 50 bars.

2.5.3 Adsorption

Adsorption refers to the selective removal of impurities through their physical attachment to the surface of a solid material, known as an adsorbent. This process is an energy-efficient process as the adsorbent can be used many times in the adsorption-desorption cycle as it is regenerable. That is why adsorption processes are widely used in chemical and petrochemical industries.

In the removal of hydrogen sulfide from a gas mixture containing CH_4, CO_2, N_2, H_2, and H_2O, various adsorbents such as metal oxides [54] [55] [56], metals [57], metal-organic frameworks [58], zeolites and carbon-based materials [59] are utilized. To be an effective adsorbent in the process, it must have some properties such as high adsorption capacity, regenerability, high-temperature stability and high selectivity towards the molecule to be removed.

2.6 H_2S REMOVAL USING ZEOLITES

Synthetic and natural zeolites are employed as adsorbents due to their good adsorption properties. Zeolites are also widely used in the chemical industry as catalysts. The point of using zeolites is that they have pores through which molecules with smaller diameters can be adsorbed, while large molecules cannot. This makes them effective for removing impurities like hydrogen sulfide, carbon dioxide, and moisture from natural gas due to their excellent adsorptive properties.

Natural zeolites exhibit adsorption capabilities that are significantly higher than those of synthetic zeolites. However, according to literature, only a limited number of natural zeolites have been explored for gas purification purposes.

Yaşyerli et al. [60] carried out H_2S adsorption by natural zeolite namely Clinoptilolite in the fixed bed adsorption system and investigated 0.03 g S/g (total sulfur adsorption capacity) capacity at 600℃. Jafari et al. [61] studied Y and ZSM-5 zeolites modified with 3% and 5 % weight ratios of magnetite nanoparticles in hydrogen sulfide removal from the air. Meso/micro-porosity of zeolite Y was increased due to loading magnetite nanoparticles compared to ZSM-5. Due to the modification of pores during high-temperature desulfurization, Y/Fe_3O_4-5 % was successful. Yokogawa et al. [62] synthesized LTA (Zeolite A) and MFI (ZSM-5) zeolites by a wet method and doped Ag onto them. Studies have shown that substituting univalent metal ions with alkali atoms in zeolites enhances their H_2S absorption capabilities. Furthermore, Ag-doped LTA zeolite demonstrated a greater capacity for hydrogen sulfide uptake than Ag-doped MFI zeolite. Oliveira et al. [63] inspected H_2S adsorption on NaY zeolite in equilibrium and fixed bed conditions. The zeolite was prepared naturally using kaolin clay and examined its adsorption properties for the H_2S removal from natural gas in continuous PSA. It was found that raising the bed height (6 cm) increased the adsorption capacity of the synthetic zeolite by 5.345mg/g at 25℃. Pourzolfaghar et al. [64] have reached 94% of hydrogen sulfide adsorption from biogas using raw zeolite. A number of experiments showed that this zeolite had natural regeneration. Ahmad et al. [65] examined Diatomite and it's water and acid-treated modification in biogas purification. Results showed that acid treatment facilitated modifying surface area and functional group of Diatomite. Thus it reached 6.87 mg/g of H_2S adsorption capacity while water treated Diatomite showed 3.82 mg/g. Lee et al., [66] evaluated adsorption properties of iron incorporated NaA

zeolite synthesized from melting slug towards NH_3 and H_2S. As the concentration of iron in the solution was raised, the surface area of iron enriched NaX zeolite pellets grew, resulting in a higher H_2S adsorption capacity compared to commercial 4A and 13X zeolites.

Nguyen and his team [67] synthesized Faujasite zeolite by hydrothermal and ion-exchange method with divalent metal ions (Co^{2+}, Mn^{2+}, Ni^{2+}, Cu^{2+}, Ca^{2+}, Zn^{2+}) and examined them in continuous fixed-bed H_2S adsorption. The synthesized ZnX zeolite exhibited an H_2S adsorption capacity that was over 24 times greater than that of the raw X zeolite.

Theoretical approaches of removal of H_2S were also considered. Kristóf [68] assessed the adsorption of hydrogen sulfide from a simple gas mixture by molecular simulation. Highly polar zeolite NaA was used as an adsorbent and it exhibited a remarkable ability to capture H_2S. Kristóf and Bucsai [69] unveiled the adsorption behaviours of the all-silica zeolite frameworks DDR, CHA, ACO, and CAS in the removal of H_2S from binary mixtures with CH_4, C_2H_8, C_3H_{10} using atomistic molecular simulation. In terms of CH_4/H_2S adsorption, ACO, CAS, zeolites that have small pores showed high adsorption performance. Shah et al. [70] examined 386 all silica for zeolites to identify the best zeolites for the removal of high concentration of H_2S from H_2S/CH_4 and H_2S/ C_2H_6 binary mixtures using Monte Carlo simulations and selected the best candidates for natural gas sweetening. The authors concluded that the optimum zeolite selection for H_2S removal may differ depending on the value of CO_2 removal and the reduction of C_2H_6 and other alkane losses. Lasich [71] evaluated the efficiency of alkali metals doped bentonite for H_2S adsorption from natural and landfill gases using Monte Carlo simulation. In terms of overall efficiency, the findings showed that the three doped bentonite adsorbents should be ranked as follows: $K^+ > Li^+ > Na^+$. K^+ doped bentonite may be used as the best candidate for the selective H_2S adsorption from gas streams in PSA.

Nowadays, despite the low adsorption capacity of synthetic zeolites compared to natural zeolites, they are widely used in many industrial processes. Molecular sieves which are zeolite-based adsorbents such as 3A, 4A, 5A, 13X, that differ from each other based on their pore size and chemical composition, are used in the purification of industrial gases. They are produced on an industrial scale. Among them, molecular sieves of type 4A are very effective. This molecular sieve can reduce sulfur content to

4 ppmv [72]. Many researchers have studied the different adsorption properties of these molecular sieves to remove H_2S from natural gas [73] [74] and biogas [8] [75] [76] [30], [77] [78] from CO_2 [79] from feed stream [80] [77] and air [78].

Alonso-Vicario et al. [8] compared Clinoptilolite with 5A and 13X zeolites for removal of H_2S in the upgrading of biogas in PSA. Activation of Clinoptilolite was carried out by washing and calcination while 13X and 5A zeolites were activated only by calcination. Clinoptilolite showed an excellent property among the zeolites, with 1.39 mg H_2S/g and 173.9 mg CO_2/g adsorption capacity for both purification and upgrading of biogas.

Modified molecular sieve zeolites were also tested in the purification of natural gas from hydrogen sulfide, and their various properties in the process were studied ([75] [81] [82] [83] [77]. Jalil et al. [83] studied the adsorption value of 3A, 4A, and 5A zeolites prepared from Iraqi kaolin by the ion-exchange method. H_2S adsorption capacity increased with the decrease of the temperature from 55℃ to -5 ℃ and 5A zeolite exhibited adsorption capacity of 79.384 μmol/g (2.7mg/g). Liu et al. [77] carried out hydrogen sulfide removal using 4A zeolite synthesized from natural attapulgite. 4A zeolite synthesized under optimal condition showed high adsorption capacity of 8.36 mg/g-sorbent and saturation sulfur sorption capacity of 12.4 mg/g-sorbent at 50℃. Due to its characteristics, 4A zeolite emerges as a favourable option for H_2S adsorption. Starke et al. [84] studied LTA (4A) zeolite on the adsorption of H_2S exchanging with Ca^{2+} in different percentage. It was concluded that increasing of Ca^{2+} cations on the zeolite increases physical adsorption sites. Zhu et al. [85] prepared 13X zeolite modified by Ag and Cu to remove organic sulfur compounds from natural gas. Modification of 13X with Ag increased adsorption capacity by 1.6 times compared to the raw 13X. Cu/13X also showed high adsorption capacity in the following sequence ethyl mercaptan > methyl sulfide > dimethyl disulfide. Chen et al., [86] tested ion-exchanged NaX zeolite with Zn, Co and Ag to identify adsorption performance of H_2S and COS from Claus tail gas. AgX had the largest H_2S and COS breakthrough capacity, with 1.53 mmol/g (51mg/g) and 10.5 mmol/g (630mg/g), respectively. Kumar et al. [82] examined Ag and Cu modified Faujasite to separate H_2S from dilute streams containing He, N_2, N_2 CO_2, CO, and H_2O. Although the presence of the various gases in the mixture, AgX and AgY zeolites were able to remove H_2S, however CuX and CuY were unsuccessful in the presence of 2% CO.

Abdul Hadi et al. [87] investigated the influence of ZnO impregnated on Na-A zeolite synthesized from Malaysian kaolin in biogas desulfurization and discovered adsorption capacity of 15.75 mg S/g sorbent H_2S when 20 wt.% ZnO was loaded onto Na-A.

In order to evaluate the effect of silver on NaA zeolite, Bahraminia et al. [88] studied synthesized such nano zeolite and its Ag exchanged sample. The adsorption capacity of NaA zeolite with Ag^+ ions was found to be increased (33.24 mg/g). Li et al. [89] inspected ZnO-loaded 3-D structural mesoporous silica materials (SBA-16, MCM-48, and KIT-6) to evaluate the performances on H_2S removal at room temperature. Rezaei et al. [90] compared ETS-2 adsorbent exchanged with Ag, Ca, Cu, and Zn metals to commercially available adsorbent R3-11G. Metal exchanged ETS-2 zeolite showed more effective adsorption properties. Cu exchanged ETS-2 zeolite had the highest H_2S capacity of 29.7mg H_2S/g adsorbent. Bayu et al. [91] used high-intensity ultrasonic waves to modify Bayah natural zeolites with Ferric chloride hexahydrate solution. The performance of natural zeolite modified increased by 70% to 117 %. Bowen et al. [92] investigated hydrogen sulfide removal from natural gas using titanosilicite zeolite in presence of hydrogen peroxide and examined the effect of reaction temperature and H_2O_2 concentration on the catalytic oxidation. The findings indicated that a higher reaction temperature and an increased concentration of H_2O_2 enhance the catalytic oxidation of TS-1 in converting H_2S. Sung et al., [93] studied H_2S adsorption properties of multivalent cation-exchanged zeolites including Zn(II)Y, Ni(II)Y, and Ga(III)Y zeolites using DFT calculation. Results indicated that GaY might be used for the desulfurization of Claus tail gas followed by Cu (II)Y dehydration. Simultaneous removal of H_2S and SO_2 using the 13X zeolite was carried out by Yang et al. [46]. The adsorption was performed in a simulated Claus gas containing 20,000 ppmv H_2S, 10,000 ppmv SO_2, 15 vol% water vapours, and the balance N_2 gas at 150 °C. According to the breakthrough curve, the fresh 13X zeolite showed an adsorption sulfur capacity of 179.7 mg S/g for H_2S and SO_2. Regeneration was done by purging of N_2 at 490 °C for 120 min with the space velocity of 1000 h^{-1}. The adsorption sulfur capacity decreased to 148.1 mg S/g after five adsorption–regeneration cycles due to formation of sulphate in the pores of 13X, which causes the blockage of pores.

Bareschino et al. [48] recently conducted studies to determine the saturation of NaX zeolite with H_2S. The effects of H_2S concentration, temperature, and adsorbent age were investigated, and it was discovered that the adsorbent does not fully saturate since H_2S oxidation occurs:

$$H_2S + 1.5O_2 = SO_2 + H_2O \quad (2.12)$$

$$H_2S + 0.5O_2 = S + H_2O \quad (2.13)$$

At high temperatures, elemental S is formed in the pores of zeolite; thus, no zero H_2S concentration can be achieved by regenerating the adsorbent.

The process of treating natural gas is complicated due to the presence of various contaminants in it. This occurs because substances compete for adsorption sites on the zeolites. Thompson [94] investigated adsorption performance of the Na-SSZ -13 zeolite to treat natural gas containing CH_4, C_2H_6, CO_2, H_2S, H_2O. the sequence of adsorption affinity was determined to be $H_2O > H_2S > CO_2 > C_2H_6 > CH_4$ according to experimental outcomes.

2.7 MODIFICATION OF ZEOLITES TOWARD H_2S REMOVAL

The adsorbent modification will provide opportunities to increase efficiency of adsorption. Both natural and synthetic zeolites can be modified by ion-exchange and impregnation methods. [28]. In order to tailor adsorbents and catalysts, ion exchange is carried out for post synthesis modification of microporous materials [95]. To prepare metal exchanged zeolite, ion exchange and impregnation methods can be applied [2]. Traditionally, ion exchange is performed by immersing the zeolite powder in water-based solutions of salts that contain the necessary cation. Impregnation and ion-exchange are the most widely used techniques in the modification of zeolites to improve their adsorption properties.

Tran et al. [96] ion exchanged Faujasite NaX zeolite with Co for the removal of H_2S from nitrogen. $Co(NO_3)_2$ solution of various concentration was used as ion exchange cation with Na cations. The samples were dried at 120°C for 12 h and underwent thermal treatment at various temperatures (400, 500, 600, and 700°C) for 3 hours, with a heating rate of 20°C min^{-1}. Iron-Incorporated Na-A Zeolites Synthesized from Melting Slag was prepared by Lee et.al. [66] to adsorb NH_3 and H_2S gases. Pellets prepared from 78mM $FeCl_3$ solution calcined at 200°C showed highest hydrogen

sulfide adsorption capacity. The pellets made from a solution of $FeCl_3$ with a concentration of 78mM and then heated to 200°C, had the greatest capacity for adsorbing hydrogen sulfide. Abdullah et al. [87] studied the influence of ZnO on Na-A zeolite synthesized by impregnation from Malaysian kaolin in biogas desulfurization. ZnO was employed to increase the adsorption capacity of zeolite and because its low cost compared to other oxides. When the loading rate was increased from 10 to 20 wt%, both the micropore area and the micropore volume decreased. However, there was no substantial change found even after increasing the loading rate from 20 to 30 wt%, which indicates that the loading rate was exceeded. It was noticed that the highest adsorption capacity of 15.75 mg S/g when 20 wt% ZnO was loaded onto Na-A. The fact that the characteristics of the used adsorbent were not recovered because of regeneration at temperatures of 100 and 200 °C is evidence that chemical adsorption took place by the following equation:

$$ZnO + H_2S(g) = ZnS + H_2O \quad (2.14)$$

2.7.1 Silver nanowires modification

Nanowires exhibit a range of unique properties that are absent in three-dimensional or bulk materials. This is attributed to the quantum confinement of electrons within the nanowires, resulting in energy levels that diverge from those found in bulk materials. Nanowires are nanostructures with a diameter in the order of 10^{-9} m. They have aspect ratios of more than 1000, and hence they are commonly referred to as one-dimensional nanomaterials. Silver nanowires have distinct optical, electrical, and thermal properties and are being incorporated into a wide range of products from photovoltaics to biological sensors. Nanowires excel in absorbing and scattering light with remarkable efficiency. Their characteristics are determined using analytical methods like scanning electron microscopy (SEM), transmission electron microscopy (TEM), and atomic force microscopy (AFM). When silver nanowires are in solution, molecules interact with the nanowire surface to form a double layer of charge which prevents aggregation and stabilizes the nanowires. The new attention on nanostructured noble metals is primarily driven by their prospective uses in catalysis, optoelectronics, and microelectronics [97].

Ul'yanova and Golubeva [98] conducted a study to alter zeolites by adding silver nanoparticles and clusters in order to examine their catalytic efficiency in the oxidation

reactions of H_2 and CO. The findings indicated that the zeolite, which had been altered with Ag_8^+ clusters, achieved a complete conversion rate of 100% at 250°C. formation of silver nanowires in within SBA-15 was reported by Huang et.al [99]. Adhyapak et. al. [97] synthesized silver nanowires inside mesoporous MCM-41 to study its optical properties.

2.8 SYNTHESIS OF ZEOLITES FROM KAOLIN

On an industrial scale, one of the most important things that contributes to effective development is the utilization of the least expensive raw materials. As a result, a significant portion of the research is focused on the achievement of novel compounds through the utilization of less expensive and prevalent materials. Rice husk, kaolinite, clay minerals, fly ash, asbestos, slag, and sludge are some of the materials that are utilized in the process of zeolites synthesis. The synthesis of zeolites is a highly active area of research because of the significant role that zeolites play in several industrial processes involving catalysis, separation, and adsorption [2]. The synthesis of LTA type zeolites from diverse materials, such kaolin [100], [101], coal fly ash [102] , attapulgite [77] [103], is the subject of numerous studies.

Kaolin is commonly chosen for producing zeolites as it contains both Si and Al. Jalil with colleagues [104] investigated the microwave-assisted synthesis of Zeolite 5A from Iraqi kaolin. The results showed that 5A zeolite synthesized by this method had a higher adsorption capacity for H_2S (37.19 µmol/g) compared to Zeolites 4A and 3A. Liu et.al [77] carried out an experiment on H_2S removal using 4A zeolite synthesized from attapulgite. Their findings indicated that 4A zeolite, when synthesized under optimal conditions, has the ability to remove H_2S, exhibiting a breakthrough adsorption capacity of 8.36 mg/g. Mohamed et al. [101] prepared 5A zeolite from local kaolin for dehydration and desulfurization of LPG. Synthesized 5A showed excellent dehydration and desulfurization propertied. 5A zeolite extrudates were synthesized from kaolin, as reported by Shams et al. [105]. The highest purity and optimal sieving results were obtained using 30 wt% kaolin as a binder.

Kaolin is the one of the most used minerals for the synthesis of zeolite in many studies. Kaolin has a chemical composition of $Si_2Al_2O_5(OH)_4$ and 1:1 layered structure composed of SiO_4 tetrahedra joined $Al(O,OH)_6$ octahedra with pseudohexagonal symmetry [106]. Kaolinite is the primary component of kaolin, a mineral that is white

or greyish white in color. It is composed of small, thin, and flexible sheets of triclinic crystals. [107]. Uzbekistan ranks among the countries with the largest kaolin resources, alongside the United States, Colombia, the Czech Republic, Brazil, Guyana, Suriname, Ghana, Australia, and Europe [108] [107]. Angren Kaolin is the only factory in Central Asia that manufactures enriched kaolin. AKF-78, AKC-30, and ACT-10 are types of enriched kaolin that have multiple applications, such as the production of kaolin wool, ceramics, cables, plastic, adhesives, and as a filler in paper manufacturing. They are also used as coagulants and glazes [109]. Unfortunately, there is currently no comprehensive study available on the process of synthesizing zeolites from Angren kaolin, despite its potential as a source of Al and Si. Zeolites are synthesized via conventional hydrothermal, microwave-assisted, and fusion-hydrothermal techniques, which utilize different resources. The hydrothermal synthesis approach is utilized due to its characteristics that improve the water's solvation ability, enhance the solubility of the reactants, and stimulate the reactivity of the source materials. The first step in hydrothermal synthesis involves the initial formation of the hydrated aluminosilicate, followed by the crystallization process of the gel [2].

2.9 DETERMINATION AND MEASUREMENT OF HYDROGEN SULFIDE CONCENTRATION.

The presence of hydrogen sulfide in natural gas is a significant quality metric, necessitating the application of different techniques to measure its concentration. These techniques differ from each other in cost, complexity of application, and accuracy of measurement. Therefore, a variety of approaches are applied depending on the intended purpose. To achieve this goal, international bodies like OSHA and IUPAC have established and documented standardized methods for highly precise measurements.

The concentration of H_2S is one of the most crucial quality standards for natural gas and biogas. Standards for accurate measurements have been developed and registered by international organizations as ASTM, UOP, and GPA [110]. The following approaches have been employed in lab settings in numerous research studies because they are straightforward to use despite the complexity of these basic test methods.

2.9.1 Gas chromatography

Gas chromatography is one of the most exact ways for determining the precise concentration of the components in a mixture. This approach is based on the measurement of signals generated by sample components that are separated in the column. As GC column porous polymers (Poropack [111], Hayesep-Q column, sulfur chemiluminescence detector (SCD) [112]) are used. For comprehensive compositional analysis, this approach is used [110].

2.9.2 Analyzers

Analyzers are commercially available and are widely used [30], [113] to monitor or detect targeted gas for a variety of purposes. They are based on a variety of techniques, and the following are some of the most common H_2S measurement methods that used to develop analyzers.

Electrochemical

Detectors are primarily used for personnel protection and to offer information about workplace pollution. However, it can be seen from the several studies have been reported in the literature [114], [115] detectors were employed to measure H_2S concentration for research purposes too. In the electrochemical detectors, when H_2S molecules replace oxygen molecules, free electrons are released, and the resistance between the two electrodes is reduced. This change is proportional to the amount of H_2S in the gas and can be measured directly. Electrochemical sensors can be utilized to measure H_2S concentration in different ranges (0-1000ppm) on lab scale.

Lead acetate

H_2S tape analyzers utilize a lead acetate-coated tape to detect the presence of H_2S in a gas sample which is based on the reaction between H_2S and lead acetate to form lead sulfide. Darkness of the stain on the type is proportional to the amount of the H_2S. Low-level H_2S can be reliably measured with these tape analyzers, but they come at a high upfront cost.

Tuneable diode lasers

Tuneable diode lasers (TDL) are commonly used to measure the concentrations of the gas's constituents. To measure the concentration of a target gas, the technology uses the absorption characteristics of various gases. To determine the target gas concentration, a detector measures the intensity of the laser light after it passes through

the gas sample. At very low levels of H_2S, a properly engineered TDL analyzer can provide accurate and extremely reliable measurements.

Although determination methods have their merits, the choice of technique or analyzer depends on the intended purpose.

2.10 SUMMARY AND IMPLICATIONS

H_2S, a corrosive and toxic compound found in natural gas, needs to be eliminated for several reasons, including enhanced safety, compliance with pipeline quality standards, and environmental protection. The removal of H_2S from various sources is commonly achieved by the utilization of absorption, adsorption, and membrane separation techniques. Adsorption is a highly effective technique that employs a range of adsorbents, including MOFs, activated carbons, zeolites, silica gel sand other substances. Zeolites such as 4A, 5A, and 13X are utilized for the purpose of desulphurisation and dehydration in gas processing. The literature suggests that the adsorption performance of zeolites can be enhanced by modifying them with Cu, Zn, Ag, and Co. Utilizing inexpensive materials to manufacture adsorbents for the natural gas sweetening process results in cost reduction for the final product and is also environmentally sustainable.

Promising findings have been obtained from considerable study on the utilization of molecular sieves as adsorbents for the separation of H_2S from various sources such as natural gas, biogas, syngas, refinery gas, and coal gas. However, there is only one experimental approach where molecular sieves type 4A, 5A, 13X in PSA were used to remove acid gases from $CH_4/CO_2/H_2S$ mixture [73]. In this research, synthetic zeolites of types 4A, 5A, and 13X, as well as samples modified with Ag and AgNWs using ion exchange and impregnation techniques, were evaluated. The focus was on analysing their fundamental adsorption properties for removing trace levels of H_2S from natural gas.

Chapter 3: Research Design and Methodology

This chapter discusses reagents and materials used, synthesis and modification procedures and the adsorption method to assess adsorption properties of zeolites both silver-modified and synthesized from kaolin. The discussion also included characterisation techniques, along with the giving of characterization parameters.

3.1 MATERIALS AND METHODS

3.1.1 Reagents and materials

The choice of reagent and appropriate selection of materials are crucial elements that significantly impact the quality and efficacy of the investigation. Thus, for the research study on the removal of hydrogen sulfide from natural gas, we have chosen the subsequent beginning reagent and material.

1. Molecular sieves: 4A, 5A and 13X (from Hurtland LLC, Poland),
2. $AgNO_3$ (from Stanlab LLC, Poland),
3. 5000 ppm H_2S in CH_4 (from Air Liquide Polska LLC, Poland),
4. Deionized water.
5. 100 ppm H_2S in N_2 (from Air Liquide Polska LLC, Poland),
6. NaOH as an alkaline activating agent from Stanlab LLC, (Poland),
7. $CaCl_2$ from Chempur LLC, (Poland),
8. AKC-30 type of enriched kaolin provided courtesy of Angren Kaolin LLC, Uzbekistan.
9. Ammonia solution
10. Polyvinylpyrrolidone
11. Ethylene glycol

3.2 SYNTHESIS METHODS

3.2.1 Synthesis of silver modified 13X zeolite

Ag ion-exchanged 13X was prepared by stirring 10 g of 13X molecular sieve in various molar concentrations of $AgNO_3$ water solution (0.02 M, 0.05 M, and 0.1 M in 200 mL) for 24 h. Ag ion-exchanged 13X molecular sieves were labelled as AgI-13X, AgII-13X, and AgIII-13X, respectively. Then, the samples were washed with deionized water, filtered, and dried at 110 °C for 12 h. Calcination was carried out at 600 °C overnight in the oven. Samples were cooled and kept in a desiccator.

3.2.2 Fusion/hydrothermal synthesis of 4A zeolite from kaolin

Fusion/hydrothermal technique was used to synthesize 4A molecular sieve from kaolin adopted by [108] with some required modifications. Prior to synthesis, the kaolin was dried in an oven at a temperature of 110 °C for 10 h. 10 grams of Kaolin were mixed with 8.0, 10.0, and 12.0 grams of NaOH (synthesized zeolites were labelled 4A-I, 4A-II, and 4A-III, respectively) and ground. Fusion was conducted at 550 °C for 1 h. Fused product then pulverized and dissolved in 100 ml of deionized water. To augment crystallization 0.1 g of commercial 4A was added. The mixture was aged in autoclave at 30 °C for 5 h and heated at 90 °C for 5 h.

3.2.3 Hydrothermal synthesis of 4A zeolite from kaolin

The Si/Al ratio typically has a significant impact on the synthesis of zeolite to ensure correct formation. Zeolites such as A (LTA), hydroxysodalite (SOD), KH, and KJ can form crystals when there is a low Si/Al ratio and strong alkalinity. On the other hand, Mordenite (MOR) and beta (BEA) can form crystals when there is a high Si/Al ratio and weak alkalinity in the gel [2].

4A zeolite was synthesized from kaolin by hydrothermal method by the following manner.

First, 20 g of kaolin with mixed with different molar concentration of NaOH solutions (2.0, 2.5, 3.0 M) and 2 g of sodium silicate (Na_2SiO_3) was added as a source of silica. Samples were aged at 60 °C for 4 h with stirring at 500 rpm. Crystallization occurred at 90 °C for 3.5 h. The samples were labelled as S1, S2, and S3 respectively.

Second, 20 g of kaolin with mixed with 2.0 M of NaOH solution and 4 g of Na_2SiO_3 was added. Samples were aged at 60 °C for 4 h. Crystallization of the samples was done at 90 °C for 8, 10 and 12 h. The samples were labelled as S4, S5, and S6 respectively.

Third, 20 g of kaolin mixed with 2.0 M of NaOH solution and no Na_2SiO_3 was added this time. Aging was carried out at 60 °C for 12 h. Samples were crystallized at 90 °C for 12, 24 and 36 h. Following these processes, all samples were dried at 110°C overnight and stored in a desiccator. The samples were labelled as S7, S8, and S9 respectively.

3.2.4 Synthesis of 5A from 4A by ion-exchange

The preparation of 5A zeolite was achieved by utilizing a 1 M calcium chloride solution to facilitate ion exchanges with the 4A-III zeolite, which had been synthesized from kaolin. Aging was carried out at 95 °C for 4 h with stirring at 300 rpm. The 5A product was cleansed four times with deionized water, dried at 110 °C for 2h, then calcinated at 500 °C for 4 h. Sample was placed in a desiccator for storage until adsorption experiments.

3.2.5 Synthesis of silver nanowires

Silver nanowires were fabricated by the following procedure: 200 ml of EG pure was measured and put into the flask. After that 0.603 g of PVP was added to the flask and mixed with the help of magnetic stirrer until a uniform transparent solution in obtained. Then add 0.08 mL of $CuCl_2$ from 50 mM stock solution and the mixture was stirred and heated until it reached 150 °C. Finally, 0.594 g of $AgNO_3$ was added to the solution and it was stirred continuously. The reaction time was 75 minutes with the continuous purging of argon, maintaining temperature to 150 °C.

Purification of AgNWs was performed by centrifugation at 4000-4200 rpm for 20 minutes and subsequently washed with deionized water (6 cycles) and in the last step AgNWs were washed with the ammonia solution to remove the chloride impurities.

3.2.6 Impregnation of silver nanowires on zeolite

The process of impregnating silver nanowires onto zeolites involved the addition of 10 grams of 5A and 13X zeolite to a solution containing 100 ml of silver nanowires.

The mixture was impregnated at room temperature for a period of 12 hours. Afterward, the product obtained was dried at a temperature of 110°C for 12 hours, and then it was stored in a desiccator. The samples were labelled as 5ANWs and 13XNW for silver nanowire-modified zeolites.

3.3 ZEOLITE SHAPING

The zeolite shaping was carried out using the extruder shown in Figure 3-1.a. Figure 3-1.b displays the dimensions of the extruder. The dimension of the extruder is shown in A mixture of synthesized 4A and 5A was placed in the extruder using a spatula. Subsequently, with the assistance of a press, they were transformed into spaghetti-like noodle shapes Figure 3-2. The spaghetti-like noodle has a diameter of 3 mm. To remove the water, the 4A and 5A shapes were dried at 110°C for 12 hours. Next, the samples underwent calcination at 550°C for 2 hours in order to enhance their mechanical and textural properties. Calcined noodles were then crushed.

a)

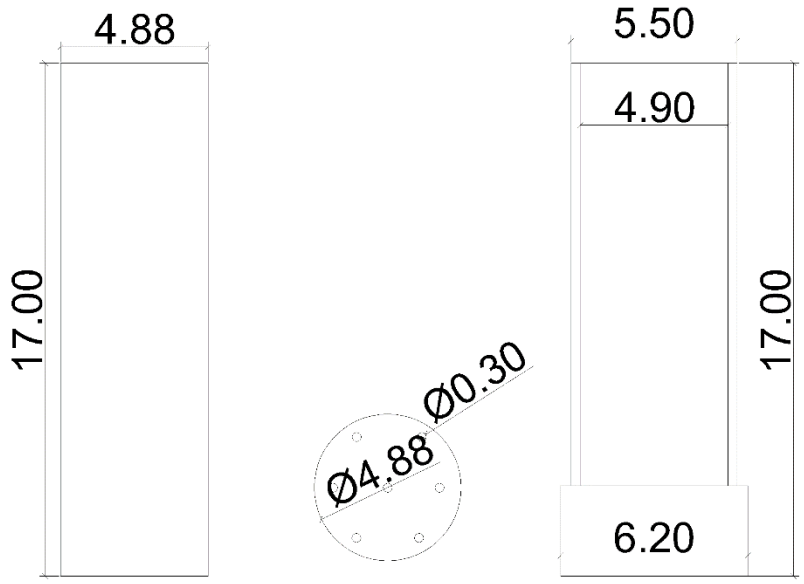

b)

Figure 3-1. Photo and scheme of the extruder used for shaping samples.

(All measurements are in centimeters)

Figure 3-2. Photo of spaghetti-like noodles of 5A-III

3.4 H_2S REMOVAL FROM NITROGEN

Initially, a basic adsorption unit was constructed to conduct adsorption tests aimed at eliminating H_2S from nitrogen. Nitrogen is an inert gas that is safe for

personnel to use in studies. Adsorption tests were performed using commercially zeolites including 5A and 13X and silver modified 13X. Below is a description of a typical laboratory adsorption unit.

A laboratory scale setup was used to carry out H_2S adsorption, as shown in Figure 3-3. Ten grams of adsorbent was placed in the Teflon adsorber (400 mm long and 15 mm internal diameter) and attached to the system. The nitrogen containing 100 ppm H_2S were introduced at the top of the adsorption column with a flow rate of 400 mL/min (24 l/h) under atmospheric pressure. BH-4S Portable Multi-gas Detector from Bosean (China) were used to measure inlet and outlet concentrations of H_2S. H_2S concentrations were recorded in both outlet and inlet by connecting detector ta a computer using software.

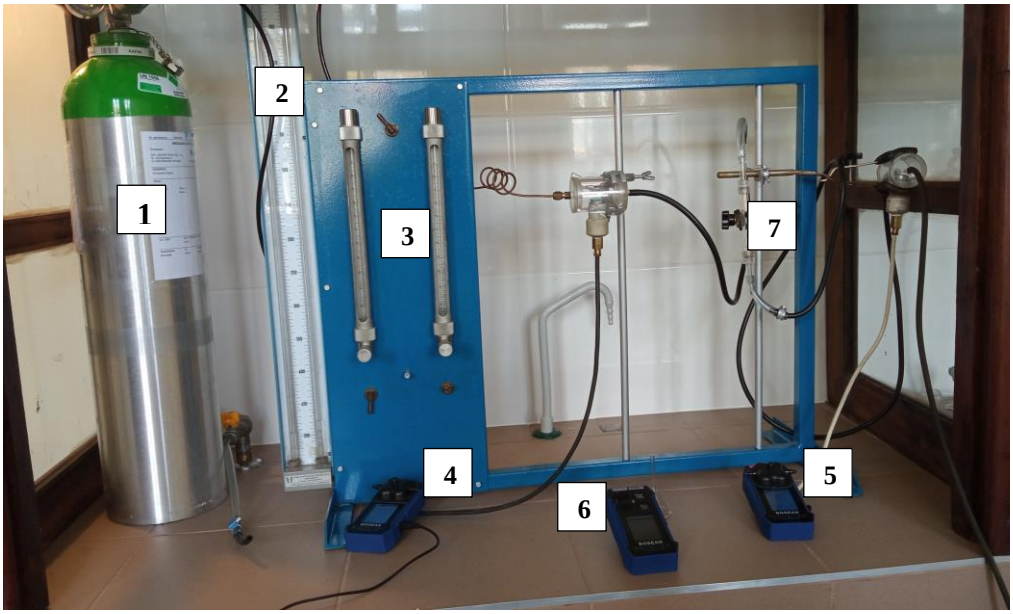

a)

Labels [1] H_2S/N_2 mixture (100 ppm), [2] Monometer, [3] Rotameters, [4] Inlet H_2S detector, [5] Personnel gas detector, [6] Outlet H_2S detector, [7] Adsorber,

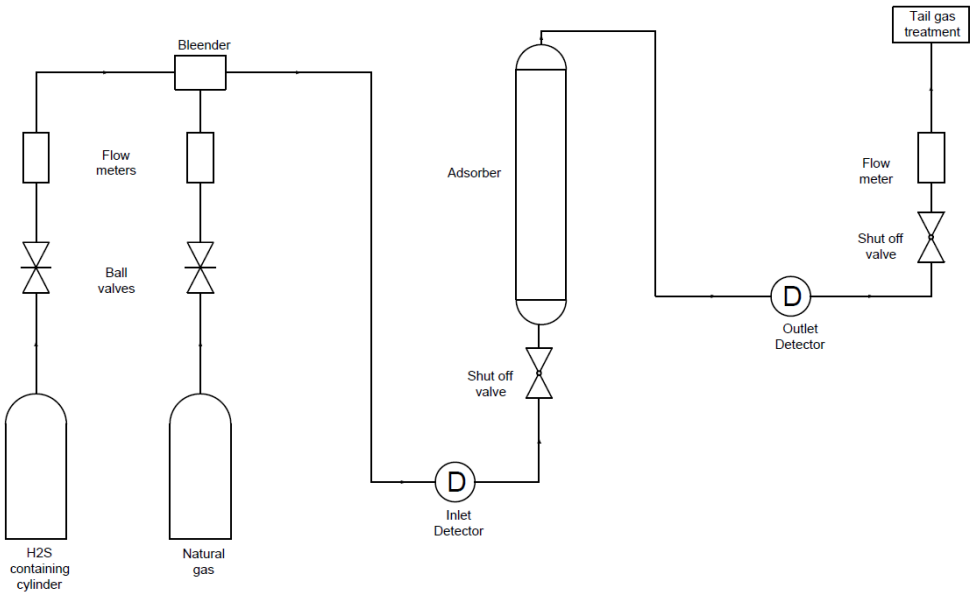

b)

Figure 3-3. a) photo and b) scheme of laboratory set-up for H_2S adsorption from nitrogen.

To prevent inhalation of H_2S, we wore gas protective masks during the experiment.

3.5 H_2S REMOVAL FROM METHANE

While a basic adsorption unit is adequate for evaluating the adsorption characteristics of zeolite, it becomes challenging to investigate the impact of the incoming gas concentration due to the limitations of detectors, which can only measure H_2S concentration up to 100 ppm. Therefore, we reconstructed the adsorption unit with the necessary improvements in order to achieve accurate outcomes. To precisely monitor H_2S concentrations in the intake and outflow, it is crucial to replace detectors with precise measurement equipment. Therefore, we choose to utilize an analyzer capable of quantifying H_2S concentrations up to 2000 ppm. By employing this type of analyzer, we can establish appropriate levels of H_2S in the inlet stream and investigate the influence of the initial H_2S concentration on the adsorption efficiency. Here below, we provide a detailed explanation of the reconstructed adsorption laboratory setup.

A laboratory scale setup was used to carry out H_2S adsorption, as shown in Figure 3-4. Ten grams of adsorbent was placed in the Teflon adsorber (400 mm long and 15 mm internal diameter) and attached to the system. The primary objective of employing 10 g of adsorbent was to replicate the authentic process, as the flow rate of

400 mL/min may prevent H_2S molecules present in methane coming into contact with the surface of the adsorbent. As a result, analyzers in the outlet flow may quickly detect the presence of H_2S gas that is not in direct contact with the adsorbent, allowing for the early detection of breakthrough time. The installation was carefully checked to ensure all connections had no leakage. The mixture was fed directly to a scrubber unit until the desired H_2S concentration in methane was achieved. Desired concentrations (within the 150–500 ppm range) of H_2S were introduced at the top of the adsorption column with a flow rate of 400 mL/min under atmospheric pressure. A rotameter was used to keep the mixed gas flow rate constant at 400 mL/min for each of the experiments. To measure initial and breakthrough H_2S concentrations, two analyzers (Southland Sensing Ltd., USA) were installed before and after the adsorber. Analyzers are able to measure the concentration of hydrogen sulfide in a broad range, from 0 to 2000 ppm. H_2S concentrations were recorded in the input and output every second to obtain accurate results. Outlet gas was treated with a NaOH (pH 13.4) solution and burned before being released. Phenolphthalein was used to indicate the H_2S saturation of the NaOH solution. Pipelines and fittings made of stainless steel were used to prevent corrosion.

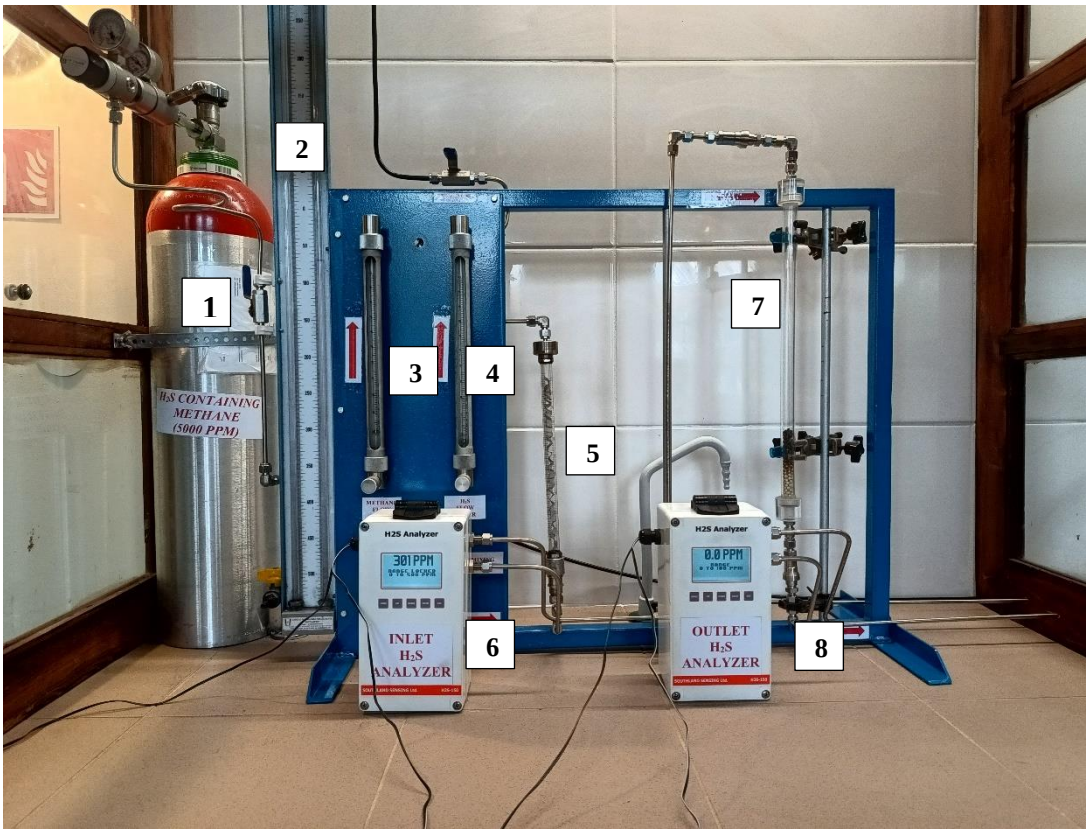

Labels [1] H_2S containing methane cylinder (5000 ppm), [2] Monometer, [3] Methane flow meter, [4] H_2S+CH_4 flow meter, [5] Gas mixing chamber, [6] Inlet H_2S analyzer, [7] Adsorber, [8] Outlet H_2S analyzer,

a)

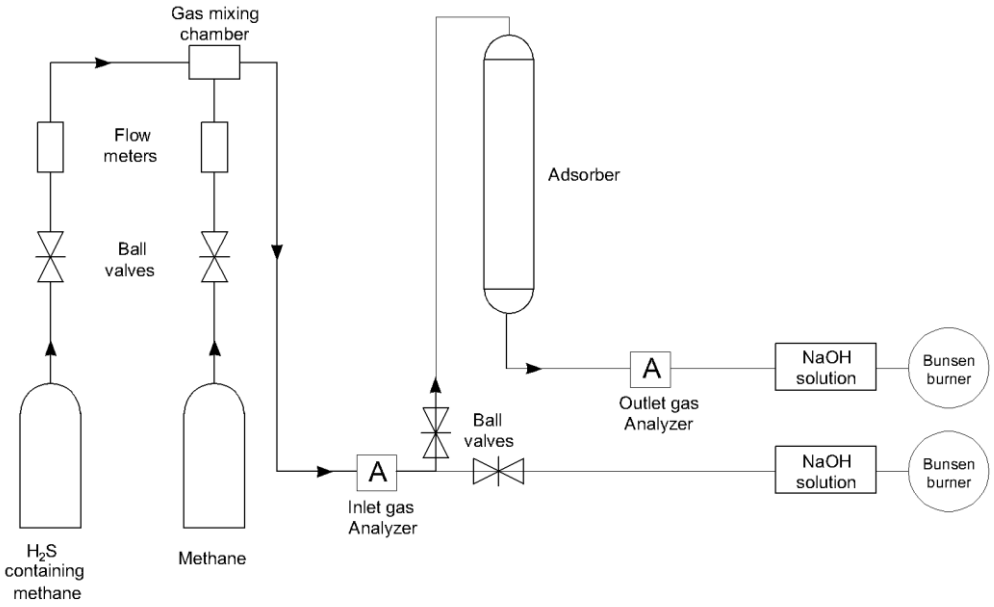

b)

Figure 3-4. a) Photography and b) scheme of laboratory setup with a single adsorber for the H_2S adsorption

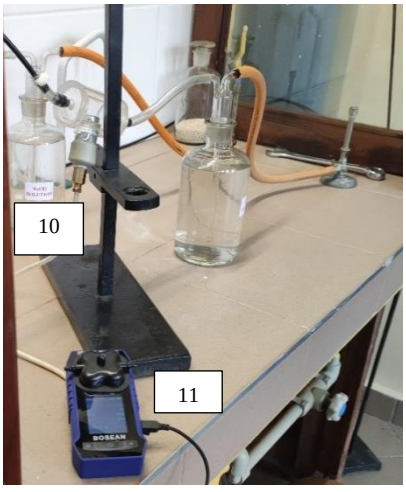

Label:

[10] NaOH solution

[11] Personal gas detector

Figure 3-5. Outlet gas treatment

3.6 ADSORPTION CAPACITY CALCULATION

The adsorption capacity for continuous adsorption can be calculated from the breakthrough curves using the following Equation 3.1 [116]:

$$C_{ads} = \frac{Q_{tot} \cdot MW \cdot [C_{in} \cdot t_1 - (t_1 - t_0)] \cdot 0.5}{V_m \cdot m \cdot 10^3} \quad (3.1)$$

where

Q_{tot} – total gas flow rate (Nl/h),

MW – molecular weight of H_2S,

C_{in} – inlet H_2S concentration,

t_1 – breakthrough time when the outlet concentration is 1 ppmv (h),

t_0 – breakthrough time at the last detection of 0 ppmv (h),

V_m – molar volume (24,414 Nl/mol)

m – mass of adsorbent material (g).

Typically, Adsorption capacity data are gathered at constant temperature and various adsorbate concentrations in the mixture and then the data are plotted as an isotherm [27].

3.7 ADSORPTION ISOTHERMS

Adsorption isotherm can be used to study the performance of an adsorbent. Series of laboratory experiments are conducted to obtain isotherm data. By modelling of isotherm data, performance of adsorbent can be predicted and compared.

An adsorption isotherm refers to the relationship between the concentration of adsorbate in a mixture and the amount of adsorbate that is adsorbed on the surface of an adsorbent at a specific temperature and equilibrium. Brunauer-Emmett-Teller adsorption isotherm, Langmuir, Freundlich, Kelvin equation, Dubinin-Radushkevich equation, Temkin, Redlich-Peterson, Toth and Sip model, Kolbe-Corrigan, Hill, Khan, Flory-Huggins are widely used to explain the microscopic process of adsorption. The adsorption experimental data are often analysed to determine how well they fit a specific isotherm model. This analysis helps to identify the type, nature, and mechanism of the adsorption system [117]. Adsorption isotherms typically represent the relationship between the amount of adsorbate adsorbed and the concentration of the adsorbate, displayed as a graph. [118]. The Langmuir and Freundlich isotherm models were selected for this study due to their widespread usage.

Langmuir isotherm

The following Langmuir isotherm Equation 3.2 was used:

$$q_e = \frac{K_L q_{max} C_e}{1 + C_e K_L} \quad (3.2)$$

where

q_e – H_2S uptake concentration,

C_e – H_2S equilibrium concentration,

K_L – Langmuir isotherm constant related to the binding energy,

q_{max} – is the theoretically calculated adsorption capacity.

Freundlich isotherm

The Freundlich model adsorption parameters were obtained using the following Equation 3.3

$$q_e = K_F C_e^{1/n} \quad (3.3)$$

where

K_F – Freundlich constant or maximum adsorption capacity,

C_e – is the concentration of adsorbate under equilibrium condition (mg/L),

q_e – the amount of adsorbate adsorbed per unit mass of adsorbent (mg/g).

3.8 CHARACTERIZATION

Characterization of zeolites is an advantageous approach for creating new variations and examining their various characteristics. Through characterization, one can identify and analyse several physical and chemical transformations during the modification process. Therefore, structure determination is essential for understanding of their performance in diverse applications. Zeolites are characterized using scanning electron microscopy (SEM), X-ray powder diffraction (XRD), infrared spectroscopy (IR spectroscopy), and Brunauer-Emmett-Teller (BET) techniques. In this research, the zeolites underwent the characterization processes defined below.

3.8.1 Scanning electron microscopy

Morphological features of the sample surfaces were obtained by scanning electron microscope (SEM) images using a Phenom ProX SEM (Phenom-World BV, Eindhoven, The Netherlands). For the SEM imaging, the samples were coated with a

thin layer of gold and mounted on a slab using double-sided tape. The elemental analysis of the samples was also carried out by energy dispersive X-ray spectroscopy (EDS) during SEM image acquisition (Phenom-World BV, Eindhoven, The Netherlands).

3.8.2 X-ray diffraction

Peak position, peak intensities and peak shapes are the basic parameters to look for in a diffraction pattern. The peak position of the crystalline zeolite are determined by the size and shape of the unit. Peak positions are considered fingerprint since all zeolites have unique framework. The peak intensities are dictated by the spatial arrangement and chemical composition of the atoms within the unit cell. The difference in intensities provides insights into the chemical composition and spatial arrangement of atoms within the unit cell. The morphology and dimensions of the peaks provide insights on the crystallite's quality [119].

X-ray diffraction (XRD) is employed to analyse the crystal structure of zeolites, determine the size of their crystals, estimate the degree of heteroatom substitution, and identify any defects present in the zeolite structure [120]. The process of determining the crystal structure of zeolites using X-ray diffraction methodology involves the following stages: (i) obtaining an appropriate sample, (ii) gathering the data, (iii) establishing a preliminary structure using ab initio methods, and (iv) refining the data [121] .

Phase identification is achieved using powder diffraction, which allows for the determination of the kind of zeolite. Each form of zeolite produces a distinct pattern, making it simple to identify. The relative overall intensities of the peaks in zeolite are directly proportional to the quantity of each phase present, when there is more than one phase.

The phase composition of samples was determined using a powder X-ray diffractometer (Seifert 3003TT) with a Cu X-ray tube (kλ1 = 1.540598 Å, kλ2 = 1.544426 Å, kβ = 139,225 Å). The powder samples were analysed between 5° and 80° of 2Theta with 0.05° step. In order to validate the crystal structures, the X-ray diffraction patterns that were acquired were compared with the information that was collected from the Joint Committee on Powder Diffraction Standards (JCPDS) [28].

3.8.3 BET analysis

The Brunauer-Emmett-Teller (BET) method is used to calculate the specific surface area by analysing nitrogen adsorption isotherm data obtained at 77 K. This model assumes multilayer adsorption of gas on the surface of the adsorbent.

The BET surface of the samples was measured using a Micromeritics ASAP 2020 adsorption analyzer (Micromeritics Inc., Norcross, GA, USA). Brunauer - Emmett - Teller (BET) equation was employed for their surface area calculation based on the gathered nitrogen adsorption isotherms.

3.8.4 Characterization of samples synthesized from kaolin

The samples synthesized from Angren kaolin using the conventional hydrothermal method were characterized using the following equipment:

XRD data is collected using a Rigaku SmarLab X-ray Diffractometer (Rigaku Holdings Corporation, Matsubara-cho, 3-9-12 Akishima-shi, Tokyo, Japan). The data were collected with Bragg-Brentano para-focusing geometry and in continuous scan mode, with a 2theta scan between 5 to 90 degrees and a scan speed of 3 degrees/minute.

XRF analysis was done using Bruker S8 TIGER Series 2 Wavelength Dispersive X-ray Fluorescence Spectroscopy (WDXRF). The samples were pressed using a pallet press with 20T pressure. A standardless Quant-Express analysis method was used to analyse the samples.

A Thermo Fisher Apreo S Field-Emission Scanning Electron Microscope (Thermo Fisher Scientific Inc.) equipped with an energy-dispersive X-ray Spectrometer (EDS) was used to study the samples' morphology and elemental composition.

Chapter 4: Experimental results

This chapter details characterization results of the materials and their adsorption performance, mechanism of the silver modification and adsorption.

4.1 SEM IMAGES

4.1.1 SEM images of 13X and silver modified 13X

Figure 4-1 shows the SEM images of the samples. The framework of the Faujasite zeolite is built by connecting sodalite cages by six rings [19]. SEM analysis verified that both silver-modified and fresh 13X are composed of very well- shaped crystallites with a spherical (octahedral) morphology. However, the fresh 13X molecular sieve shows much smoother surfaces as compared to the silver ion-exchanged 13X particles.

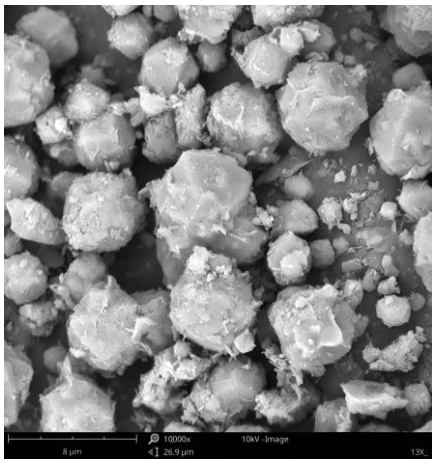

(a)

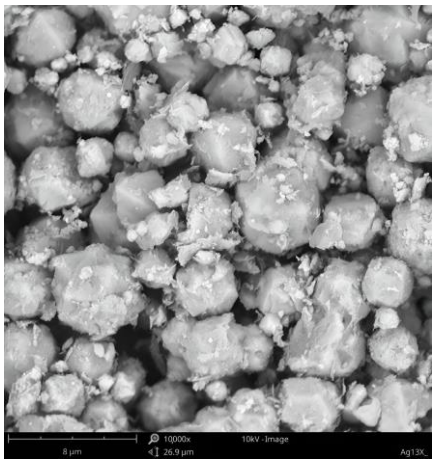

(b)

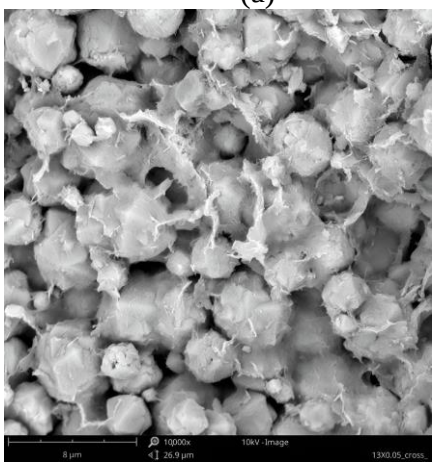

(c)

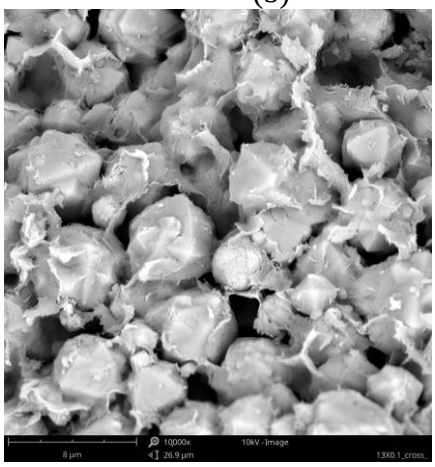

(d)

Figure 4-1. SEM images of (a) 13X; (b) AgI-13X; (c)AgII-13X, and (d)AgIII-13X. mag. 10000×.

4.1.2 SEM images of commercial 4A and 5A

Commercial 4A and 5A zeolites were characterized by SEM technique. Figure 12 shows the SEM images of the 4A and 5A zeolites. It is evident that both types of zeolites consist of well-formed cubic crystals, which are constructed by connecting sodalite cages through four-ring structures.

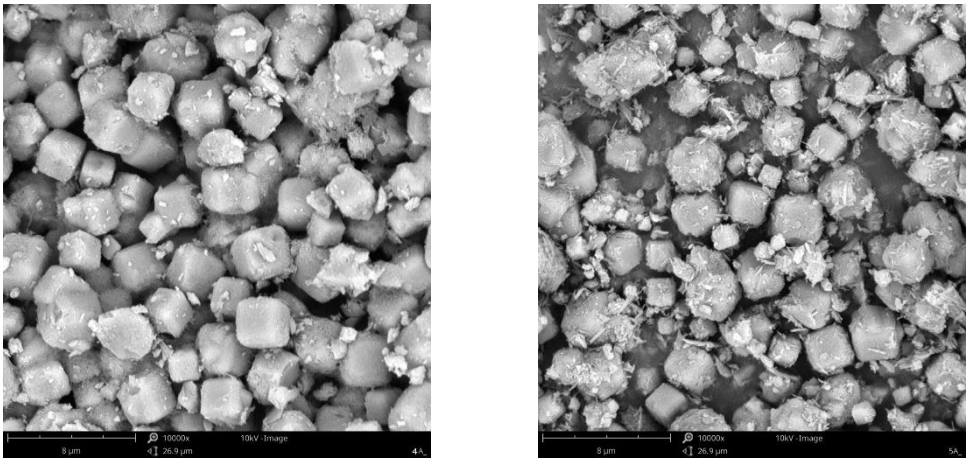

(a) (b)

Figure 4-2. SEM images of (a) 4A, and (b) 5A. mag. 10000×.

4.1.3 SEM images of kaolin, 4A and 5 A zeolites synthesized from Angren kaolin via fusion/hydrothermal method

SEM Images of the kaolin and zeolites obtained from the SEM are presented in Figure 4-3. Kaolin is composed of morphological assemblage of laminar or platelet shapes (Figure 4-3.a). Synthesized samples from kaolin adding NaOH changed its morphology to cubic shapes (Figure 4-3.b-d).

The element content in the 4A and 5A zeolites synthesized from Angren kaolin is shown in Table 4-3. It is evident that there were no appreciable differences in the elemental weight concentration of 4A synthesized with different kaolin/NaOH ratios compared to the commercial version. Moreover, 5A zeolite prepared from 4A by ion exchange has almost similar element content with commercial 5A. Therefore, it can be concluded that the zeolites 4A and 5A were successfully synthesized.

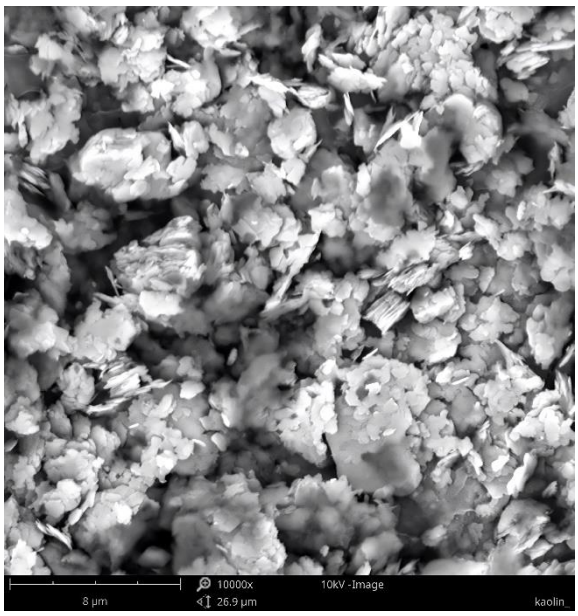
10000x
10kV -Image
8 µm
26.9 µm
kaolin

a)

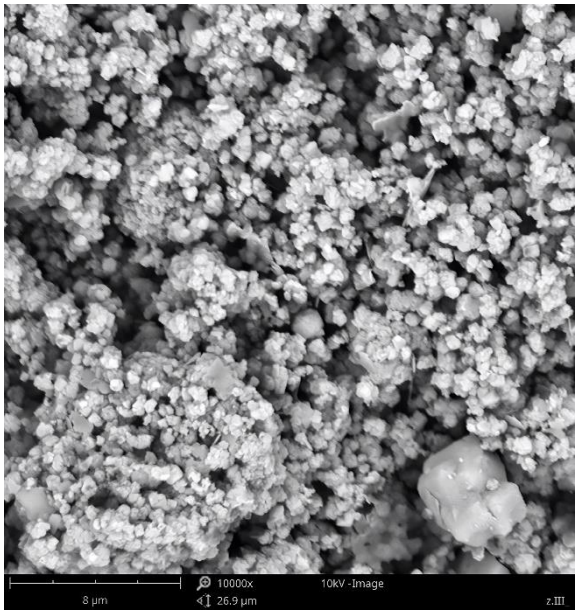
10000x
10kV -Image
8 µm
26.9 µm
z.III

b)

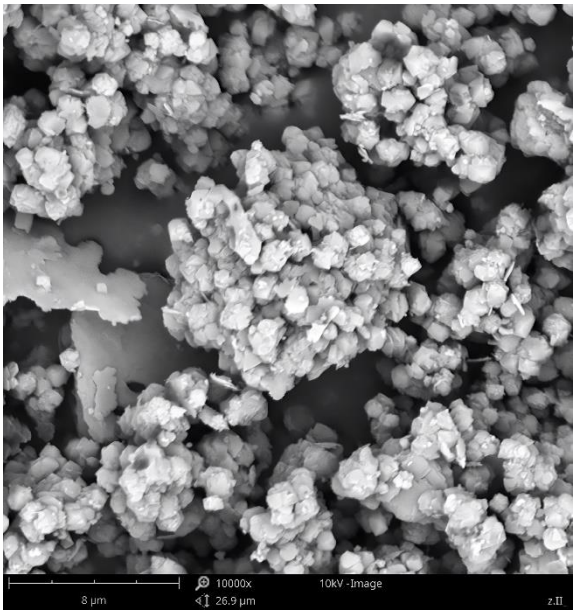
10000x
10kV -Image
8 µm
26.9 µm
z.II

c)

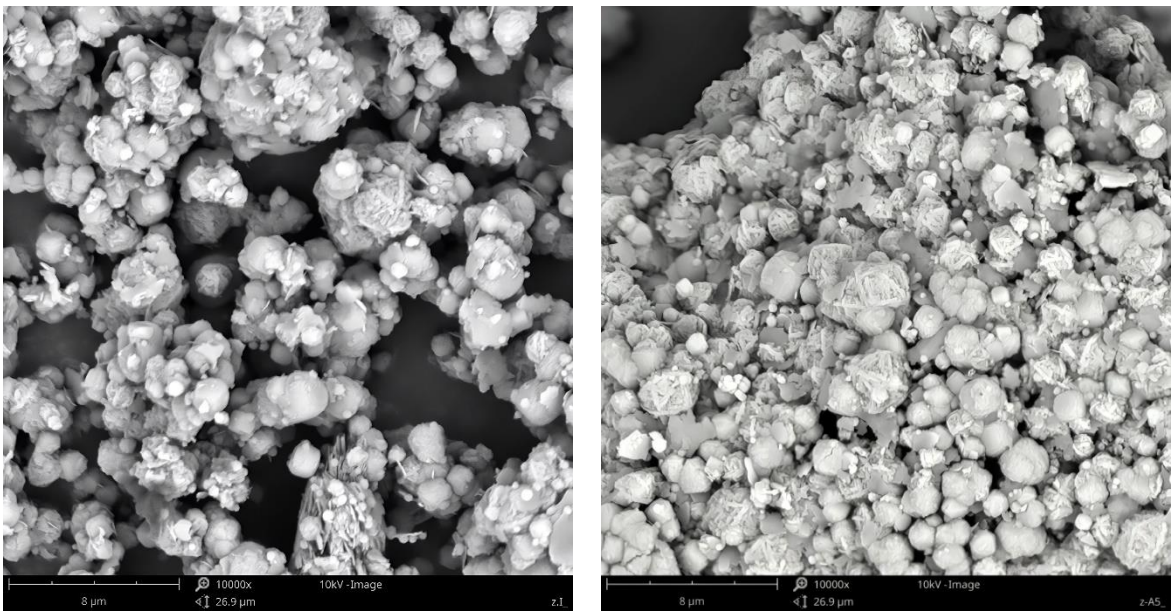

d) e)

Figure 4-3. SEM images of a) raw kaolin, b) 4A-I, c) 4A-II, d) 4A-III samples synthesizes by fusion/hydrothermal method e) 5A-III zeolite synthesized by ion-exchanging 4A-III. mag. 10000×.

4.1.4 SEM images of kaolin and 4A zeolites synthesized from Angren kaolin via hydrothermal method

SEM images of the kaolin and zeolites synthesized from Angren kaolin via hydrothermal method are presented in Figure 4-4. Kaolin is composed of morphological assemblage of laminar or platelet shapes (Figure 4-4.a). It can be seen from the SEM images that, the crystal shapes of the samples transformed from platelet shapes to cubic shapes (Figure 4-4. b-d).

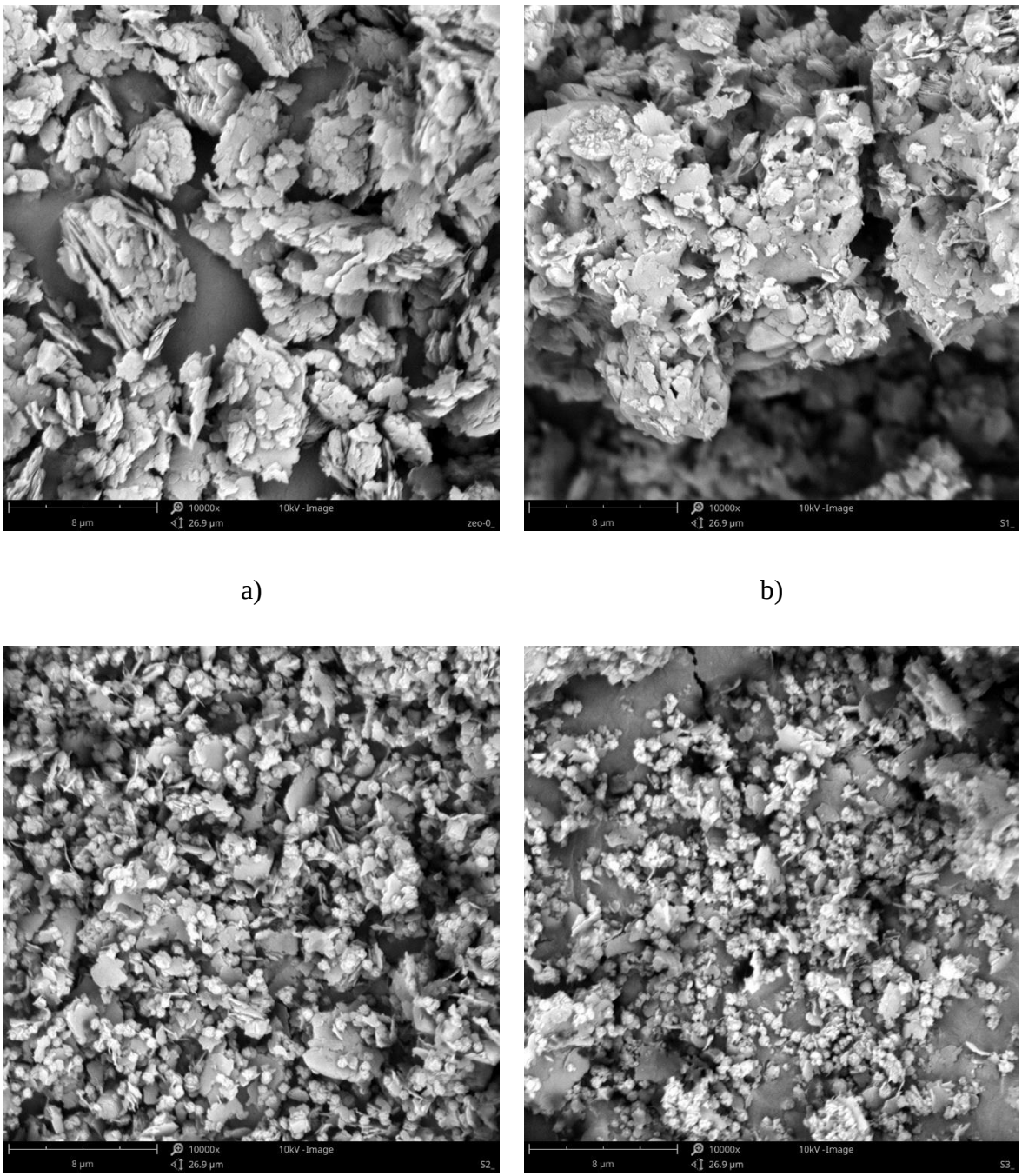

a) b)

c) d)

Figure 4-4. SEM images of a) metakaolin, b) S1, c) S2, d) S3 samples synthesized by hydrothermal method. mag. 10000×.

Figure 4-5 displays SEM images of the samples synthesized within a crystallization time range of 8-12 hours. The images illustrate that the cubic crystal structure of the zeolites yielded higher results in comparison to samples synthesized with varying concentrations of NaOH (Figure 4-4). Particularly, Figure 4-5.c provides visual evidence of this.

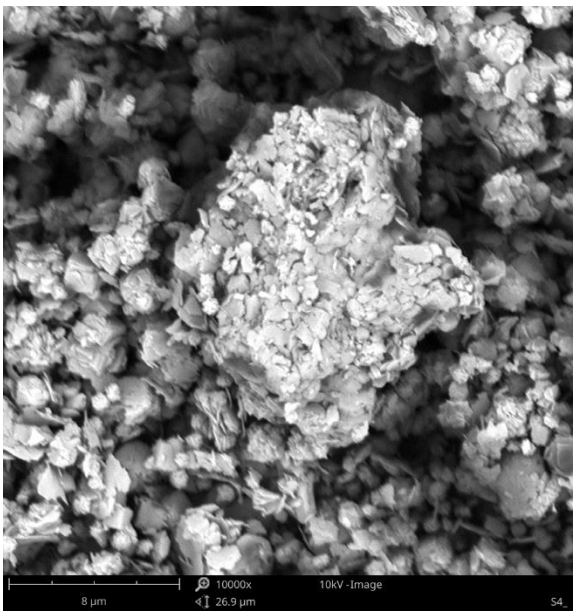

a)

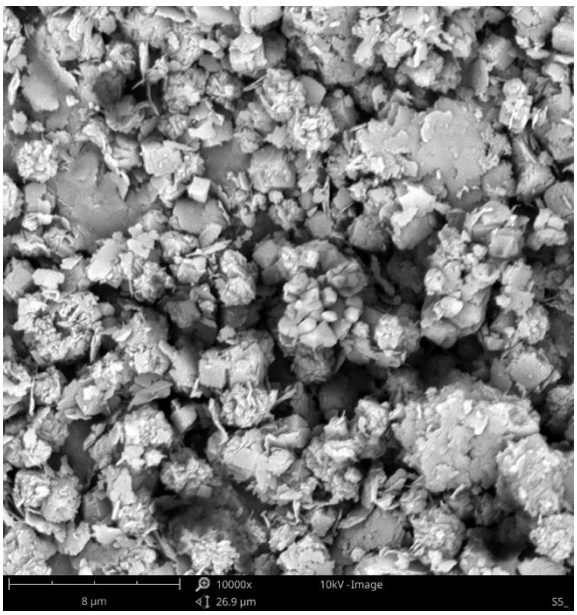

b)

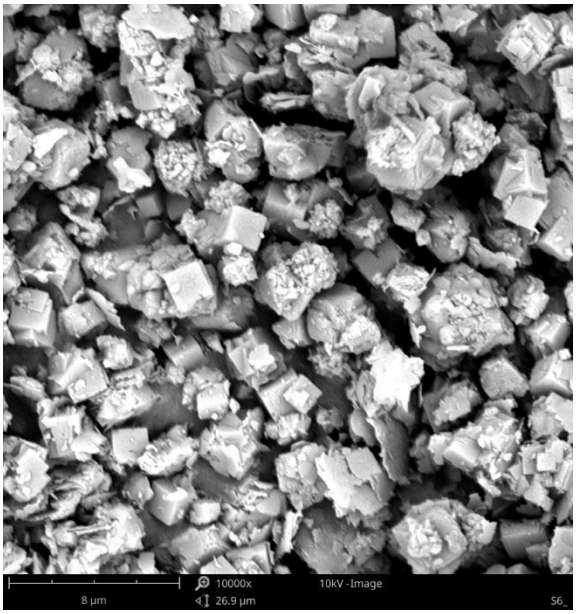

d)

Figure 4-5. SEM images of a) S4, b) S5 and d) S6 zeolites synthesized by hydrothermal method. mag. 10000×.

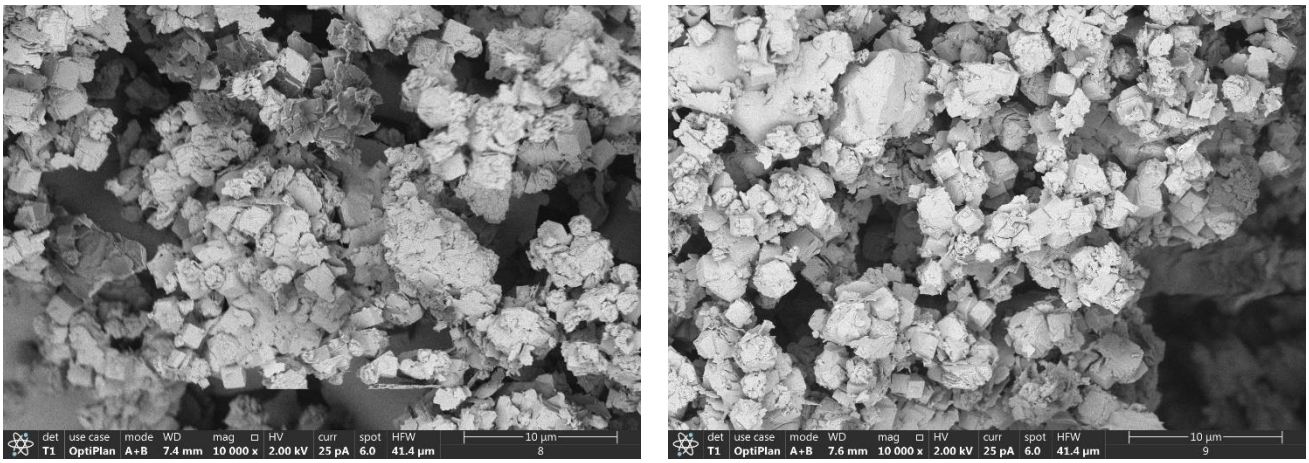

a) b)

Figure 4-6. SEM images of a) S8 and b) S9 zeolites synthesized by hydrothermal method. mag. 10000×.

4.1.5 SEM images of 5A and its modification by silver nanowires.

Figure 4-7 illustrates the SEM images of 5A and 5ANWs samples. The LTA 5A zeolite framework is composed of four rings connecting sodalite structures [19]. The SEM examination verified that both the modified and unmodified 5A silver nanowires are composed of cubic crystallites with exceptional definition.

Compositional characterization of the samples was done by energy dispersive X-ray spectroscopy (EDS) during SEM image acquisition. The element content in the samples was shown in Table 1. The weight concentration of silver in 5ANWs confirmed that impregnation was carried out partly.

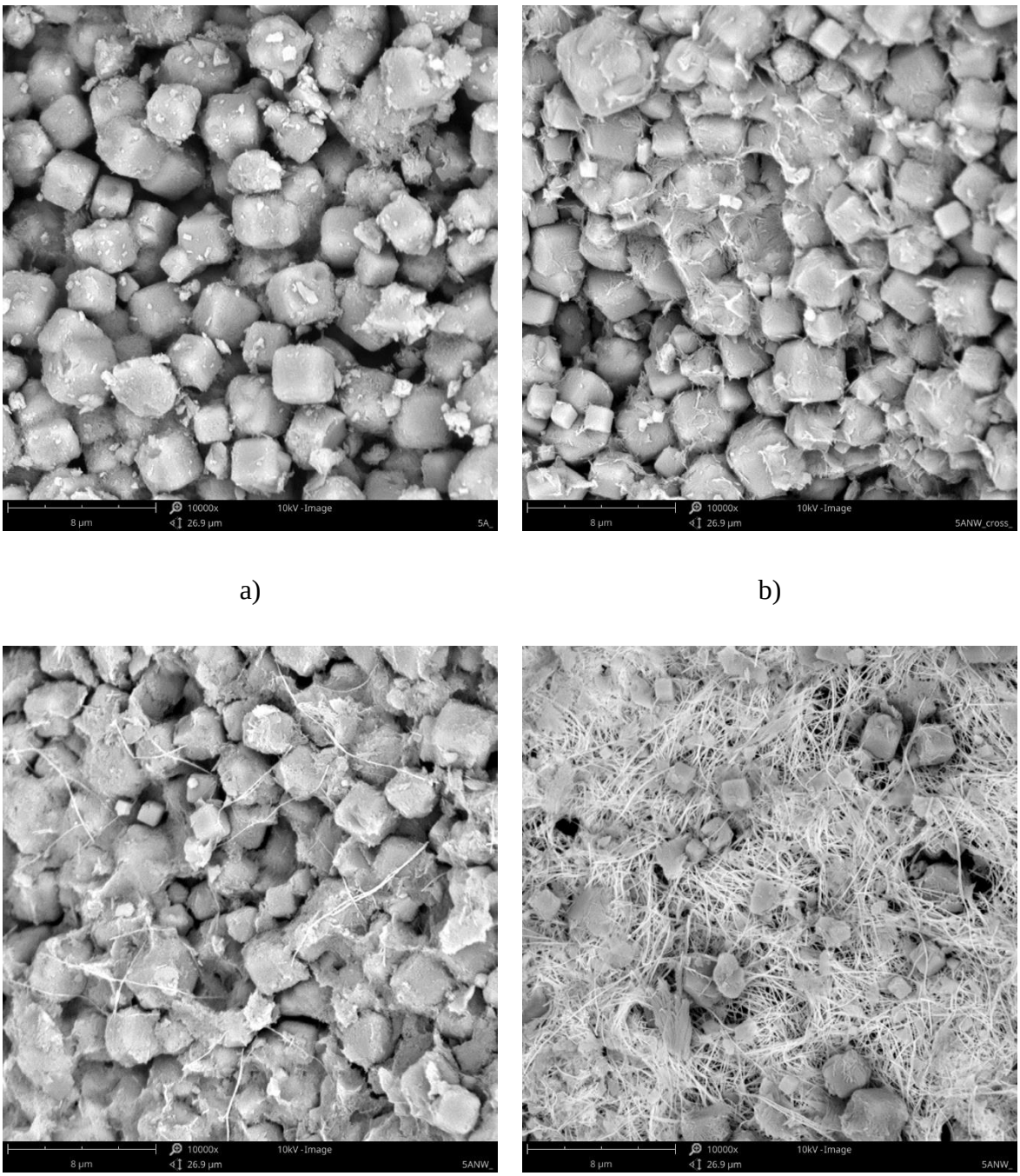

a) b)

c) d)

Figure 4-7 SEM images of (a) 5A zeolite; b-d) 5ANWs. mag. 10000×.

4.2 EDS SPECTRA

4.2.1 13X and silver modified 13X zeolites

Compositional characterization of the samples was done by energy dispersive X-ray spectroscopy (EDS) during SEM image acquisition. At least 3 spots on the surface of the zeolites were analysed to get accurate results. Average elemental content

was provided. For better results, some elements were disabled during the compositional analysis. The element content in the samples and their EDS spectra were shown in Table 4-1 and in Figure 6-1 (Appendix C), respectively. It can be seen that the high weight concentration of silver in AgI-13X (10.24 wt. %), AgII-13X (21.38 wt. %) and AgIII-13X (32.38 wt. %).

Table 4-1. The element content in 13X, AgI-13X, AgII-13X, and AgIII-13X was determined by the EDS analysis.

Element	**Elemental Composition in wt.%**			
	13X	**AgI-13X**	**AgII-13X**	**AgIII-13X**
O	55.81	51.83	46.80	39.24
Si	21.20	18.93	16.20	14.31
Al	15.74	12.27	9.40	11.13
Na	6.89	5.79	2.38	2.07
Mg	0.35	0.94	1.55	0.43
Ag	-	10.24	21.32	32.38
Σ	99.99	100	97.65	99.56

4.2.2 Commercial 4A and 5A

In order to compare synthesized zeolites, commercial 4A and 5A molecular sieves were characterized. Their elemental analysis was determined. EDS spectra of commercial 4A and 5A was given in Figure 6-2 (Appendix C).

Table 4-2. The element content in commercial 4A and 5A

Element	**Elemental Composition in wt.%**	
	4A	**5A**
O	56.65	55.28
Si	15.55	16.77
Al	13.70	14.49
Na	11.55	1.91
Mg	0.95	3.26
Fe	1.60	-
Ca	-	8.28
	100	99.99

4.2.3 Kaolin, 4A and 5 A zeolites synthesized from Angren kaolin via fusion/hydrothermal method

The elemental composition of kaolin, 4A-I, 4A-II, 4A-III and 5A-III along with their EDS spectra are presented in Table 4-3 and Figure 6-3 (Appendix C). It is evident that the Na content increases in 4A-I, 4A-II, and 4A-III as the NaOH concentration rises. The presence of Ca in 5A-III indicates that ion exchange was effectively performed.

Table 4-3. The element content in raw kaolin, 4A-I, 4A-II, 4A-III and 5A-III samples

Element	Elemental Composition in wt.%				
	Raw kaolin	4A-I	4A-II	4A-III	5A-III
O	59.342	53.505	52.38	52.52	62.04
Si	18.402	20.26	21.53	20.62	16.47
Al	16.096	16.78	16.965	16.36	13.61
K	0.75	-	0.195	-	-
Mg	0.44	-	-	-	-
P	0.37	-	-	-	-
Na	-	8.2775	8.93	10.49	0.76
Ca	-	-	-	-	7.10
	99.99	100	98.82	99.56	99.98

4.2.4 4A zeolites synthesized via hydrothermal method

The synthesis of 4A zeolite samples was carried out under three different settings, each with unique characteristics. The EDS spectra and elemental compositions of the samples are compared and shown in separate figures and tables. EDS spectra and element composition of S1, S2 and S3 were given in Figure 6-4 (Appendix C) and Table 4-4.

Table 4-4. The element content in S1, S2 and S3 samples

Element	Elemental Composition in wt.%		
	S1	S2	S3
O	59.342	52.52	53.505
Si	18.402	20.62	18.26
Al	16.096	16.36	14.78
K	0.75	-	-
Mg	0.44	-	-
P	0.37	-	-
Na	-	10.49	8.2775
C	-		5.175
Ca	-	-	-
	99.99	100	97.65

EDS spectra and element composition of S4, S5 and S6 were given in Figure 6-5 (Appendix C) and Table 4-5.

Table 4-5. The element content in S4, S5 and S6 samples

Element	Elemental Composition in wt.%		
	S4	S5	S6
C	6.447	7.693	7.433
O	46.570	45.109	45.460
Na	7.604	8.522	8.423
Al	15.203	14.568	14.443
Si	22.298	22.356	22.267
K	0.855	0.838	0.734
Ti	0.292	0.838	0.838
Fe	0.731	0.646	0.402
	100	100	100

EDS spectra and element composition of S8 and S9 were given in Figure 6-6 (Appendix C) and Table 4-6.

Table 4-6. The element content in S8 and S9 samples

Element	Elemental Composition in wt.%	
	S8	**S9**
C	8.334	5.637
O	45.097	43.353
Na	8.689	9.977
Al	13.164	15.247
Si	23.944	23.611
K	0.691	0.959
Ti	-	-
Fe	-	0.911
Mg	0.080	-
	100	100

4.2.5 5A and 5ANWs

It is clear that silver nanowires may be deposited on the surface of zeolite. Even though no ion exchange occurs, analysing the elemental content by averaging the concentrations at different spots can provide an estimate of the silver nanowires' content on the zeolite. Figure 6-7 (Appendix C) shows the EDS spectra of 5A and 5ANWs.

Table 4-7 The element content in 5A and 5ANWs

Element	Elemental Composition in wt.%			
	5A		**5ANWs**	
	Atomic conc.	**Weight conc.**	**Atomic conc.**	**Weight conc.**
O	70.638	56.972	73.697	68.326
Si	11.736	16.512	6.57	10.41
Al	10.484	14.192	5.21	8.07
Ca	4.15	8.288	1.97	4.566
Ag	-	-	9.998	5.46
Mg	1.6075	1.945	1.73	1.89
Na	1.558	1.812	0.80	1.267
Σ	100.1735	99.721	99.975	99.989

4.3 XRD SPECTRA

4.3.1 XRD spectra of 13X and silver-modified 13X

The XRD patterns corresponding to 13X and AgI-13X, AgII-13X were presented in Figure 4-8. The samples feature significant crystallinity, as shown by the strength and broadening of the XRD peaks. The investigated samples showed mainly a crystalline phase composed of sodium aluminium silicate ($Na_{14}Al_{14}Si_{34}O_{96}$) according to the PDF card no. 04-010-5065. The main diffraction peaks at 2 θ = 6.1, 10.0, 11.9, 15.2, 18.3, 20.11 23.2, 26.9, 31.0 are characteristic of the Faujasite structure (JCPDS No: 12-0228) [119]. Between 5° and 15° of 2Theta the characteristic bump

was identified characteristic for the amorphous phase. In this part, some of the Ag-based compounds could be identified, however not in the crystalline phase.

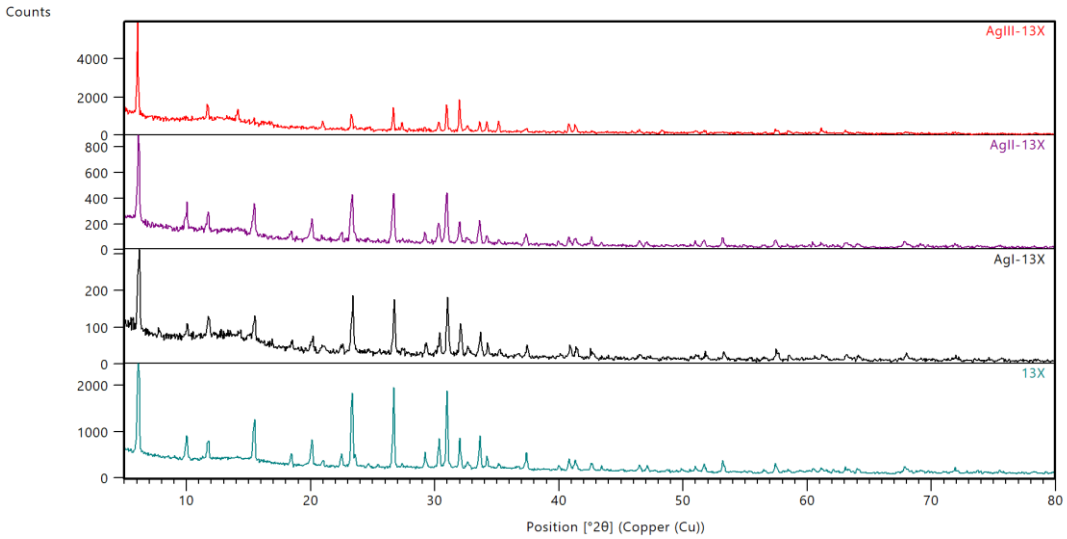

Figure 4-8. XRD pattern registered for the 13X, AgI-13X and AgII-13X samples.

4.3.2 XRD spectra of commercial 4A and 5A

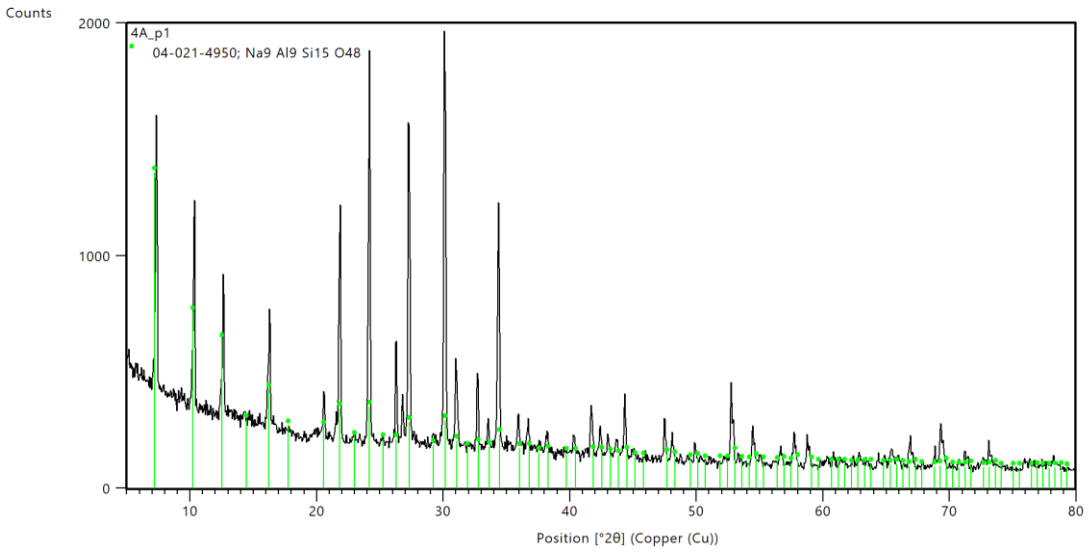

a)

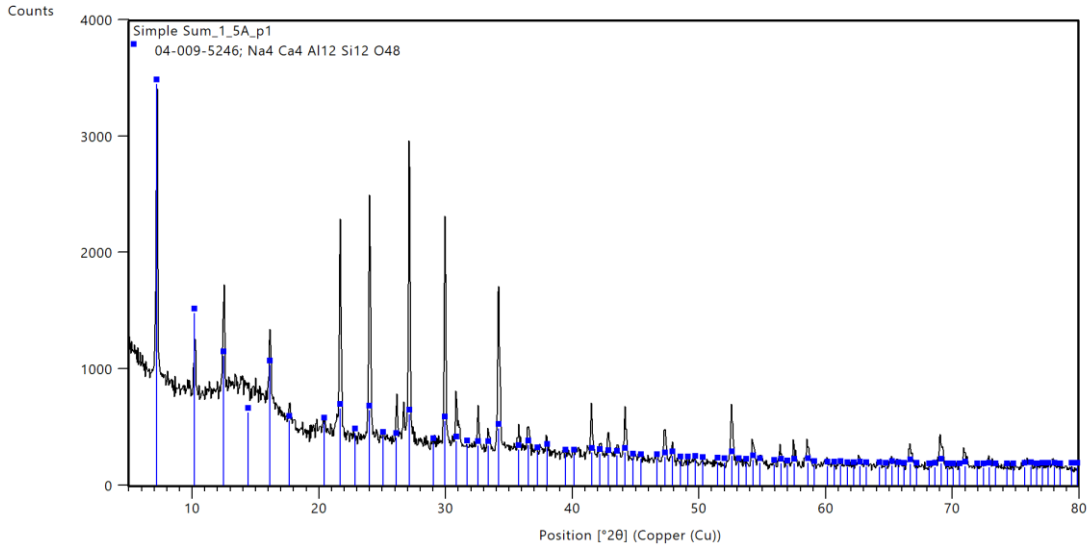

b)

Figure 4-9. XRD pattern registered for commercial a) 4A and b) 5A.

4.3.3 XRD spectra of zeolites synthesized from Angren kaolin via fusion/hydrothermal method

The XRD patterns corresponding to 4A-I, 4A-II, 4A-III and 5A-III were illustrated in Figure 4-9. The samples feature significant crystallinity, as shown by the strength and broadening of the XRD peaks. 4A-I, 4A-II, 4A-III zeolites synthesized from Angren kaolin via fusion/hydrothermal method. 5A-III was synthesized from 4A-III by ion exchange.

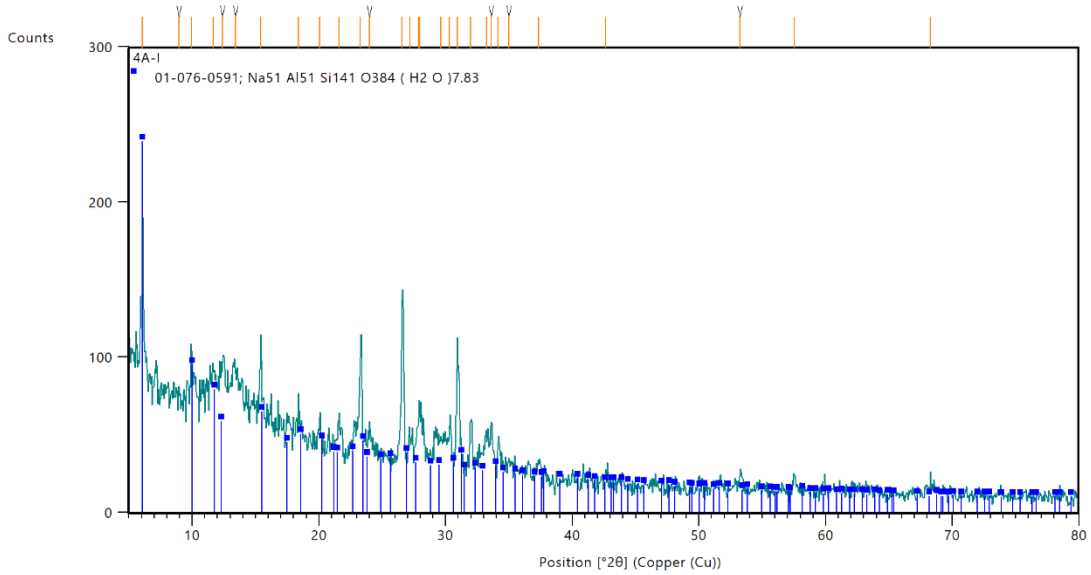

a)

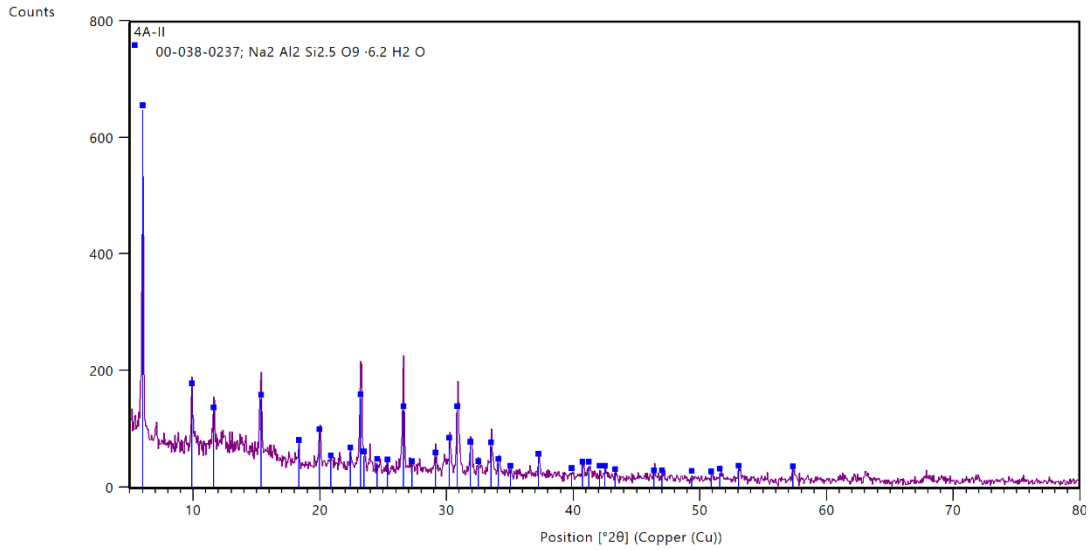
Counts
4A-II
00-038-0237; Na2 Al2 Si2.5 O9 ·6.2 H2 O
800
600
400
200
0
10
20
30
40
50
60
70
80
Position [°2θ] (Copper (Cu))

b)

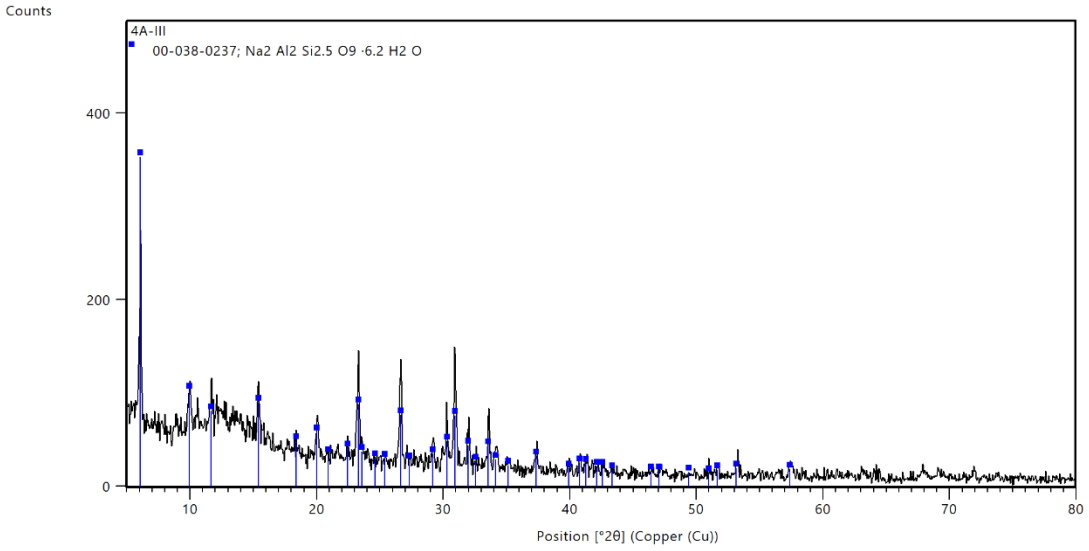
Counts
4A-III
00-038-0237; Na2 Al2 Si2.5 O9 ·6.2 H2 O
400
200
0
10
20
30
40
50
60
70
80
Position [°2θ] (Copper (Cu))

c)

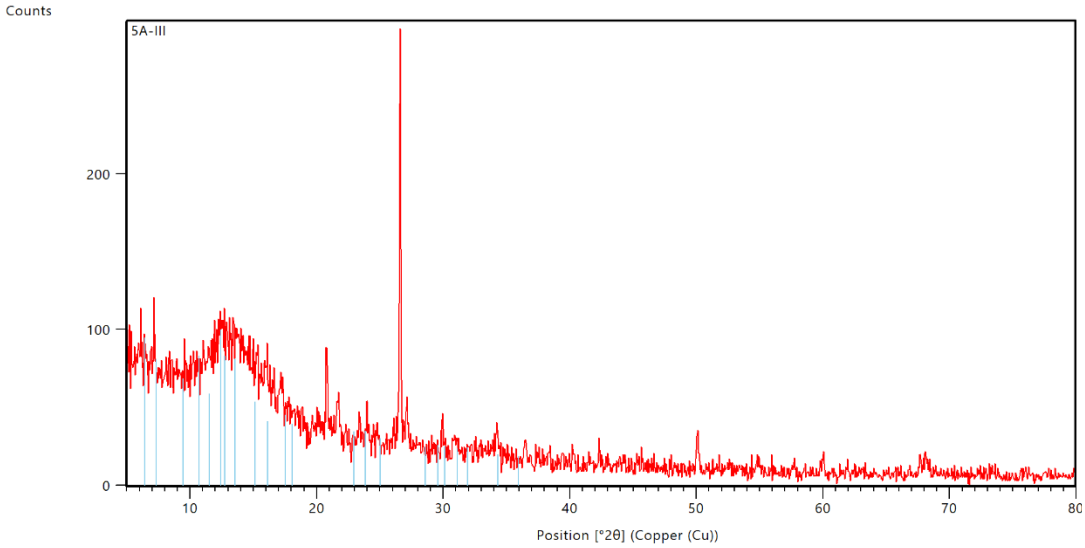

d)

Figure 4-10. XRD pattern registered for synthesized from Angren Kaolin via fusion/hydrothermal method a) 4A-I, b) 4A-II, c) 4A-III and d) 5A-III samples

4.3.4 XRD spectra of 4A and 5 A zeolites synthesized from Angren kaolin via hydrothermal method

In order to compare the samples XRD patterns were presented in one graph for the same methods. Figure 4-11 shows the XRD patterns for samples S1, S2, and S3. All samples display very similar XRD patterns, with the main diffraction peaks observed at 2θ = 7.18, 10.17, 12.46, 14.03, 20.83, and 26.6 for S1, S2, and S3.

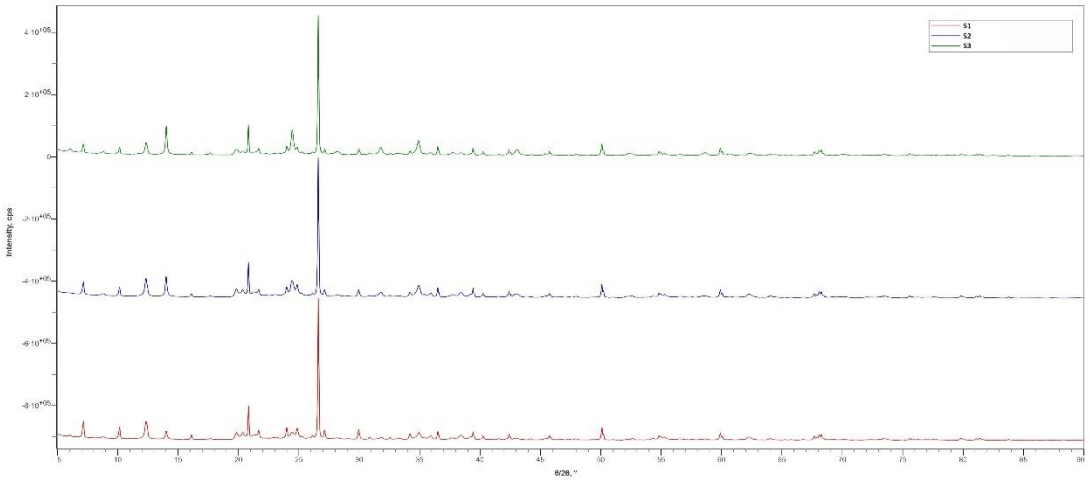

Figure 4-11. XRD pattern registered for synthesized S1, S2 and S3 samples

Figure 4-12 displays the X-ray diffraction (XRD) patterns of the S4 and S5 samples. The patterns show an increase in intensities, with the main diffraction peaks for S4 and S5 being the same and observed at 2θ = 6.1, 7.18, 10.16, 12.33, 20.83, 26.6.

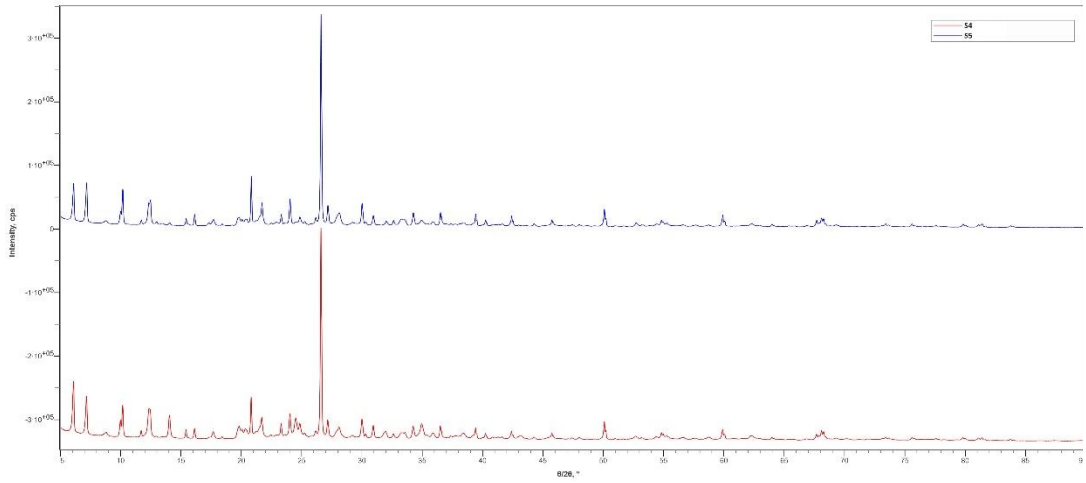

Figure 4-12. XRD pattern registered for synthesized S4 and S5 samples

The XRD patterns of the S7, S8 and S9 are given in Figure 4-13. The synthesized samples show reflections located at 2θ = 7.18, 10.14, 12.45, 20.83, 21.65, 23.98, 26.6, 29.94 and 34.18. These samples exhibit several XRD peaks with great intensity, unlike other specimens. The S7, S8, and S9 samples, which underwent extended crystallization time, demonstrated a significant increase in crystallinity.

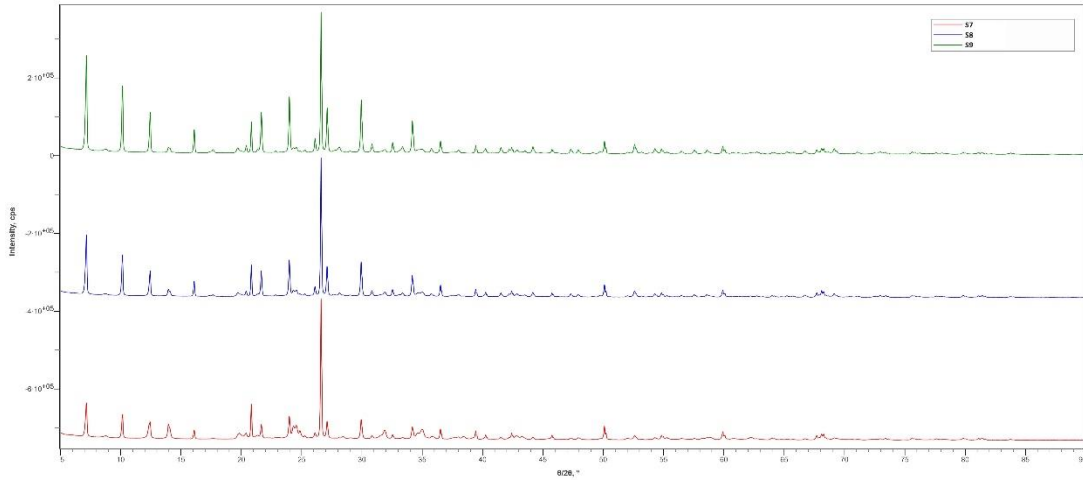

Figure 4-13. XRD pattern registered for synthesized S7, S8 and S9 samples

4.4 XRF RESULTS

XRF analysis was conducted solely on 4A samples that were synthesised using the hydrothermal technique. Table 4-8 provides the XRF analysis results for the samples.

Table 4-8. XRF analysis of 4A samples synthesized via hydrothermal method

Component	Weight percent							
	S1	**S2**	**S3**	**S4**	**S5**	**S7**	**S8**	**S9**
SiO_2	54.9	52.8	54.6	50.8	51.9	51.5	49.5	48.1
Al_2O_3	27.8	28.7	26.1	28.8	27.4	27.5	26.4	27.2
Na_2O	9.5	11.4	13.5	13.4	14.4	14.2	16.2	17.0
K_2O	0.784	0.827	0.768	0.801	0.755	0.720	0.648	0.668
Fe_2O_3	0.659	0.689	0.666	0.675	0.656	0.639	0.583	0.628
TiO_2	0.478	0.451	0.477	0.438	0.445	0.437	0.435	0.439
CaO	0.211	0.194	0.179	0.208	0.2	0.212	0.199	0.196
MgO	0.159	0.18	0.159	0.152	0.181	0.169	0.157	0.164

4.5 BET SURFACE AREA

4.5.1 BET surface area of 13X and silver-modified 13X

The specific surface area was determined by low-temperature nitrogen adsorption (ASAP 2020, Micromeritics Inc., Norcross, GA, USA) using the Brunauer–Emmett–Teller equation [122]. Prior to taking the nitrogen adsorption measurements, each selected sample was outgassed for 24 h at 350 °C. The BET surface area of the samples is given in Table 2.

Table 4-9. BET surface area of the samples.

Adsorbents	BET surface area (m2/g)
13X	501.33
AgI-13X	436
AgII-13X	416
AgIII-13X	405

4.5.1 BET surface area of commercial 4A and 5A

The same procedure was applied to determine surface are of 4A and 5A. The BET surface area of the samples is provided in the Table 4-10 below.

Table 4-10. BET surface area of the 4A and 5A.

Adsorbents	BET surface area (m^2/g)
4A	12.6
5A	392

4.5.1 BET surface area of 4A-III and 5A-III

The BET surface areas of 4A-III and 5A-III were measured for comparison with commercial 4A and 5A. The BET surface area values of the samples are presented in the Table 4-11 below.

Table 4-11. BET surface area of the 4A-III and 5A-III.

Adsorbents	BET surface area (m^2/g)
4A-III	233.0248
5A-III	302.7657

4.6 ADSORPTION ISOTHERMS

4.6.1 Adsorption isotherms

The Langmuir and Freundlich adsorption models were applied to assess adsorption parameters and to investigate adsorption mechanisms at ambient temperature. The Langmuir model describes monolayer adsorption of adsorbate onto homogenous solid surface sites, while the Freundlich model does not have a maximum adsorption limit.

Two adsorption models were implemented for the 13X and silver modified 13X zeolites. Due to its high adsorption capacity, the adsorption isotherm parameters of AgII-13X for the Langmuir and Freundlich models were provided in Table 4-12.

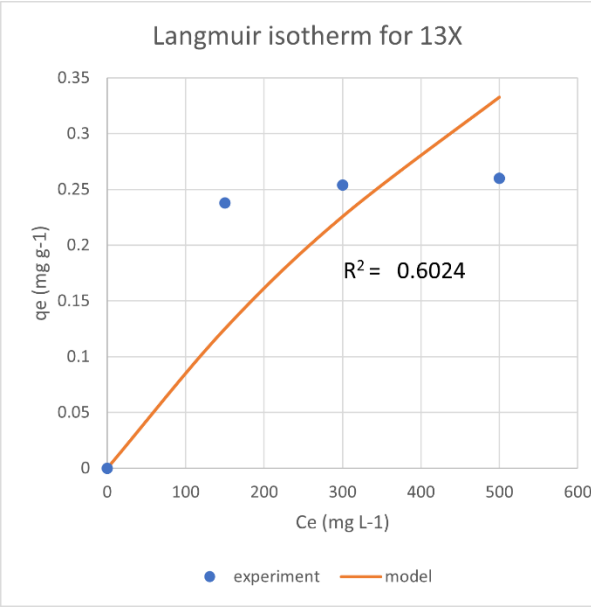

a)

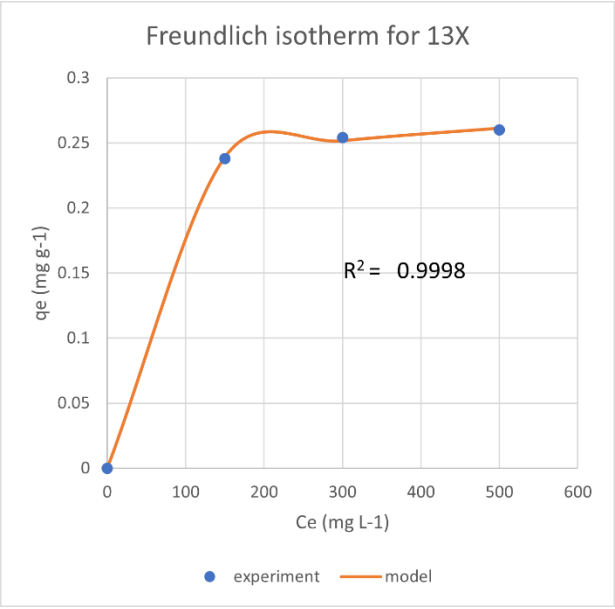

b)

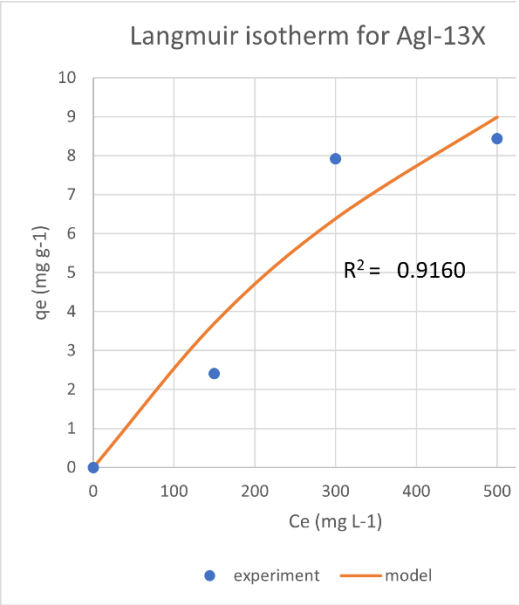
Langmuir isotherm for AgI-13X
qe (mg g-1)
Ce (mg L-1)
R² = 0.9160
experiment
model

c)

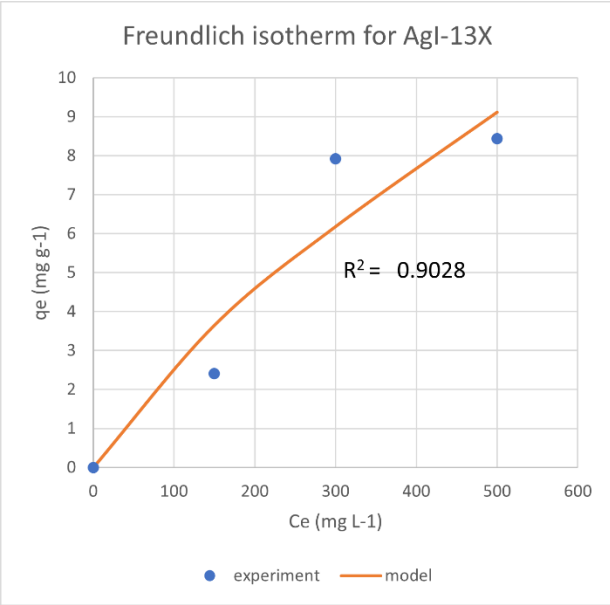
Freundlich isotherm for AgI-13X
qe (mg g-1)
Ce (mg L-1)
R² = 0.9028
experiment
model

d)

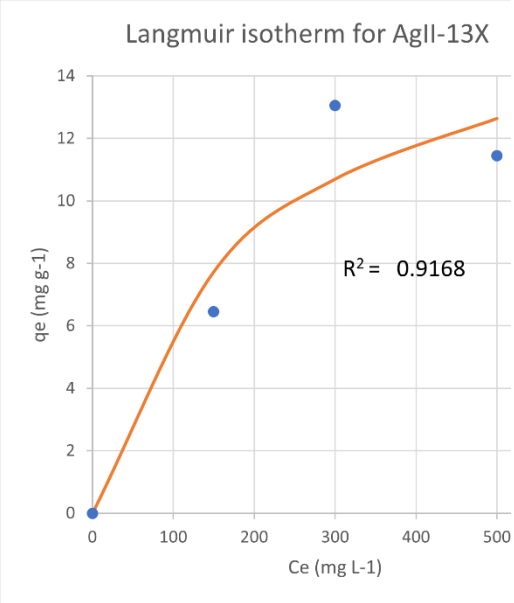
Langmuir isotherm for AgII-13X
qe (mg g-1)
Ce (mg L-1)
R² = 0.9168

e)

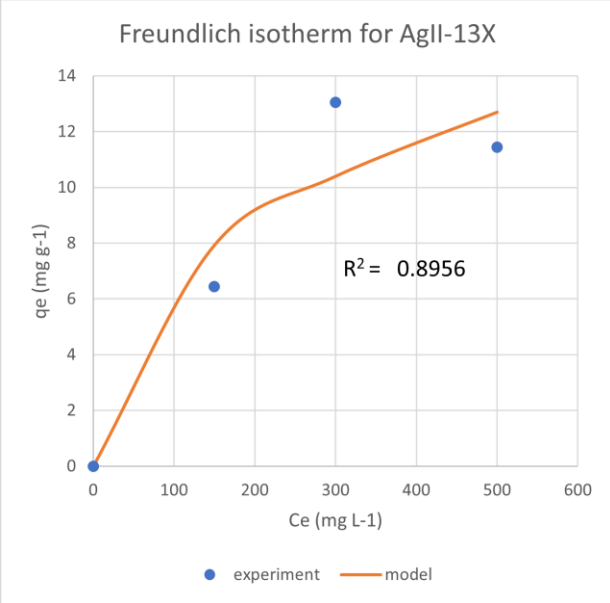
Freundlich isotherm for AgII-13X
qe (mg g-1)
Ce (mg L-1)
R² = 0.8956
experiment
model

f)

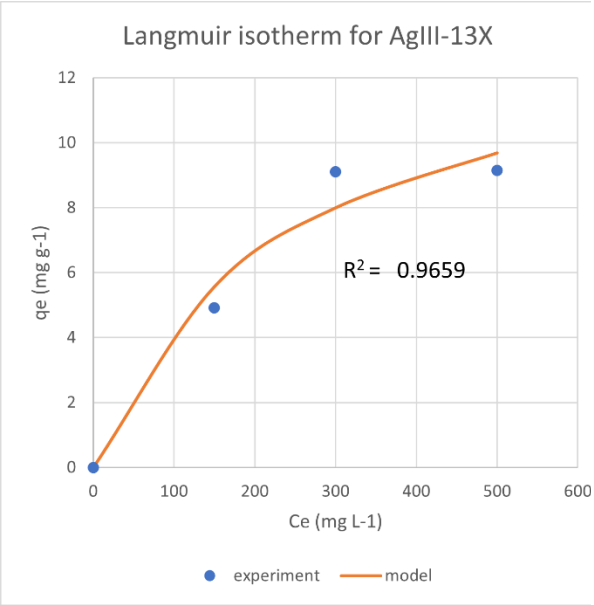

g)

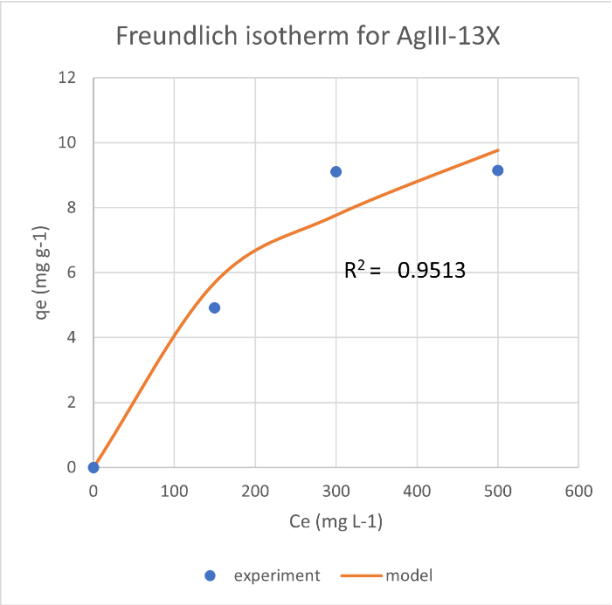

h)

Figure 4-14. Langmuir and Freundlich adsorption isotherm models at ambient temperature for 13X and silver modified 13X

Table 4-12. Adsorption isotherm parameters for AgII-13X.

Langmuir	**Value**	**Freundlich**	**Value**
K_L (μM^{-1})	0.002229	K_F (mmol m^{-2} μM^{-1}/n)	0.347795
R^2 (C_e vs. q_e)	0.9168	R^2 (C_e vs. q_e)	0.8956
qmax (mg g^{-1})	29.42685	n	1.632228

4.7 H_2S REMOVAL FROM NITROGEN

Commercial 5A, 13X and silver modified 13X zeolites were used in the adsorption of H_2S from nitrogen. Results of adsorption experiments were given below.

Commercial 5A zeolite

First, experiments were operated with the 15g and 20 g of commercial 5A to investigate impact of the operation parameters. The breakthrough curve of H_2S adsorption is displayed in Figure 4-15. The recorded breakthrough point, which is the moment when the output H_2S concentration reached 1 ppm, was provided for both runs in Table 4-13.

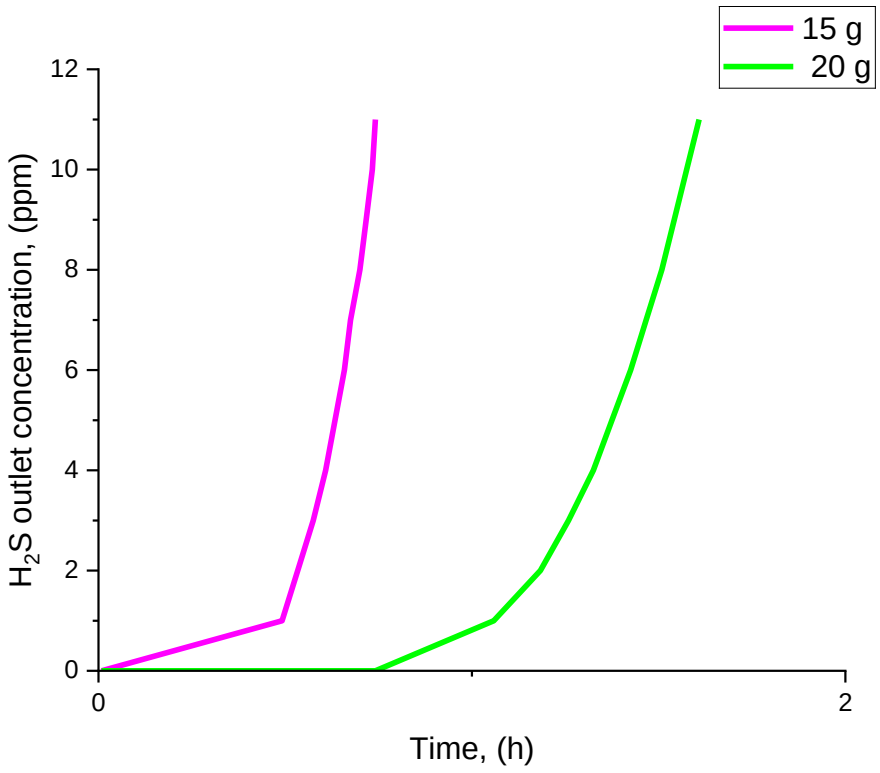

Figure 4-15. Comparison of breakthrough experiments of H_2S using 15g and 20g of 5A

Table 4-13. Breakthrough times for 5A

Adsorbents	**Breakthrough Time (h)**	
	15g	**20 g**
5A	0.49167	1.0583

Commercial 13X zeolite

Subsequently, adsorption experiments were conducted using 15 grams of commercial 13X, with flow rates of 20 and 30 l/h and H_2S concentration of 100 ppm to examine the influence of the flow rate. The Figure 4-16 shows the comparison of breakthrough curves for H_2S adsorption at different flow rates. Table 4-14 displays the breakthrough points at different flow rates.

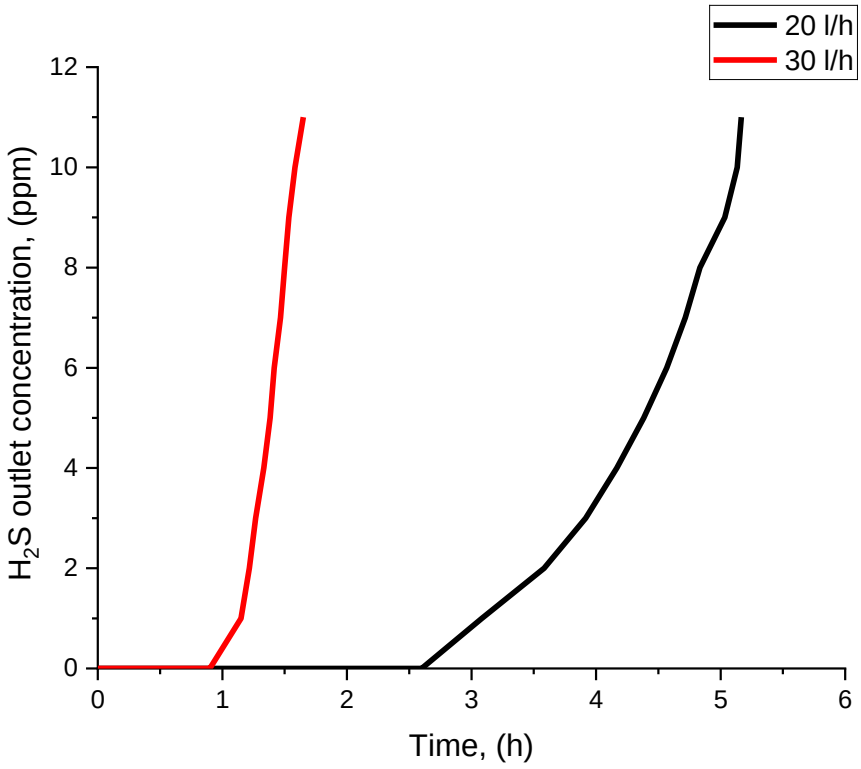

Figure 4-16. Comparison of H_2S breakthrough curves using 13X at various flow rates

Table 4-14. Breakthrough times for 13X

Adsorbents	Breakthrough Time (h)	
	20 l/h	30l/h
13X	3.083	1.15

Ag-13X zeolite

To assess the adsorption capabilities of Ag-13X compared to the non-modified version, experiments were conducted under identical conditions. The flow rate was set 20 l/h, and 10 grams of each material was used in the adsorption process. Inlet concentration of H_2S is 100 ppm. Comparison of H_2S breakthrough and recorded breakthrough points on 13X and Ag-13X were presented in Figure 4-17 and Table 4-15.

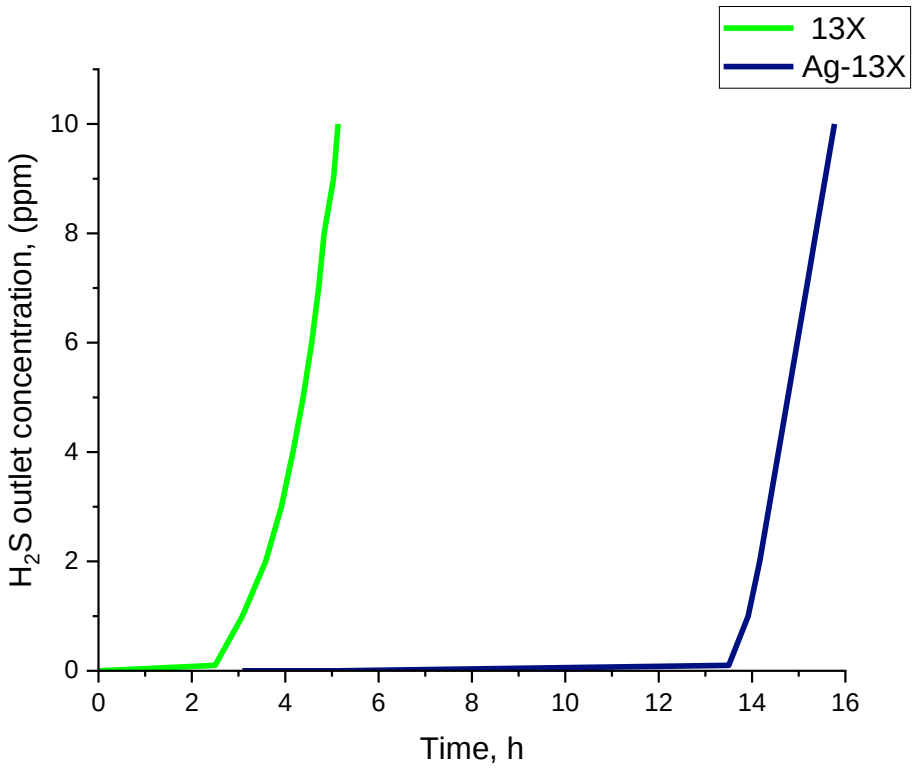

Figure 4-17. Comparison of H_2S breakthrough experiments on 13X and Ag-13X

Table 4-15. Breakthrough times for 13X and Ag-13X

Adsorbents	Breakthrough Time (h)
13X	3.083
Ag-13X	13.9167

4.8 H_2S REMOVAL FROM METHANE

Given that methane is the primary component, studying real natural gas yields accurate findings. Therefore, in this instance, adsorption tests will be conducted using actual natural gas with different amounts of H_2S at the input.

Commercial 13X and silver modified 13X zeolites

The H_2S removal from methane was conducted by varying the H_2S inlet concentration and the ion exchange rate of silver in 13X zeolite, in contrast to previous investigations. The effects of inlet concentration were measured in samples with H_2S concentrations of 150 ppm, 300 ppm, and 500 ppm at ambient temperature. The breakthrough curves for 13X and modified zeolites are demonstrated in Figure 4-18.

The concentration of H_2S in the outlet stream was zero for a significant amount of time before it broke through. The experiments were stopped when the outlet

concentration reached 10% of the initial concentration, indicating an effective adsorption time [85]. Adsorption capacity of the 13X, AgI-13X, AgII-13X, and AgIII-13X was calculated from the experimental breakthrough times (Table 4-16) and is shown in Table 4-21. Breakthrough time was determined when the outlet concentration was 1 ppm. Increased inlet H_2S concentration resulted in earlier breakthrough times for all samples, as anticipated. The 13X molecular sieve exhibited the earliest breakthrough time over all concentration ranges (150–500).

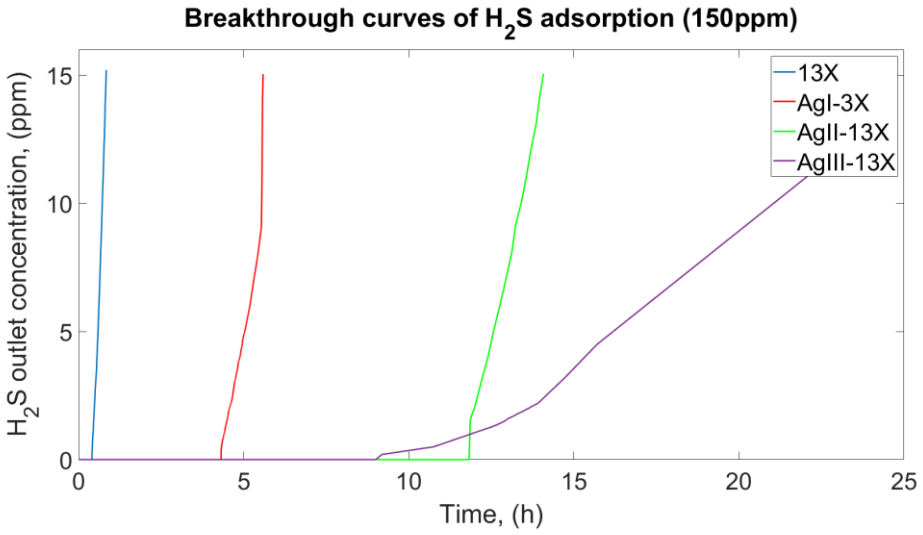

(**a**)

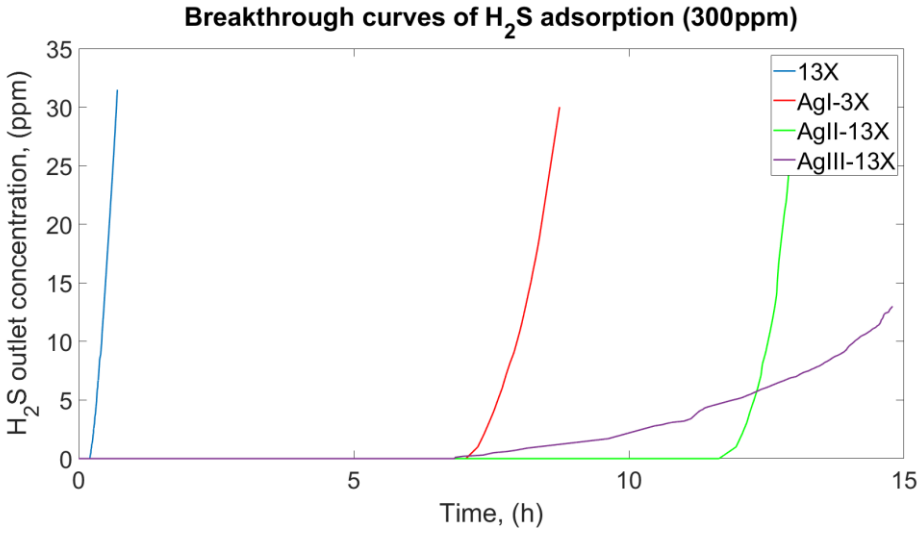

(**b**)

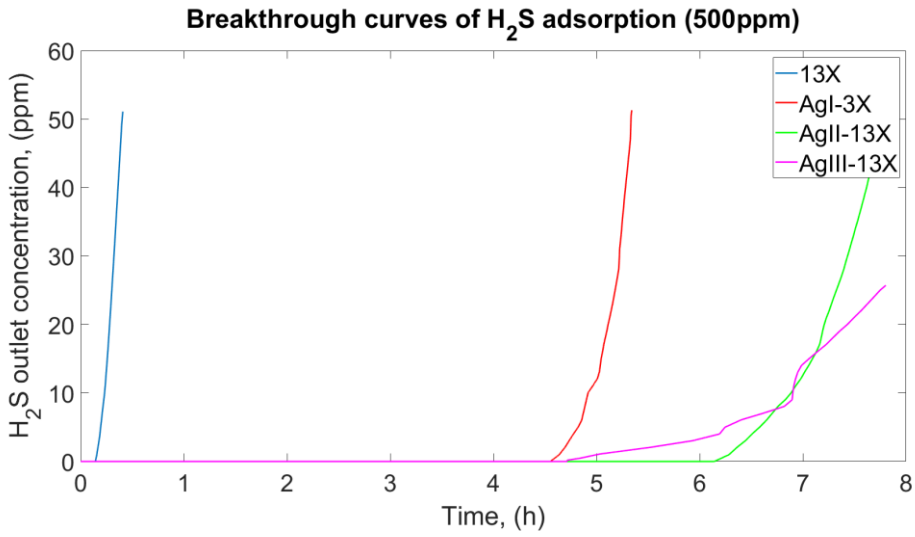

(**c**)

Figure 4-18. Breakthrough curves of zeolites in the range of (a) 150 ppm, (b) 300 ppm, and (c) 500 ppm H_2S in methane.

Table 4-16. Breakthrough times for the 13X, AgI-13X, AgII-13X, and AgIII-13X samples in the range of 150–500ppm.

Adsorbents	**Breakthrough Time (h)**		
	150 ppm	**300 ppm**	**500 ppm**
13X	0.435833	0.232778	0.1425
AgI-13X	4.403889	7.253611	4.638611
AgII-13X	11.84806	11.9475	6.284444
AgIII-13X	11.87917	8.338889	5.03

Silver nanowires modified 5A

A study was conducted to examine the impact of silver nanowires on the adsorption of H_2S from methane in 5A zeolites. The results were then compared to those obtained from non-modified 5A zeolites. The initial concentration of H_2S in the mixture was 150 ppm, with a flow rate of 24 l/h. Figure 4-19 and Table 4-17 display the breakthrough curve and breakthrough times for comparison.

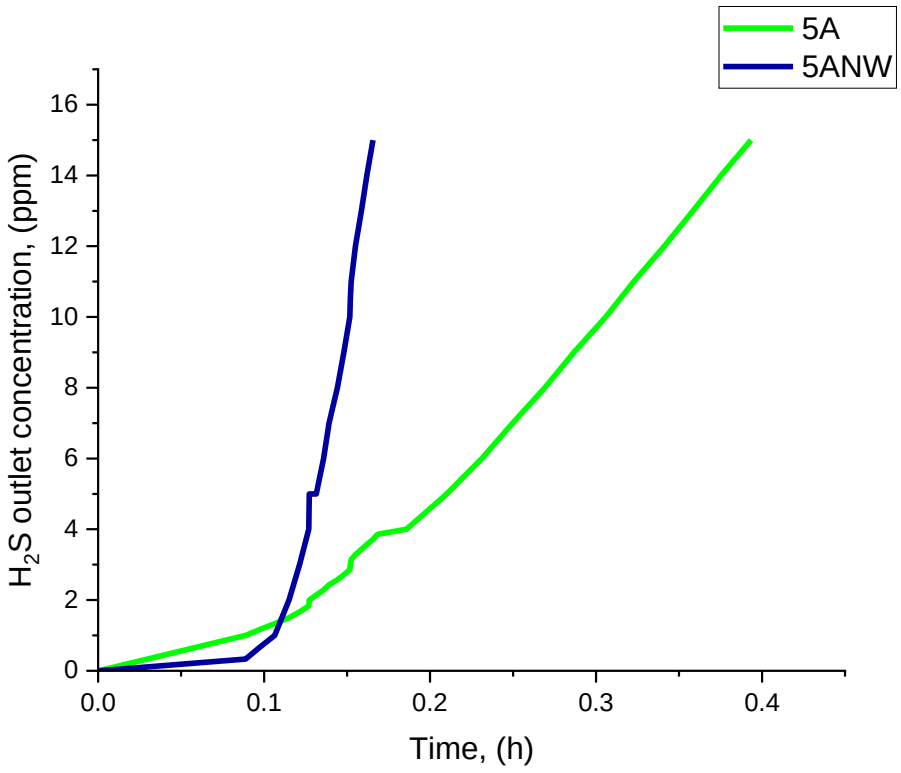

Figure 4-19. Comparison of H_2S breakthrough curves on 5A and 5ANWs

Table 4-17. Breakthrough times for 5A and 5ANWs

Adsorbents	Breakthrough Time (h)
5A	0.089
5ANWs	0.106

4A-III and 5A-III

A study was conducted on the adsorption of H_2S from methane to evaluate the performance of 4A-III and 5A-III. The obtained results were compared with those obtained from a commercial one. The initial concentration of H_2S in the mixture was 150 ppm, and the flow rate was set at 24 l/h. Figure 4-20 presents the breakthrough curves of commercial 4A, 5A, 4A-III and 5A-III for comparison.

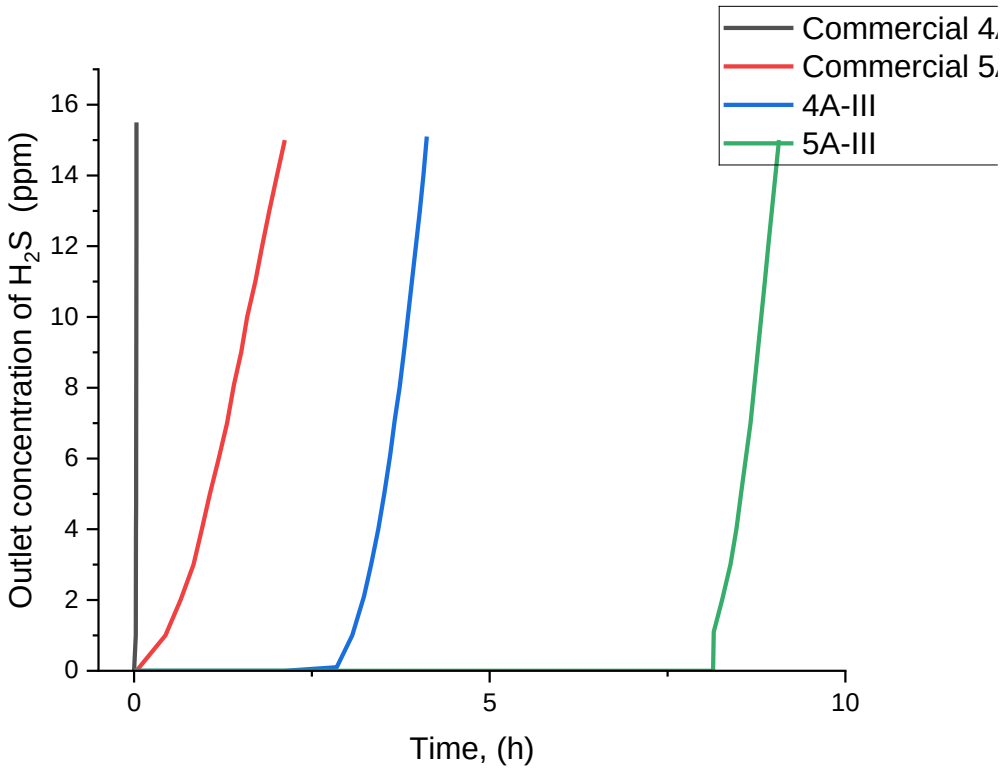

Figure 4-20. Comparison of H_2S breakthrough curves on commercial 4A, 5A, synthesized 4A-III, and 5A-III

Table 4-18. Breakthrough times for commercial 4A, 5A, synthesized 4A-III, and 5A-III

Adsorbents	Breakthrough Time (h)
Commercial 4A	0.023
4A-III	3.06
Commercial 5A	0.44167
5A-III	8.15

4.9 ADSORPTION CAPACITY

By calculating the adsorption capacity of the samples based on adsorption data, we may obtain evidence of the materials' effectiveness in removing H_2S. The adsorption capacity of the samples was measured according to Equation 3.1.

4.9.1 H_2S removal from nitrogen

The composition of inlet gas may affect on the adsorption performance of adsorbents. Hence, adsorption capacity of adsorbents was calculated for H_2S removal from both nitrogen and methane.

Adsorption capacity of commercial 5A

The adsorption capacity of commercia 5A was determined using the weight difference method, namely by comparing the weights of 15 g and 20 g samples. As previously said, it is crucial to observe the breakthrough point in order to calculate the adsorption capacity. The adsorption capacity of 5A is given in Table 4-19.

Table 4-19. Adsorption capacity of the 5A

Adsorbents	Effective Adsorption Capacity (mg/g)	
	15g	20 g
Commercial 5A	0.149	0.214

Adsorption capacity of 13X

In order to examine the impact of flow rate on the adsorption of H_2S using 13X, two different flow rates of 20 l/h (333.33 ml/min) and 30 l/h (500 ml/min) were utilized throughout the adsorption process. Inlet concentration of H_2S was 100 ppm. The adsorption capacity of 13X under different flow rates is presented in Table 4-20.

Table 4-20. Adsorption capacity of the 13X at various flow rates

Adsorbents	Effective Adsorption Capacity (mg/g)	
	20 l/h	30 l/h
Commercial 13X	0.935	0.35

Adsorption capacity of 13X

Adsorption tests were conducted under identical operational settings to investigate the effectiveness of silver modification in removing H_2S from nitrogen. The adsorption capacities of both 13X and Ag-13X are presented in Table 4-21.

Table 4-21. Adsorption capacity of the 13X and Ag-13X

Adsorbents	Effective Adsorption Capacity (mg/g)
Commercial 13X	0.935
Ag-13X	4.22

4.9.2 H_2S removal from methane

Adsorption capacity of 13X and silver modified 13X

In the tables below, adsorption capacities of 13X and its silver modified ones are given.

Table 4-22. Adsorption capacity of the samples

Adsorbents	Effective Adsorption Capacity (mg/g)		
	150 ppm	300 ppm	500 ppm
13X	0.238	0.254	0.26
AgI-13X	2.405	7.92	8.44

AgII-13X	*6.47*	13.05	11.44
AgIII-13X	4.92	9.1	9.15

Adsorption capacity of 4A, 5A, 4A-III and 5A-III

Given that only the 4A-III and 5A-III samples exhibited strong characteristics of Linde type A, adsorption experiments were conducted for these samples, and their adsorption capacities are presented in Table 4-23.

Table 4-23. Adsorption capacity of commercial 4A, 5A, 4A-III and 5A-III

Adsorbents	Effective Adsorption Capacity (mg/g)
Commercial 4A	0.013
4A-III	1.674
Commercial 5A	0.0486
5A-III	4.45

Adsorption capacity synthesized 5A and 5ANWs

Table 4-24. Adsorption capacity of the samples

Adsorbents	Effective Adsorption Capacity (mg/g)
Commercial 5A	0.0486
5ANWs	0.0579

In order to assess the affinity of all the materials toward H_2S, the average adsorption capacity of each material was determined. The values obtained under identical conditions (adsorbent mass of 10 g, flow rate of 400 ml/min, and H_2S concentration of 150 ppm for methane adsorption and 100 ppm for nitrogen adsorption) are shown in Table 4-25 below.

Table 4-25. Adsorption capacity of the samples

Adsorbents	Effective Adsorption Capacity (mg/g)	
	Nitrogen	Methane
Commercial 5A	0.1215	0.24
Commercial 4A	-	0.013
Commercial 13X	0.6425	0.27
5ANWs	-	0.0579
4A-III	-	1.67
5A-III	-	4.45
Ag-13X	4.22	-
AgI-13X	-	6.255
AgII-13X	-	10.32
AgIII-13X	-	7.723333

Chapter 5: Discussion

Based on the prior discussion and literature, it can be concluded that the addition of silver to zeolites is an effective method for enhancing the adsorption properties of the zeolites to remove H_2S. In order to assess the adsorption performance of silver-modified 13X for H_2S, it is crucial to analyse the characterisation data of the samples. In addition, an analysis of the characterisation results of kaolin and zeolites synthesized from kaolin provides a comprehensive overview of the progress made in synthesizing zeolites from Angren kaolin.

The adsorption performance of various materials towards H_2S will be discussed based on experimental data. This study offers insights into the characteristics of zeolitic materials through the analysis of adsorption phenomena.

5.1 SEM ANALYSIS

5.1.1 13X and silver modified 13X

The morphology of the zeolite materials was studied using the SEM technique. The preparation and interpretation of morphological information from the images of a typical zeolite powder sample was straightforward and efficient. It can be seen from SEM images of silver-modified 13X, lattice destruction might happen during the ion-exchange or high temperature calcination (Figure 4-1). These observations are consistent with the findings of the XRD investigation. Additionally, it is evident that when the ion exchange rate increased in silver modified 13X, the number of minor additives in the surface morphology also increased. The smaller particles observed between the zeolite crystals can likely be attributed to the binder, made of clay, which is used to shape the crystals into beads.

5.1.2 Commercial 4A and 5A

The commercial 4A and 5A zeolites exhibited a larger number of well-formed cubic crystals, as shown in Figure 4-2, which is characteristic of Zeolite A. It is barely possible to observe the presence of amorphous material, which is potentially unreacted reagents.

5.1.3 Kaolin, 4A and 5A zeolites synthesized from Angren Kaolin via fusion/hydrothermal method

Increasing the ratio of kaolin to sodium hydroxide from 0.8 to 1.2 has resulted in a rise in the size of the cubic crystals and crystallinity. Figure 4-3, shows that the 4A-I sample has a little amount of cubic crystal among a high number of microscopic crystals, indicating that zeolite synthesis was not carried out effectively. However, it is evident that the size of the cubic crystals in 4A–II is increasing, suggesting that the additional NaOH contributed to the formation of more zeolite crystals (Figure 4-3.b). Using a high ratio of 1.2, 4A-III zeolite with a cubic crystalline structure was synthesized from kaolin (Figure 4-3.d). This is clearly shown in the SEM images (Figure 4-3.f). Therefore, to synthesize using the fusion/hydrothermal method, a larger amount of NaOH is required, which leads to the formation of significant quantities of zeolite crystals and an enhanced yield.

The well-defined cubic crystals seen in the SEM images of 5A suggest that the ion exchange of 4A successfully led to the effective synthesis of 5A.

5.1.4 4A zeolites synthesized from Angren kaolin via hydrothermal method

S1, S2 and S3 samples

The initial phase of the synthesis involved conducting experiments using different concentrations of NaOH (2.0, 2.5, 3.0). The morphology of the S1, S2, and S3 samples, characterized by small cubic crystals, is different from that of kaolin, indicating the beginning of zeolite crystal formation. However, these crystal structures do not fully represent the zeolite. This may be due to an insufficient crystallization time.

S4, S5 and S6 samples

In the second phase of the synthesis, 4g of Na_2SiO_3 was used, and the crystallization time ranged from 8 to 12 hours. The surface morphology of samples in Figure 4-5 shows significant differences compared to S1, S2, and S3 (Figure 4-4). As the crystallization time increases, there is a corresponding increase in the formation of cubic crystals that represent the LTA zeolite framework. The duration of crystallization has a positive impact on the production of zeolite crystals. In particular, the S6 exhibits cubic crystals with well-defined shapes. The crystals in the micrographs are distinct and contain a small amount of amorphous material, which may suggest the presence of unreacted metakaolin (Figure 4-5.d).

S8 and S9 samples

No sodium silicate was added during the third phase of the synthesis. The aging process was conducted at 60 °C for 12 hours. The duration of crystallization ranged from 24 to 36 hours. Zeolites can be produced since the crystallization period is sufficient. It is evident that both the S8 and S9 samples exhibit well-defined cubic crystals surrounding unreacted kaolin. There is minimal disparity in the morphology of the S8 and S9 samples, suggesting that extending crystallization time does not yield any beneficial effects on the production of zeolite molecules.

5.1.5 5A modified by silver nanowires

Silver nanowires were detected in specific areas within the 5A zeolite. However, the lack of silver nanowires on the 5A zeolite surface indicates that the concentration of silver nanowires in the solution was either too low or the impregnation process was incomplete.

5.2 EDS ANALYSIS

5.2.1 13X and silver modified 13X

The substantial silver content found in the silver-modified samples indicates that the ion-exchange process was successful. This suggests that the Na^+ cations in the zeolite were replaced by Ag^+ cations, as alkali metals tend to exchange with silver ions . Table 7 shows a decrease in Na^+ cations and an increase in Ag^+ cations, supporting this conclusion.

5.2.2 Commercial 4A and 5A

Based on the constituent content in Table 4-2, it is evident that commercial 4A and 5A have nearly identical compositions of oxygen (O), silicon (Si), and aluminium (Al). Generally, 4A zeolite is characterized by the presence of Na as a cation, whereas 5A zeolite is known for retaining Ca as a cation [100], [123]. This is reflected in the fact that 4A contains 11.55 wt.% of Na and 5A has 8.28 wt.% of Ca. In addition, 4A includes 0.95 wt.% of Mg, while 5A has a slightly higher amount of 3.26 wt.%. Fe was only detected in 4A.

5.2.3 4A and 5A zeolites synthesized from Angren Kaolin

The element content in the samples is shown in Table 4-3. It is crucial to compare the levels of Si, Al, Na, and Ca in the synthesized 4A and 5A samples with those in

the commercial ones. The Si weight concentration in 4A-I, 4A-II, and 4A-III is 20 wt.%, but it is 16.47 wt.% in 5A-III. The higher Si concentration compared to raw kaolin is due to the ion exchange of Mg, Ka, and P with Na, which were not detected in the synthesized samples. The Na concentration in 4A-I, 4A-II, 4A-III, and 5A-III are 10.49, 8.27, 8.89, and 0.76, respectively. Ca is exclusively found in the 5A-III at a concentration of 7.10 wt.%. There are no significant differences in the elemental weight concentration of 4A synthesized with different kaolin/NaOH ratios compared to the commercial one. Moreover, 5A zeolite prepared from 4A by ion exchange has almost similar element content with commercial 5A. Therefore, it can be concluded that the zeolites 4A and 5A were successfully synthesized.

5.2.4 Silver nanowires modified 5A

The atomic and weight concentrations of the elements were measured at four different locations to obtain an average. The weight concentration of Ag in 5ANWs is 5.64 %, confirming the successful impregnation. However, it is clear that the Ag presence on the zeolite surface led to a drop in the weight concentrations of Si, Al, and Ca.

5.3 XRD ANALYSIS

The XRD spectra obtained from the samples should be compared to those of the reference zeolite. Typically, multiple diffraction peaks are employed for the purpose of comparison. The ASTM technique D3906 for Faujasite materials involves comparing eight distinct peaks, while the ASTM method D5357 for LTA zeolite utilizes the six most prominent peaks. Modifications in the highest levels of intensity can be utilized to observe and assess the progress of the therapy procedure. For instance, a general reduction in the highest level of intensity could suggest the deterioration of zeolite, while variations in peak intensities could suggest a change in atomic positioning due to the treatment.

5.3.1 13X and silver-modified 13X

No significant difference was observed between fresh 13X, and the Ag modified samples as shown in Figure 4-8. It should be noted, however, that the intensity of some peaks for the samples that had been exchanged with silver was diminished. It indicates that the crystal structure of the 13X molecular sieve remains intact after the Ag ion-exchange treatment.

5.3.2 Commercial 4A and 5A

XRD pattern of 4A showed mainly a crystalline phase composed of sodium aluminium silicate ($Na_9Al_9Si_{15}O_{48}$) according to the PDF card no. 04-021-4950. The main diffraction peaks at 2 θ = 7.1, 10.1, 12.3, 16.2, 18.3, 20.5 21.8, 24.2, 26.2, 27.3, 30.2, 34.5 are characteristic of the Linde Type A structure. XRD pattern of 5A confirmed mainly a crystalline phase composed of sodium, calcium aluminium silicate ($Na_4\ Ca_4Al_{12}Si_{12}O_{48}$) according to the PDF card no. 04-009-5246. The main diffraction peaks at 2θ = 7.1, 10.1, 12.3, 16.2, 18.3, 20.5 21.8, 24.0, 27.1, 30.0, 34.2 are characteristic of the Linde Type A structure.

5.3.3 4A and 5 A zeolites synthesized from Angren kaolin via fusion/hydrothermal method

XRD pattern of 4A-I showed mainly amorphous phase with crystalline phase composed of sodium aluminium silicate ($Na_{51}Al_{51}Si_{141}O_{384}(H_2O)_{7.83}$) according to the PDF card no. 01-076-0591. The main diffraction peaks were observed only at 2 θ = 6.1, 10.1, 11.9, 15.5, 18.3, 23.5 26.6, 31.1. Nevertheless, the XRD spectra of the 4A-II and 4A-III primarily exhibited a crystalline phase. Because, the crystallinity increases with the increase of alkali solution (NaOH) [124]. Both samples consist of sodium aluminium silicate ($Na_2Al_2Si_{2.5}O_96.2\cdot(H_2O)$) as indicated by the PDF card no. 00-038-0237. The main diffraction peaks at 2 θ = 6.1, 10.0, 11.6, 15.2, 18.3, 20.5 23.4, 31.3, 33.2, 34.5 are characteristic of the Linde Type A structure. All samples exhibited a diffraction peak at 2θ=26.6, which is indicative of quartz [125]. Quartz present in kaolin remains intact during metakaolinization and subsequent conversion to zeolite [126].

It can be concluded that 4A-II and 4A-III were successfully synthesized as a zeolite. We determined the diffraction peaks corresponding to 5A, despite the XRD pattern for the 5A-III primarily showing an amorphous phase alongside a crystalline phase. Diffraction peaks (2θ = corresponding to quartz were observed in the phase of 5A-III and persisted after ion exchange.

5.3.4 4A zeolite synthesized from Angren kaolin via hydrothermal method

S1, S2 and S3

Despite the presence of diffractions at 2θ = 7.18, 10.17, and 12.36, which correspond to the 4A zeolite, their intensity is minimal, implying low weight content.

There is a single intensity peak at 26.6 that exhibits a high level of crystallinity for all samples. The diffraction intensity observed at 26.65 and 20.83 correlates to the presence of quartz as an impurity, which remains stable during hydrothermal synthesis [127], [128]. This indicates that the synthesis has not been entirely achieved.

S4 and S5

As the crystallization time increases, there is a corresponding rise in XRD peaks observed in the S4 and S5 samples (Figure 4-12). These results suggest the formation of 4A zeolite molecules. However, due to the relatively small size of these peaks, the formation of 4A zeolites cannot be conclusively confirmed. Even within these samples, we can definitely observe intensities that are characteristic of quartz.

S7, S8 and S9

XRD patterns of samples S7, S8 and S9 show a high degree of crystallinity (Figure 4-13), indicating that the reaction was successfully carried out. According to the Collection of Simulated XRD Powder Patterns for Zeolites [125], the characteristic diffraction peaks of Linde Type A (Hydrated) occur at 2θ = 7.18, 10.17, 12.46, 16.11, 20.41, 21.67, 23.99, 26.11, 27.11, 29.94 and 34.18. However, similar to the aforementioned samples, quartz remains unchanged by temperature and was observed by a diffraction peak at 2theta= 26.6 in all samples. As the crystallization duration increases, intensity of the reflection peaks corresponding to the zeolitic products also increases, reaching its highest value for the synthesized sample at 90℃ for 36 h.

5.4 XRF ANALYSIS

Table 4-8 shows the primary constituents of zeolite found in its structure, together with small quantities of impurities linked to the kaolin. High percentages of SiO_2 and Al_2O_3 were observed for all samples. The percentage of Na_2O exhibited a positive correlation with the concentration of NaOH solution for S1, S2, S3. Furthermore, the content of the Na_2O increased proportionally with the synthesis duration, suggesting the formation of more zeolites. Fe_2O_3, TiO_2, CaO and MgO were observed as impurities.

5.5 BET

5.5.1 13X and silver-modified 13X

The BET surface area was calculated as 501.33 m^2/g for 13X. However, this surface area was influenced by the ion exchange of Ag. The increase in silver ions most likely led to a decrease in the BET surface area, since the silver ion exchange of 13X resulted in a slight decrease in the specific surface area of AgIII-13X from 501.33 to 405 m^2/g. Similar findings were given by Chen et al., who found that the BET-specific surface area of silver-exchanged X was reduced by 33% [86].

5.5.2 Commercial 4A and 5A

The pore diameter of type A (4Å) zeolites is almost equal to the molecular diameter of N_2 molecules, which hinders their ability to enter the pore structure [129]. This leads to a low BET surface area of 4A, specifically less than 15 m^2/g. However, 5A has a pore diameter of 5Å, enabling the entry of molecules with a kinetic diameter smaller than 5 mm. As a result, the BET surface area of 5A was determined to be 392 m^2/g.

5.5.3 4A-III and 5A-III

The calculated BET surface areas of the synthesized 4A-III and 5A-III are 233.02 m^2/g and 302.76 m^2/g, respectively. The BET surface area of 4A-III exceeds that of commercial 4A, which is 12.6 m^2/g. However, the BET surface area of 5A-III is lower than that of the commercial one. The adsorption capacity of 4A-III is anticipated to be significantly greater than that of commercial 4A for H_2S adsorption.

5.6 ADSORPTION ISOTHERMS

Only the 13X samples treated with silver were subjected to the adsorption isotherms model, which revealed a significant capacity for adsorption relative to other materials. The Langmuir and Freundlich isotherm models were applied to AgI-13X and AgIII-13X to achieve a better match. The graphs also included the presented fitting parameters. The average determination coefficient for the AgI-13X is 0.9602 in the Langmuir model and 0.9028 in the Freundlich model. The value of Langmuir model was around 0.9659, while the value of Freundlich model was 0.9513 for AgIII-13X. The average determination coefficient (R^2) for AgII-13X zeolites was 0.9160 in Langmuir and 0.8956 in Freundlich, indicating that Langmuir's isothermal model was

better in this case. The maximum adsorption capacity was calculated as 29.42 mg/g, which was higher than the effective adsorption capacity of 13.06 mg/g.

5.7 H_2S REMOVAL FROM NITROGEN

The utilization of 5A and 13X zeolites for H_2S adsorption is widely applied in the industrial sector for natural gas processing [4]. We conducted H_2S adsorption experiments using nitrogen to examine operational factors such as the amount of adsorbent and the flow rate of the incoming gas.

It is hypothesized that large quantities of 5A zeolites could adsorb significant amounts of H_2S. Due to the large quantity of zeolites, the breakthrough point may be detected later, resulting in a higher adsorption capacity. The breakthrough time for 15g of 5A zeolite was observed to be 29.5 minutes, while for 20g of 5A zeolite it was 63.5 minutes (Figure 4-15).

Similarly, at a high flow rate, the target molecule has less contact time with the adsorbent, resulting in a quicker determination of the breakthrough point and a lower adsorption capacity. As shown in Figure 33, H_2S adsorption at a high flow rate reached 1 ppm after 69 minutes from the start of the process. At a flow rate of 20 l/h, this level was reached in 185 minutes. This demonstrates that, as mentioned earlier, there was limited contact between H_2S and the adsorbent, reducing the adsorbent's ability to capture H_2S. Therefore, it is generally preferable to conduct the adsorption process with more adsorbent and at a lower flow rate.

5.8 H_2S REMOVAL FROM METHANE

5.8.1 Commercial 13X and silver modified 13X zeolites

It is noteworthy to mention that the breakthrough time for AgIII-13X was detected earlier than that of AgII-13X. However, the breakthrough curves demonstrated that AgIII-13X was capable of adsorbing substantial quantities of H_2S molecules even after breakthrough time. Across all ranges, the longest breakthrough time for AgII-13X samples was discovered, indicating their high effective adsorption capacity.

5.8.1.1 Adsorption mechanism

After the procedure was started, it was observed that the initially white adsorbent surface underwent a colour change, transitioning to a darker shade. This alteration in

coloration served as an indication that chemical adsorption was taking place. Sodium (Na^+) ions present in 13X replaced silver (Ag^+) cations, leading to a subsequent chemical reaction with hydrogen sulfide (H_2S) molecules, resulting in the formation of black silver sulfide (Ag_2S). The possible adsorption mechanism of H_2S on silver-modified 13X was presented in Figure 5. Na^+ cations present in 13X molecular sieves can be replaced by Ag^+ cations. The H_2S molecules are strongly attracted to the Ag^+ cations. In fact, the large number of Ag cations contained in the zeolite had to increase their attraction to H_2S molecules. However, the zeolite interacts with H_2S molecules at the initial time of adsorption of Ag ions on the surface of the zeolite, forming Ag_2S and preventing other Ag ions in the inner layer from showing activity. As a result, no matter how much the amount of Ag cations contained in the zeolite increases, it does not have a positive effect on the increase in H_2S adsorption. Although AgII-13X contains fewer silver cations than AgIII-13X, its adsorption capacity becomes higher. π-complexation and sulfur-metal (S–M) bond formation may take place between sulfur compounds and metal ions. Previous research also stated that [86] the S–M bond was found to exist between the metal ion and H_2S. The Ag–sulfide bond was found to have the highest strength according to the Mayer bond order (0.639), which was determined by employing density functional theory (DFT).

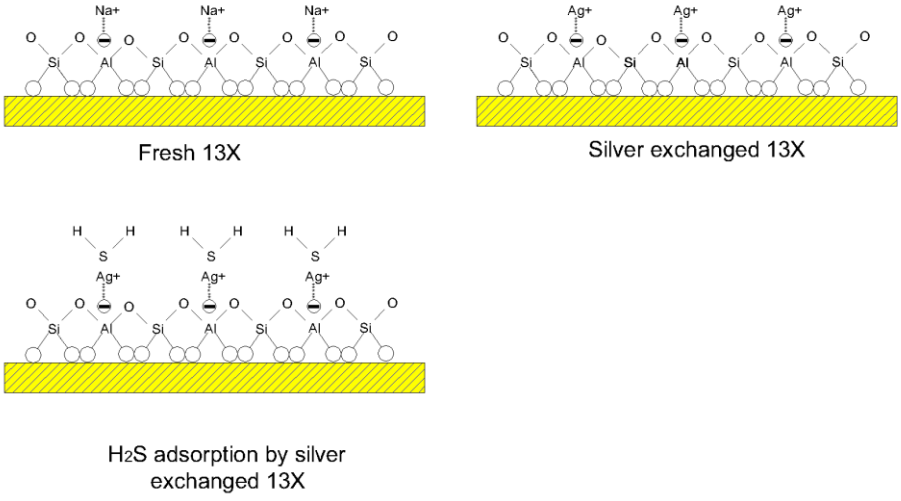

Figure 5-1. The possible adsorption mechanism of H_2S on silver-modified 13X.

5.8.1.2 Effect of inlet gas composition

The influence of H_2S concentration in the inlet gas composition was evaluated to determine its impact on adsorption capacity. Initially, three concentrations of H_2S

in natural gas were considered: 150 ppm, 300 ppm, and 500 ppm. The breakthrough curve, the corresponding breakthrough time, and the effective H_2S adsorption capacity are shown in Figure 4 and Table 3, respectively. When high H_2S concentrations of 500 ppm were used, the breakthrough was reached, as expected, significantly earlier (Figure 4c) than with the concentration of 150 ppm. At a 300 ppm H_2S inlet concentration, a greater adsorption capacity of 13.05 mg/g was achieved for AgII-13X. The lowest adsorption capacity of 0.238 mg/g was observed for non-modified 13X when the H_2S inlet concentration was 150 ppm. Table 4 provides the breakthrough times for the samples.

5.8.1.3 Effect of silver concentration

The effect of the concentration of Ag ions on the adsorption capacity of modified zeolite during H_2S uptake was investigated in the range of molar concentrations of 0.02–0.1M $AgNO_3$ water solution. The results are reported in Figure 4 and Table 3, respectively. It can be seen in Figure 4 that the increase of silver ions on zeolite samples led to an increase in breakthrough time and H_2S adsorption capacity. However, when the silver ion concentration was too large (Figure 4a for AgIII-13X, 0.1 M $AgNO_3$), the breakthrough time was observed earlier with respect to AgII-13X, resulting in a decrease in the adsorption performance. In spite of observing an earlier breakthrough time for AgIII-13X, its breakthrough curve changed marginally compared to those of the other samples. The use of a high-$AgNO_3$ solution concentration resulted in an increase in the cost of the adsorbent. Therefore, modification of the 13X molecular sieve using 0.05 M $AgNO_3$ solution was believed appropriate. It was determined that AgII-13X possessed a greater adsorption capacity, measuring 13.06 mg/g. AgII-13X showed about 50 times more adsorption capacity than non-modified 13X, which only had 0.238 mg/g of adsorption capacity.

5.8.1.4 Colour transformation.

Following the silver ion exchange process on the 13X zeolite, the original white yellowish colour of the 13X transformed into a light green. In 1962, Rálek et al. [130] observed a phenomenon of colour transformation in silver modified zeolite A, where the zeolite transformed from white to yellow.

a) b)

Figure 5-2. Colour transformation of silver modified 13X a) Non modified 13X zeolite and b) Ag ion exchanged 13X zeolite

5.8.2 4A-III and 5A-III zeolites

When both 4A-III and 5A-III zeolites were used for H_2S adsorption from methane, a significant difference in the breakthrough times was observed between the synthesized and commercial zeolites. For commercial zeolites, the breakthrough point was reached after just a few minutes of adsorption, whereas the breakthrough points for synthesized ones were observed after 31.9 h and 8.15 h, respectively, demonstrating a significantly higher capacity for H_2S adsorption.

Among all the zeolites, 5A-III exhibited a markedly superior adsorption capability compared to commercial 4A, 5A, and 4A-III. The adsorption capacities determined from breakthrough points were 1.67 mg/g for 4A and 4.45 mg/g for 5A. The results demonstrate that both 4A and 5A zeolites produced from Angren kaolin possess remarkable adsorption properties for H_2S.

The 4A and 5A zeolites synthesized via fusion/hydrothermal techniques exhibited advantageous properties for H_2S adsorption, comparable to those of commercial zeolites.

It is noteworthy that although the synthesis of 4A and 5A zeolites from kaolin can be achieved by fusion/hydrothermal and standard hydrothermal procedures, the former is favored due to its shorter time requirements.

5.8.3 Silver nanowires modified 5A

The adsorption capacity of silver nanowires modified with 5A was found to be 0.0579 mg/g, which is somewhat greater than that of the non-modified 5A (0.0486 mg/g). However, the difference is not statistically significant. It can be inferred that silver nanowires do not have a beneficial impact on zeolite 5A for the elimination of H_2S from methane.

Chapter 6: Conclusions and recommendations

6.1 SUMMARY

This chapter will provide a summary of the main research findings in relation to the research aims and questions, highlighting their value and contribution. Additionally, it will assess the limitations of the study and offer recommendations for future research.

Due to its corrosive nature, H_2S is commonly removed from natural gas to avoid damage to pipelines and equipment used in gas processing and transportation. Furthermore, it presents risks to both human health and the environment. Zeolites play a vital role in adsorbing H_2S from natural gas due to their exceptional properties, such as high adsorption capacity, regenerability, thermal stability, and low cost.

This work mainly studied the H_2S removal from nitrogen and methane using various zeolitic materials. To enhance the adsorption properties of the 13X, silver modifications in various concentrations were carried out. The performance of 13X and its silver modified samples was done in laboratory set up. Moreover, synthesis of 4A and 5A zeolites from Angren Kaolin (Uzbekistan) was conducted via fusion/hydrothermal and conventional hydrothermal methods. Characterization of the materials was done by XRD, SEM and BET techniques. To evaluate the adsorption efficiency of silver nanowires modified 5A zeolites, silver modified 13X zeolites, and 5A zeolites synthesized from kaolin, we carried out adsorption experiments with H_2S and methane under different conditions. The adsorption capacity of each sample was determined from the breakthrough time and then compared. Various modifications and synthesis techniques were applied to the zeolites. A brief summary of the results for each sample is provided below:

6.1.1 Silver modification of 13X

Various concentrations of $AgNO_3$ solution were used to modify 13X to assess the effect of the Ag^+ cation level on the adsorption properties. The effect of the inlet concentration of H_2S was evaluated in the range of 150–500 ppm. The results demonstrated that the ion exchange of 13X with silver ions positively influenced the

adsorbent capacity. The highest adsorption capacity of 13.05 mg/g was achieved using AgII-13X zeolite and was highly effective in removing H_2S from natural gas.

6.1.2 Fusion/hydrothermal synthesis of 4A and 5A

The synthesis of zeolites using low-cost raw materials is an environmentally friendly approach on a global scale. Therefore, we have utilized kaolin as the primary substance for producing 4A zeolites, which were subsequently converted into 5A zeolites to eliminate H_2S from natural gas.

Angren Kaolin, sourced from Uzbekistan, was chosen as the raw material for synthesizing zeolites due to its high content of silica and aluminium. It is also motivated by the fact that, to date, no research has been conducted on synthesizing zeolites using Angren Kaolin. The synthesis of 4A zeolite samples involved the application of both fusion/hydrothermal and hydrothermal methods. Meanwhile, 5A zeolite was produced by ion-exchanging 4A with $CaCl_2$. The fusion/hydrothermal method was performed on kaolin using NaOH at a mass ratio ranging from 0.8 to 1.2.

The results of H_2S adsorption employing 4A-III and 5A-III zeolites demonstrated a remarkably high adsorption capacity of 1.67 mg/g and 4.45 mg/g, respectively. These capacities are 130 and 90 times greater than those of the commercial zeolites. This suggests that the successful synthesis of 4A and 5A zeolite from Angren kaolin as a base material could be an effective method for removing H_2S from natural gas.

6.1.3 Hydrothermal synthesis of 4A

The conventional hydrothermal method was also applied to the synthesis of 4A. The study examined the impact of various factors, such as the NaOH concentration, addition of Na_2SiO_3, crystallization time, and aging time, in the hydrothermal method.

Experiments demonstrated that the samples synthesized in the initial stage (S1, S2, and S3) did not exhibit the characteristics of 4A zeolite. As anticipated, the addition of NaOH and Na_2SiO_3 to the kaolin content was insufficient. Therefore, we increased the amount of Na_2SiO_3 in our subsequent experiment and gradually extended the crystallization time. Consequently, the formation of cubic crystals, a hallmark of 4A, became more evident as crystallization progressed, especially in sample S6. The presence of an amorphous phase in these samples indicates unreacted kaolin

molecules, as the samples were only dried at 110°C and not subjected to calcination at temperatures above 500°C before characterizations.

However, an extended period of crystallization resulted in the production of zeolite molecules, as evidenced by the S7, S8 and S9 samples. A higher quantity of cubic crystals measuring 4A were observed in these samples. An increase in crystallization time resulted in the observation of high crystallinity.

The study also focused on examining the effects of extended aging and crystallization times on the synthesis process at its final stage. It can be concluded that prolonged aging and crystallization will lead to a greater formation of 4A crystals. It can be concluded from this that the optimal aging time for synthesizing type 4A zeolite from Angren kaolin using the conventional hydrothermal method is 12 h, while the optimal crystallization time is 36 h.

Since the ion exchange process successfully converted 4A zeolites into 5A zeolites and effectively removing H_2S in the first method of synthesis (i.e. fusion/hydrothermal method), there was no need to repeat the procedure.

6.1.4 Silver nanowires modified 5A zeolite

5A zeolite was modified with silver nanowires to improve its adsorption characteristics. The SEM examination techniques were utilized to examine the morphology of both the unaltered and silver nanowires modified 5A. The SEM micrographs revealed that the silver nanowires were deposited on the zeolite surface, though not uniformly. Although the breakthrough points delayed, the breakthrough curve showed a rapid increase in comparison to the unmodified 5A. The point at which the breakthrough is delayed leads to a greater capacity for adsorption, but a fast increase in the breakthrough curve leads to a lower saturated adsorption capacity. The presence of silver nanowires on the surface of 5A caused a hindrance in the adsorption of H_2S molecules. Thus, it can be inferred that the addition of silver nanowires does not enhance the efficiency of 5A zeolite in removing H_2S from natural gas.

6.2 FINAL CONCLUSIONS

The final conclusions of the research are as follows:

- Linde type A (4A and 5A) and Faujasite (13X) zeolites play an important role in natural gas processing in order to remove H_2S, CO_2 and water.

- As suggested in the literature, modification of zeolites with metals can improve H_2S adsorption capacity of zeolites.
- The silver modification of 13X offers advantages in enhancing the adsorption efficiency for removing H_2S from natural gas. Silver concentrations in ion exchange play crucial role in this process.
- Silver modification does not damage to the surface morphology of 13X.
- To obtain more accurate results for adsorption capacity, it is necessary to conduct additional experiments with zeolites, varying factors such as the mass of the adsorbent, inlet H_2S concentration, and flow rate.
- The adsorption capacity of zeolites can vary depending on the inlet concentration of H_2S and the flow rate.
- The addition of silver nanowires to modify 5A does not enhance the adsorption capacity, hence it is unnecessary to pursue this modification.
- Based on the literature and findings of this study, both fusion/hydrothermal and conventional hydrothermal methods can be applied for the synthesis of zeolites from kaolin.
- Angren Kaolin from Uzbekistan is suitable material for the synthesis of 4A and 5A via fusion/hydrothermal and standard hydrothermal techniques.
- Synthesis of 4A and 5A zeolites can be applied for the purpose of H_2S elimination.
- 4A and 5A zeolite synthesized from Angren kaolin demonstrate a higher adsorption capacity compared to the commercial zeolites.
- Synthesized 4A and 5A and silver modified 13X samples, can be produced industrially and used in natural gas processing plants on an industrial scale.

6.3 NOVELTY OF THIS WORK

Since there have been several attempts to study the adsorption of H_2S from nitrogen and methane using commercial adsorbents and their modified versions, several novelties have been discovered in this research work.

- The commercial 13X zeolite has been modified with silver in order to enhance its adsorption capacity towards H_2S. Highest adsorption capacity of 13.05 mg/g was achieved for AgII-13X.
- The modification of 5A with silver nanowires was conducted for the first time to study the effect of silver nanowire towards H_2S. However, no significant enhancement was observed in adsorption capacity.
- We have studied experimentally the impact of flow rate, inlet H_2S concentrations, and mass of adsorbent on adsorption capacity. The results indicate that the adsorption capacity is influenced by these factors. The determination of adsorption capacity can be achieved by calculating the average of all measurements. Therefore, we recommend the creation of an international standard to quantify the adsorption capacity of adsorbents under uniform conditions. The mass of the adsorbent, flow rate, inlet concentration of the adsorbate, temperature, and pressure should all be standardized.
- We have successfully synthesised 4A and 5A zeolites from Angren Kaolin for the first time using both the fusion/hydrothermal and hydrothermal methods.
- The adsorption performance of the synthesized 4A and 5A materials was assessed to determine their effectiveness in removing H_2S from methane. The adsorption capacities achieved were 1.67 mg/g for 4A and 4.45 mg/g for 5A, which are higher than those of commercially available zeolites.

6.4 RECOMONDATIONS FOR FUTURE WORKS

Although we have achieved positive outcomes in several areas, we recognize that our work, like many other endeavours, is constrained by limitations in time and resources. Therefore, we would like to emphasize some tasks that should be addressed in the future. Here are some recommendations for future research:

1. It is recommended to conduct experiments to modify 13X by other metals including Co, Zn, and Cu to enhance its ability to remove H_2S, as these metals are more cost-effective that silver.
2. Based on the findings of this study and the existing literature, it was proved that 13X exhibits a substantial adsorption capability. Therefore, it is

recommended to synthesize 13X zeolite from Angren Kaolin and investigate its adsorption performance for H_2S.

3. Adsorbents are utilized in multiple cycles following the process of regeneration. Therefore, it is crucial to examine the regeneration of spent adsorbents to evaluate their subsequent effectiveness.
4. Natural gas contains impurities beyond H_2S, including CO_2 and water. So, it is recommended to investigate the adsorption of these impurities from natural gas using zeolites synthesized from kaolin.
5. Given Uzbekistan's abundant kaolin resources and natural gas reserves, it is proposed to produce import-substituting zeolites using Angren kaolin. These zeolites would be highly valuable for gas processing plants.

Bibliography

[1] W. H. Organization, *Air quality guidelines*, no. 91. 2000.

[2] R. Xu, W. Pang, J. Yu, Q. Huo, and J. Chen, *Chemistry of Zeolites and Related Porous Materials*. Wiley, 2007. doi: 10.1002/9780470822371.

[3] IEA, "Global Energy Review 2020," *Global Energy Review 2020*. IEA, Paris, 2020. doi: 10.1787/a60abbf2-en.

[4] S. Mokhatab, W. A. Poe, and J. Y. Mak, *Handbook of natural gas transmission and processing: Principles and practices*. 2018. doi: 10.1016/C2017-0-03889-2.

[5] J. G. Speight, *Handbook of Petroleum Refining*. CRC Press, 2016. doi: 10.1201/9781315374079.

[6] S. Lee, N. Kang, M. Park, J. Y. Hwang, S. H. Yun, and H. Y. Jeong, "A review on volcanic gas compositions related to volcanic activities and non-volcanological effects," *Geosci. J.*, vol. 22, no. 1, pp. 183–197, 2018, doi: 10.1007/s12303-017-0056-y.

[7] J. G. Speight, "Corrosion in Gas Processing Plants," in *Oil and Gas Corrosion Prevention*, no. 1, 2014, pp. 67–91. doi: 10.1016/b978-0-12-800346-6.00004-1.

[8] A. Alonso-Vicario *et al.*, "Purification and upgrading of biogas by pressure swing adsorption on synthetic and natural zeolites," *Microporous Mesoporous Mater.*, vol. 134, no. 1–3, pp. 100–107, 2010, doi: 10.1016/j.micromeso.2010.05.014.

[9] W. C. Lin, Y. P. Chen, and C. P. Tseng, "Pilot-scale chemical-biological system for efficient H_2S removal from biogas," *Bioresour. Technol.*, vol. 135, pp. 283–291, 2013, doi: 10.1016/j.biortech.2012.10.040.

[10] U. R. Chaudhuri, *Fundamentals of Petroleum and Petrochemical Engineering*. 2016. doi: 10.1201/b10486.

[11] E. Latosov, M. Loorits, B. Maaten, A. Volkova, and S. Soosaar, "Corrosive effects of H_2S and NH_3 on natural gas piping systems manufactured of carbon

steel," *Energy Procedia*, vol. 128, pp. 316–323, Sep. 2017, doi: 10.1016/j.egypro.2017.08.319.

[12] T. Tork and M. M. Weiss, *Natural gas sweetening*, vol. 8, no. 5. 2003. doi: 10.1016/b978-0-12-386914-2.00007-8.

[13] C. I. Ossai, "Advances in Asset Management Techniques: An Overview of Corrosion Mechanisms and Mitigation Strategies for Oil and Gas Pipelines," *ISRN Corros.*, vol. 2012, pp. 1–10, 2012, doi: 10.5402/2012/570143.

[14] Y. T. Al-Janabi, "An Overview of Corrosion in Oil and Gas Industry," *Corros. Inhib. Oil Gas Ind.*, pp. 1–39, 2020, doi: 10.1002/9783527822140.ch1.

[15] Safety and Health Topics, "Hydrogen sulfide," *Occup. Saf. Heal. Adm.*, 2024, [Online]. Available: https://www.osha.gov/hydrogen-sulfide

[16] A. F. Cronstedt, "Om en obekant bårg art, som kallas Zeolites," *K. Sven. vetensk.akad. handl.*, pp. 120–123, 1756.

[17] H. Ghobarkar, O. Schäf, and U. Guth, "Zeolites - from kitchen to space," *Prog. Solid State Chem.*, vol. 27, no. 2, pp. 29–73, 1999, doi: 10.1016/S0079-6786(00)00002-9.

[18] E. M. Flanigen, R. W. Broach, and S. T. Wilson, "Introduction," in *Zeolites in Industrial Separation and Catalysis*, 2010, pp. 1–26. doi: 10.1002/9783527629565.ch1.

[19] C. Baerlocher and L.B.McCusker, "Database of Zeolite Structures, http://www.iza-structure.org/databases/," *Database of Zeolite Structures*. [Online]. Available: http://www.iza-structure.org/databases/

[20] R. W. Broach, *Zeolite Types and Structures*. 2010. doi: 10.1002/9783527629565.ch2.

[21] S. A. Emami Moghaddam, R. Harun, M. N. Mokhtar, and R. Zakaria, "Potential of Zeolite and Algae in Biomass Immobilization," *Biomed Res. Int.*, vol. 2018, 2018, doi: 10.1155/2018/6563196.

[22] S. Sircar and A. Myers, "Gas Separation by Zeolites," *Handb. Zeolite Sci. Technol.*, 2003, doi: 10.1201/9780203911167.ch22.

[23] A. Martin, "Zeolite catalysis," *Appl. Catal.*, vol. 6, no. 118, Apr. 2016.

[24] S. Kulprathipanja and R. B. James, “Overview in Zeolites Adsorptive Separation,” in *Zeolites in Industrial Separation and Catalysis*, 2010, pp. 173–202. doi: 10.1002/9783527629565.ch5.

[25] A. A. Ismail, R. M. Mohamed, I. A. Ibrahim, G. Kini, and B. Koopman, “Synthesis, optimization and characterization of zeolite A and its ion-exchange properties,” *Colloids Surfaces A Physicochem. Eng. Asp.*, vol. 366, no. 1–3, pp. 80–87, 2010, doi: 10.1016/j.colsurfa.2010.05.023.

[26] M. W. Ackley, S. U. Rege, and H. Saxena, “Application of natural zeolites in the purification and separation of gases,” *Microporous and Mesoporous Materials*, vol. 61, no. 1–3. pp. 25–42, 2003. doi: 10.1016/S1387-1811(03)00353-6.

[27] K. S. Knaebel, “ADSORBENT SELECTION,” *Dublin , Ohio 43016 Contents Top.*, 2004.

[28] S. Kulprathipanja, *Zeolites in Industrial Separation and Catalysis*. Wiley, 2010. doi: 10.1002/9783527629565.

[29] S. Mokhatab, W. A. Poe, and J. Y. Mak, *Handbook of natural gas transmission and processing: Principles and practices*. 2018. doi: 10.1016/C2017-0-03889-2.

[30] F. Bandarchian and M. Anbia, “Conventional hydrothermal synthesis of nanoporous molecular sieve 13X for selective adsorption of trace amount of hydrogen sulfide from mixture with propane,” *J. Nat. Gas Sci. Eng.*, vol. 26, pp. 1380–1387, 2015, doi: 10.1016/j.jngse.2015.08.019.

[31] A. De Angelis, “Natural gas removal of hydrogen sulphide and mercaptans,” *Appl. Catal. B Environ.*, vol. 113–114, pp. 37–42, 2012, doi: 10.1016/j.apcatb.2011.11.026.

[32] M. Tagliabue *et al.*, “Natural gas treating by selective adsorption: Material science and chemical engineering interplay,” *Chem. Eng. J.*, vol. 155, no. 3, pp. 553–566, 2009, doi: 10.1016/j.cej.2009.09.010.

[33] D. Stirling and J. H. Clark, “Adsorption and absorption of H_2S,” D. Stirling and J. H. Clark, Eds. 2007, pp. 16–30. doi: 10.1039/9781847552174-00016.

[34] K. Amo *et al.*, “Low-Quality Natural Gas Sulfur Removal/Recovery,” no. 415,

pp. 1–7, 1998.

[35] B. Mandald and S. S. Bandyopadhyay, “Simultaneous absorption of CO_2 and H_2S into aqueous blends of N-methyldiethanolamine and diethanolamine.,” in *Environmental science & technology*, vol. 40, no. 19, 2006, pp. 6076–84. doi: 10.1021/es0606475.

[36] X. F. Tian, L. M. Wang, D. Fu, and C. Li, “Absorption and Removal Efficiency of Low-Partial-Pressure H 2 S in a Monoethanolamine-Activated N-Methyldiethanolamine Aqueous Solution,” *Energy and Fuels*, vol. 33, no. 1, pp. 629–635, 2019, doi: 10.1021/acs.energyfuels.8b03550.

[37] W. Y. Lee, S. Y. Park, K. B. Lee, and S. C. Nam, “Simultaneous Removal of CO_2 and H_2S from Biogas by Blending Amine Absorbents: A Performance Comparison Study,” *Energy & Fuels*, vol. 34, no. 2, pp. 1992–2000, Feb. 2020, doi: 10.1021/acs.energyfuels.9b03342.

[38] G. Liu, L. Zhu, W. Cao, H. Liu, and Y. He, “New Technique Integrating Hydrate-Based Gas Separation and Chemical Absorption for the Sweetening of Natural Gas with High H_2S and CO_2 Contents,” *ACS Omega*, vol. 6, no. 40, pp. 26180–26190, Oct. 2021, doi: 10.1021/acsomega.1c03165.

[39] E. Favre, “Polymeric Membranes for Gas Separation,” in *Comprehensive Membrane Science and Engineering*, vol. 2, Elsevier Inc., 2010, pp. 155–212. doi: 10.1016/B978-0-08-093250-7.00020-7.

[40] E. Drioli and L. Giorno, *Comprehensive Membrane Science and Engineering*, vol. 1–4. Elsevier, 2010. doi: 10.1016/C2009-1-28385-7.

[41] S. Sridhar, S. Bee, and S. Bhargava, “Membrane-based Gas Separation: Principle, Applications and Future Potential,” *Chem. Eng. Dig.*, vol. 27, no. September, pp. 77–87, 2014.

[42] A. Di Pretoro and F. Manenti, “Membrane Separation BT - Non-conventional Unit Operations: Solving Practical Issues,” A. Di Pretoro and F. Manenti, Eds. Cham: Springer International Publishing, 2020, pp. 101–108. doi: 10.1007/978-3-030-34572-3_12.

[43] R. T. Sataloff, M. M. Johns, and K. M. Kost, “Intergration of membrane into bioconversions,” 2000, p. 240.

[44] H. Maghsoudi and M. Soltanieh, “Simultaneous separation of H_2S and CO_2 from CH_4 by a high silica CHA-type zeolite membrane,” *J. Memb. Sci.*, vol. 470, pp. 159–165, Nov. 2014, doi: 10.1016/j.memsci.2014.07.025.

[45] H. Maghsoudi, M. Soltanieh, H. Bozorgzadeh, and A. Mohamadalizadeh, “Adsorption isotherms and ideal selectivities of hydrogen sulfide and carbon dioxide over methane for the Si-CHA zeolite: Comparison of carbon dioxide and methane adsorption with the all-silica DD3R zeolite,” *Adsorption*, vol. 19, no. 5, pp. 1045–1053, 2013, doi: 10.1007/s10450-013-9528-1.

[46] P. Iovane, F. Nanna, Y. Ding, B. Bikson, and A. Molino, “Experimental test with polymeric membrane for the biogas purification from CO_2 and H_2S,” *Fuel*, vol. 135, pp. 352–358, Nov. 2014, doi: 10.1016/j.fuel.2014.06.060.

[47] A. Janocha and K. Wojtowicz, “Studies reducing the H_2S from natural gas of using polyimide membrane,” *Nafta-Gaz*, vol. 74, no. 7, pp. 511–517, 2018, doi: 10.18668/ng.2018.07.04.

[48] M. P. Chenar, H. Savoji, M. Soltanieh, T. Matsuura, and S. Tabe, “Removal of hydrogen sulfide from methane using commercial polyphenylene oxide and Cardo-type polyimide hollow fiber membranes,” *Korean J. Chem. Eng.*, vol. 28, no. 3, pp. 902–913, 2011, doi: 10.1007/s11814-010-0437-7.

[49] A. I. Akhmetshina *et al.*, “Acidic gases separation from gas mixtures on the supported ionic liquid membranes providing the facilitated and solution-diffusion transport mechanisms,” *Membranes (Basel).*, vol. 9, no. 1, pp. 1–14, 2019, doi: 10.3390/membranes9010009.

[50] Y. Huang and R. Wang, “Highly selective separation of H_2S and CO_2 using a H_2S-imprinted polymers loaded on a polyoxometalate@Zr-based metal-organic framework with a core-shell structure at ambient temperature,” *J. Mater. Chem. A*, vol. 7, no. 19, pp. 12105–12114, 2019, doi: 10.1039/c9ta01749f.

[51] X. Zhang, Z. Tu, H. Li, and K. Huang, “Selective separation of H_2S and CO_2 from CH_4 by supported ionic liquid membranes,” *J. Memb. Sci.*, vol. 543, no. May, pp. 282–287, 2017, doi: 10.1016/j.memsci.2017.08.033.

[52] G. Liu *et al.*, “Enabling Fluorinated MOF-Based Membranes for Simultaneous

Removal of H_2S and CO_2 from Natural Gas," *Angew. Chemie - Int. Ed.*, vol. 57, no. 45, pp. 14811–14816, 2018, doi: 10.1002/anie.201808991.

[53] S. A. M. Marzouk, M. H. Al-Marzouqi, N. Abdullatif, and Z. M. Ismail, "Removal of percentile level of H_2S from pressurized H_2S-CH_4 gas mixture using hollow fiber membrane contactors and absorption solvents," *J. Memb. Sci.*, vol. 360, no. 1–2, pp. 436–441, 2010, doi: 10.1016/j.memsci.2010.05.046.

[54] L. D. Gasper-Galvin, A. T. Atimtay, and R. P. Gupta, "Zeolite-supported metal oxide sorbents for hot-gas desulfurization," *Ind. Eng. Chem. Res.*, vol. 37, no. 10, pp. 4157–4166, 1998, doi: 10.1021/ie930439i.

[55] L. Neveux, D. Chiche, J. Pérez-Pellitero, L. Favergeon, A. S. Gay, and M. Pijolat, "New insight into the ZnO sulfidation reaction: Mechanism and kinetics modeling of the ZnS outward growth," *Phys. Chem. Chem. Phys.*, vol. 15, no. 5, pp. 1532–1545, 2013, doi: 10.1039/c2cp42988h.

[56] W. F. Elseviers and H. Verelst, "Transition metal oxides for hot gas desulphurisation," *Fuel*, vol. 78, no. 5, pp. 601–612, 1999, doi: 10.1016/S0016-2361(98)00185-9.

[57] P. R. Westmoreland and D. P. Harrison, "Evaluation of Candidate Solids for High-Temperature Desulfurization of Low-Btu Gases," *Environ. Sci. Technol.*, vol. 10, no. 7, pp. 659–661, 1976, doi: 10.1021/es60118a010.

[58] Y. Belmabkhout *et al.*, "Natural gas upgrading using a fluorinated MOF with tuned H_2S and CO_2 adsorption selectivity," *Ind. Eng. Chem. Res.*, vol. 25, no. 16, p. 111886, Jul. 2020, doi: 10.1021/la903238y.

[59] L. H. de Oliveira, J. G. Meneguin, M. V. Pereira, J. F. do Nascimento, and P. A. Arroyo, "Adsorption of hydrogen sulfide, carbon dioxide, methane, and their mixtures on activated carbon," *Chem. Eng. Commun.*, vol. 206, no. 11, pp. 1544–1564, 2019, doi: 10.1080/00986445.2019.1601627.

[60] S. Yaşyerli, İ. Ar, G. Doabreveu, and T. Doğu, "Removal of hydrogen sulfide by clinoptilolite in a fixed bed adsorber," *Chem. Eng. Process.*, vol. 41, no. 9, pp. 785–792, 2002, doi: 10.1016/S0255-2701(02)00009-0.

[61] M. J. Jafari, R. Zendehdel, A. Rafieepour, M. Nakhaei Pour, H. Irvani, and S.

Khodakarim, “Comparison of Y and ZSM-5 zeolite modified with magnetite nanoparticles in removal of hydrogen sulfide from air,” *Int. J. Environ. Sci. Technol.*, vol. 17, no. 1, pp. 187–194, Jan. 2020, doi: 10.1007/s13762-019-02348-w.

[62] Y. Yokogawa, M. Sakanishi, N. Morikawa, A. Nakamura, I. Kishida, and H. K. Varma, “VSC adsorptive properties in ion exchanged zeolite materials in gaseous and aqueous medium,” *Procedia Eng.*, vol. 36, pp. 168–172, 2012, doi: 10.1016/j.proeng.2012.03.026.

[63] L. H. de Oliveira *et al.*, “H_2S adsorption on NaY zeolite,” *Microporous Mesoporous Mater.*, vol. 284, pp. 247–257, Aug. 2019, doi: 10.1016/j.micromeso.2019.04.014.

[64] H. Pourzolfaghar and M. H. S. Ismail, “Study of H_2S Removal Efficiency of Virgin Zeolite in POME Biogas Desulfurization at Ambient Temperature and Pressure,” *Dev. Sustain. Chem. Bioprocess Technol.*, pp. 1–424, 2013, doi: 10.1007/978-1-4614-6208-8.

[65] W. Ahmad, S. Sethupathi, M. S. N. Noraini, M. J. K. Bashir, and C. Y. Chun, “Hydrogen sulfide removal using diatomite,” *AIP Conf. Proc.*, vol. 2124, no. July, 2019, doi: 10.1063/1.5117065.

[66] S. K. Lee, Y. N. Jang, I. K. Bae, S. C. Chae, K. W. Ryu, and J. K. Kim, “Adsorption of toxic gases on iron-incorporated Na-A zeolites synthesized from melting slag,” *Mater. Trans.*, vol. 50, no. 10, pp. 2476–2483, 2009, doi: 10.2320/matertrans.M2009175.

[67] Nguyen Quang Long, H. T. Vuong, H. K. P. Ha, W. Kuniawan, H. Hinode, and T. Baba, “Preparation, characterization and H_2S adsorptive removal of ion-exchanged zeolite X,” *J. Chem. Phys.*, vol. 5, no. 1, pp. 4–12, 2016, doi: 10.1063/1.1668912.

[68] T. Kristóf, “Selective Removal of Hydrogen Sulphide from Industrial Gas Mixtures Using Zeolite NaA,” *Hungarian J. Ind. Chem.*, vol. 45, no. 1, pp. 9–15, 2018, doi: 10.1515/hjic-2017-0003.

[69] T. Kristóf and D. Bucsai, “Atomistic simulation study of the adsorptive separation of hydrogen sulphide/alkane mixtures on all-silica zeolites,” *Mol.*

Simul., vol. 0, no. 0, pp. 1–12, 2021, doi: 10.1080/08927022.2021.1914336.

[70] M. S. Shah, M. Tsapatsis, and J. I. Siepmann, "Identifying Optimal Zeolitic Sorbents for Sweetening of Highly Sour Natural Gas," *Angew. Chemie - Int. Ed.*, vol. 55, no. 20, pp. 5938–5942, 2016, doi: 10.1002/anie.201600612.

[71] M. Lasich, "Adsorption of H_2S from Hydrocarbon Gas Using Doped Bentonite: A Molecular Simulation Study," *ACS Omega*, vol. 5, no. 31, pp. 19877–19883, 2020, doi: 10.1021/acsomega.0c02934.

[72] S. Mokhatab and W. A. Poe, *Handbook of Natural Gas*, vol. 53, no. 9. 2012.

[73] H. H. Heck, M. L. Hall, R. dos Santos, and M. M. Tomadakis, "Pressure swing adsorption separation of $H_2S/CO_2/CH_4$ gas mixtures with molecular sieves 4A, 5A, and 13X," *Sep. Sci. Technol.*, vol. 53, no. 10, pp. 1490–1497, 2018, doi: 10.1080/01496395.2017.1417315.

[74] D. M. A. Melo, J. R. De Souza, M. A. F. Melo, A. E. Martinelli, G. H. B. Cachima, and J. D. Cunha, "Evaluation of the zinox and zeolite materials as adsorbents to remove H_2S from natural gas," *Colloids Surfaces A Physicochem. Eng. Asp.*, vol. 272, no. 1–2, pp. 32–36, 2006, doi: 10.1016/j.colsurfa.2005.07.005.

[75] L. Micoli, G. Bagnasco, and M. Turco, "H_2S removal from biogas for fuelling MCFCs: New adsorbing materials," *Int. J. Hydrogen Energy*, vol. 39, no. 4, pp. 1783–1787, 2014, doi: 10.1016/j.ijhydene.2013.10.126.

[76] L. Sigot, M. Fontseré Obis, H. Benbelkacem, P. Germain, and G. Ducom, "Comparing the performance of a 13X zeolite and an impregnated activated carbon for H_2S removal from biogas to fuel an SOFC: Influence of water," *Int. J. Hydrogen Energy*, vol. 41, no. 41, pp. 18533–18541, 2016, doi: 10.1016/j.ijhydene.2016.08.100.

[77] X. Liu and R. Wang, "Effective removal of hydrogen sulfide using 4A molecular sieve zeolite synthesized from attapulgite," *J. Hazard. Mater.*, vol. 326, pp. 157–164, 2017, doi: 10.1016/j.jhazmat.2016.12.030.

[78] O. W. Awe, D. P. Minh, N. Lyczko, A. Nzihou, and Y. Zhao, "Laboratory-scale investigation of the removal of hydrogen sulfide from biogas and air using industrial waste-based sorbents," *J. Environ. Chem. Eng.*, vol. 5, no. 2,

pp. 1809–1820, 2017, doi: 10.1016/j.jece.2017.03.023.

[79] M. M. Tomadakis, H. H. Heck, M. E. Jubran, and K. Al-Harthi, “Pressure-Swing Adsorption Separation of H_2S from CO_2 with Molecular Sieves 4A, 5A, and 13X,” *Sep. Sci. Technol.*, vol. 46, no. 3, pp. 428–433, 2011, doi: 10.1080/01496395.2010.520292.

[80] Y. Ahn, K. Pandi, M. Lee, and J. Choi, “Removing hydrogen sulfide from a feed stream using suitable adsorbent materials,” *J. Clean. Prod.*, vol. 272, p. 122849, 2020, doi: 10.1016/j.jclepro.2020.122849.

[81] P. Cosoli, M. Ferrone, S. Pricl, and M. Fermeglia, “Hydrogen sulfide removal from biogas by zeolite adsorption. Part II. MD simulations,” *Chem. Eng. J.*, vol. 145, no. 1, pp. 93–99, 2008, doi: 10.1016/j.cej.2008.08.013.

[82] P. Kumar *et al.*, “H2S adsorption by Ag and Cu ion exchanged faujasites,” *Microporous Mesoporous Mater.*, vol. 146, no. 1–3, pp. 127–133, 2011, doi: 10.1016/j.micromeso.2011.05.014.

[83] Jalil R. Ugal, S. H. Kareem, and S. S. Hassan, “Adsorption of Hydrogen Sulphide on the Zeolite type A Synthezied from Iraqi Kaoline,” *Baghdad Sci. J.*, vol. 10, no. 3, pp. 1023–1033, 2013, doi: 10.21123/bsj.10.3.1023-1033.

[84] A. Starke, C. Pasel, C. Bläker, T. Eckardt, J. Zimmermann, and D. Bathen, “Impact of $Na^+$and Ca^{2+} Cations on the Adsorption of H_2S on Binder-Free LTA Zeolites,” *Adsorpt. Sci. Technol.*, vol. 2021, 2021, doi: 10.1155/2021/5531974.

[85] L. Zhu *et al.*, “Modification of zeolite by metal and adsorption desulfurization of organic sulfide in natural gas,” *J. Nat. Gas Sci. Eng.*, vol. 69, no. February, p. 102941, 2019, doi: 10.1016/j.jngse.2019.102941.

[86] X. Chen, B. Shen, H. Sun, and G. zhan, “Ion-exchange modified zeolites X for selective adsorption desulfurization from Claus tail gas: Experimental and computational investigations,” *Microporous Mesoporous Mater.*, vol. 261, no. November 2017, pp. 227–236, 2018, doi: 10.1016/j.micromeso.2017.11.014.

[87] A. H. Abdullah, R. Mat, S. Somderam, A. S. Abd Aziz, and A. Mohamed, “Hydrogen sulfide adsorption by zinc oxide-impregnated zeolite (synthesized from Malaysian kaolin) for biogas desulfurization,” *J. Ind. Eng. Chem.*, vol.

65, pp. 334–342, 2018, doi: 10.1016/j.jiec.2018.05.003.

[88] S. Bahraminia, M. Anbia, and E. Koohsaryan, “Hydrogen sulfide removal from biogas using ion-exchanged nanostructured NaA zeolite for fueling solid oxide fuel cells,” *Int. J. Hydrogen Energy*, vol. 45, no. 55, pp. 31027–31040, 2020, doi: 10.1016/j.ijhydene.2020.08.091.

[89] L. Li, T. H. Sun, C. H. Shu, and H. B. Zhang, “Low temperature H_2S removal with 3-D structural mesoporous molecular sieves supported ZnO from gas stream,” *J. Hazard. Mater.*, vol. 311, pp. 142–150, 2016, doi: 10.1016/j.jhazmat.2016.01.033.

[90] S. Rezaei, M. O. D. Jarligo, L. Wu, and S. M. Kuznicki, “Breakthrough performances of metal-exchanged nanotitanate ETS-2 adsorbents for room temperature desulfurization,” *Chem. Eng. Sci.*, vol. 123, pp. 444–449, Feb. 2015, doi: 10.1016/j.ces.2014.11.041.

[91] B. T. A. Prasetyo and B. Soegijono, “Hydrogen Sulfide Adsorption improvement of Bayah Natural Zeolite,” *Asian J. Appl. Sci.*, vol. 7, no. 2, pp. 194–201, 2019, doi: 10.24203/ajas.v7i2.5765.

[92] Q. Bowen, Y. Chen, Y. Li, Xiubotian, and L. Ma, “Study on the removal of hydrogen sulfide from natural gas by titanosilicite zeolite,” *IOP Conf. Ser. Earth Environ. Sci.*, vol. 657, no. 1, 2021, doi: 10.1088/1755-1315/657/1/012034.

[93] C. Y. Sung, S. Al Hashimi, A. McCormick, M. Cococcioni, and M. Tsapatsis, “A DFT study on multivalent cation-exchanged y zeolites as potential selective adsorbent for H2S,” *Microporous Mesoporous Mater.*, vol. 172, pp. 7–12, 2013, doi: 10.1016/j.micromeso.2012.12.006.

[94] J. A. Thompson, “Acid gas adsorption on zeolite SSZ-13: Equilibrium and dynamic behavior for natural gas applications,” *AIChE J.*, vol. 66, no. 10, 2020, doi: 10.1002/aic.16549.

[95] J. W. H. G. Karge, *Molecular Sieves: Post-Synthesis Modification*, vol. 3, no. I. 2002.

[96] H. L. Tran, M. S. Kuo, W. D. Yang, and Y. C. Huang, “Hydrogen sulfide adsorption by thermally treated cobalt (II)-exchanged NaX zeolite,” *Adsorpt.*

Sci. Technol., vol. 34, no. 4–5, pp. 275–286, 2016, doi: 10.1177/0263617416648964.

[97] P. V. Adhyapak, P. Karandikar, K. Vijayamohanan, A. A. Athawale, and A. J. Chandwadkar, "Synthesis of silver nanowires inside mesoporous MCM-41 host," *Mater. Lett.*, vol. 58, no. 7–8, pp. 1168–1171, 2004, doi: 10.1016/j.matlet.2003.09.008.

[98] N. Y. Ul'yanova and O. Y. Golubeva, "Zeolites Modified with Silver Nanoparticles and Clusters: Synthesis, Characterization, and Catalytic Performance in H2 and CO Oxidation Reactions," *Glas. Phys. Chem.*, vol. 44, no. 5, pp. 418–422, 2018, doi: 10.1134/S1087659618050218.

[99] M. H. Huang, A. Choudrey, and P. Yang, "Ag nanowire formation within mesoporous silica," *Chem. Commun.*, no. 12, pp. 1063–1064, 2000, doi: 10.1039/b002549f.

[100] C. R. Melo *et al.*, "Synthesis of 4A zeolites from kaolin for obtaining 5A zeolites through ionic exchange for adsorption of arsenic," *Mater. Sci. Eng. B Solid-State Mater. Adv. Technol.*, vol. 177, no. 4, pp. 345–349, 2012, doi: 10.1016/j.mseb.2012.01.015.

[101] A. A. Mohammed and Z. K. Nassrullah, "Preparation and Formation of Zeolite 5A from Local Kaolin Clay for Drying and Desuphurization of Liquefied Petroleum Gas," *Iraqi J. Chem. Pet. Eng.*, vol. 14, no. 1, pp. 1–13, 2013.

[102] J. P. Brassell, T. V. Ojumu, and L. F. Petrik, "Upscaling of Zeolite Synthesis from Coal Fly Ash Waste: Current Status and Future Outlook," *Zeolites - Useful Miner.*, no. August, 2016, doi: 10.5772/63792.

[103] L. Chen, Y. W. Wang, M. Y. He, Q. Chen, and Z. H. Zhang, "Facile synthesis of 5A zeolite from attapulgite clay for adsorption of n-paraffins," *Adsorption*, vol. 22, no. 3, pp. 309–314, 2016, doi: 10.1007/s10450-016-9776-y.

[104] U. Jalil, K. Sameer, and Hassan Sahar, "Microwave-Assisted Synthesis of Zeolites A From Iraqi Cheap Raw Materials as Adsorbents for H_2S Gas," *J. Univ. Anbar pure Sci.*, vol. 8, no. 2, 2014.

[105] K. Shams and S. J. Mirmohammadi, "Preparation of 5A zeolite monolith

granular extrudates using kaolin: Investigation of the effect of binder on sieving/adsorption properties using a mixture of linear and branched paraffin hydrocarbons," *Microporous Mesoporous Mater.*, vol. 106, no. 1–3, pp. 268–277, 2007, doi: 10.1016/j.micromeso.2007.03.007.

[106] J. Ondruška *et al.*, "Thermophysical properties of kaolin–zeolite blends up to 1100◦c," *Crystals*, vol. 11, no. 2, pp. 1–17, 2021, doi: 10.3390/cryst11020165.

[107] F. J. Adamis Zoltan, "Environmental health criteria 231: Bentonite, kaolin, and selected clay minerals," *Environ. Heal. Criteria*, no. 231, 2005.

[108] W. R. Lim, C. H. Lee, and S. Y. Hamm, "Synthesis and characteristics of Na-A zeolite from natural kaolin in Korea," *Mater. Chem. Phys.*, vol. 261, no. January, p. 124230, 2021, doi: 10.1016/j.matchemphys.2021.124230.

[109] "Angren Kaolin." [Online]. Available: http://angrenkaolin.uz/en/about-us

[110] P. J. Moore and R. W. Spitler, "Hydrogen Sulfide Measurement and Detection," pp. 118–123, 2003.

[111] S. Kulawong, R. Artkla, P. Sriprapakhan, and P. Maneechot, "Biogas purification by adsorption of hydrogen sulphide on NaX and Ag-exchanged NaX zeolites," *Biomass and Bioenergy*, vol. 159, no. November 2021, p. 106417, 2022, doi: 10.1016/j.biombioe.2022.106417.

[112] P. Kumar *et al.*, "H_2S adsorption by Ag and Cu ion exchanged faujasites," *Microporous Mesoporous Mater.*, vol. 146, no. 1–3, pp. 127–133, 2011, doi: 10.1016/j.micromeso.2011.05.014.

[113] D. Papurello, A. Lanzini, M. Bressan, and M. Santarelli, "Sewage Sludges," *Processes*, vol. 8, no. 130, pp. 1–12, 2020.

[114] L. Barelli, G. Bidini, L. Micoli, E. Sisani, and M. Turco, "13X Ex-Cu zeolite performance characterization towards H_2S removal for biogas use in molten carbonate fuel cells," *Energy*, vol. 160, pp. 44–53, 2018, doi: 10.1016/j.energy.2018.05.057.

[115] C. Liu *et al.*, "Selective removal of H_2S from biogas using a regenerable hybrid TiO2/zeolite composite," *Fuel*, vol. 157, pp. 183–190, 2015, doi: 10.1016/j.fuel.2015.05.003.

[116] E. Sisani, G. Cinti, G. Discepoli, D. Penchini, U. Desideri, and F. Marmottini, "Adsorptive removal of H_2S in biogas conditions for high temperature fuel cell systems," *Int. J. Hydrogen Energy*, vol. 39, no. 36, pp. 21753–21766, 2014, doi: 10.1016/j.ijhydene.2014.07.173.

[117] A. K. Surela, L. K. Chhachhia, V. K. Surela, and P. L. Meena, "Polypyrrole-Based Composites for Dyes Removal From Contaminated Water," in *Reference Module in Materials Science and Materials Engineering*, Elsevier, 2024. doi: 10.1016/B978-0-323-95486-0.00019-3.

[118] S. Kulprathipanja, "Aspects of Mechanisms, Processes, and Requirements for Zeolite Separation," *Zeolites Ind. Sep. Catal.*, pp. 203–228, 2010, doi: 10.1002/9783527629565.ch6.

[119] S. A. Bradley, R. W. Broach, T. M. Mezza, S. Prabhakar, and W. Sinkler, *Zeolite Characterization*. 2010. doi: 10.1002/9783527629565.ch4.

[120] T. Derbe, S. Temesgen, and M. Bitew, "A Short Review on Synthesis, Characterization, and Applications of Zeolites," *Adv. Mater. Sci. Eng.*, vol. 2021, 2021, doi: 10.1155/2021/6637898.

[121] H. van Koningsveld and J. M. Bennett, "Zeolite Structure Determination from X-Ray Diffraction," 1999, pp. 1–29. doi: 10.1007/3-540-69749-7_1.

[122] S. Brunauer, P. H. Emmett, and E. Teller, "Adsorption of Gases in Multimolecular Layers," *J. Am. Chem. Soc.*, vol. 60, no. 2, pp. 309–319, Feb. 1938, doi: 10.1021/ja01269a023.

[123] J. C. Moreira, R. A. A. B. Santa, J. Nones, and H. G. Riella, "Synthesis of zeolite 4a for obtaining zeolite 5A by ionic exchange for full utilization of waste from paper industry," *Brazilian J. Chem. Eng.*, vol. 35, no. 2, pp. 623–630, 2018, doi: 10.1590/0104-6632.20180352s20160395.

[124] N. Sazali and Z. Harun, "One Shot of the Hydrothermal Route for the Synthesis of Zeolite LTA Using Kaolin," *J. Inorg. Organomet. Polym. Mater.*, vol. 32, no. 9, pp. 3508–3520, 2022, doi: 10.1007/s10904-022-02369-y.

[125] M. M. J. Treacy and J. B. Higgins, "Collection of Simulated XRD Powder Patterns for Zeolites," *Kurinikaru sutadi = Clinical study*, vol. 4, no. 9. pp. 1063–1069, 2001.

[126] S. Chandrasekhar and P. N. Pramada, “Investigation on the synthesis of zeolite NaX from kerala kaolin,” *J. Porous Mater.*, vol. 6, no. 4, pp. 283–297, 1999, doi: 10.1023/A:1009632606671.

[127] L. Ayele, J. Pérez-Pariente, Y. Chebude, and I. Díaz, “Synthesis of zeolite A from Ethiopian kaolin,” *Microporous Mesoporous Mater.*, vol. 215, pp. 29–36, Oct. 2015, doi: 10.1016/j.micromeso.2015.05.022.

[128] P. Wang, Q. Sun, Y. Zhang, and J. Cao, “Synthesis of zeolite 4A from kaolin and its adsorption equilibrium of carbon dioxide,” *Materials (Basel).*, vol. 12, no. 9, pp. 1–12, 2019, doi: 10.3390/ma12091536.

[129] J. A. Cecilia *et al.*, “Kaolinite-based zeolites synthesis and their application in CO_2 capture processes,” *Fuel*, vol. 320, no. December 2021, 2022, doi: 10.1016/j.fuel.2022.123953.

[130] M. Rálek, P. Jírů, O. Grubner, and H. Beyer, “Molekularsiebe mit farbiger Indizierung des Wassergehaltes,” *Collect. Czechoslov. Chem. Commun.*, vol. 27, no. 1, pp. 142–146, Nov. 1962, doi: 10.1135/cccc19620142.

[131] J. William F. Carroll and BarBara l. Foster, *Prudent Practices in the Laboratory*. 2011. doi: 10.17226/12654.

[132] A. J. Kidnay, A. J. Kidnay, W. R. Parrish, and D. G. McCartney, “Fundamentals of Natural Gas Processing,” *Fundam. Nat. Gas Process.*, 2011, doi: 10.1201/b14397.

Appendices

Appendix A

Precautions

While conducting research and achieving positive outcomes is fascinating, it is essential to consider certain precautions throughout the study. Both anticipated and unforeseen events may arise during the research process. The researcher must always take immediate steps to prevent it, be prepared for such situations and take the right approach to the situation. Following safety rules in the lab is vital to ensure a culture of safety in the workplace [131]. There are also several dangerous situations in our research work, which are as follows.

1. There is a risk of natural gas leakage and consequent explosion.

2. The effect of high concentrations of hydrogen sulfide on the human.

Because the situations listed above are so dangerous, they require a thorough study of every detail.

For example, during the assembly of an experimental device, the laboratory equipment must be properly connected to each other. It is also important to check that the parts of the laboratory device are resistant to operating pressure and temperature and to conduct initial tests before starting the study.

Full compliance with the rules of laboratory work is one of the first tasks to prevent these dangerous situations. Because natural gas is prone to explosion, it is required that there be no sources of sparks in the working environment.

Exceeding the established norm of hydrogen sulfide concentration in the working environment causes various adverse conditions such as health effects. A slight hydrogen sulfide exposure concentration of 15 mg/m^3 may cause eye irritation. It is very important to constantly monitor the concentration of hydrogen sulfide in the workplace. For this purpose, it is advisable to use detectors that determine the concentration of hydrogen sulfide.

Hydrogen sulfide is unquestionably the most important chemical to focus on during the experiment. As a result, a thorough understanding of H_2S's physicochemical characteristics will serve as the foundation for conducting safe research. When handled, H_2S is a volatile, poisonous gas that can corrode and destroy laboratory equipment. This can result in a variety of negative consequences, including an increased danger of combustion owing to the gas's release into the environment, as well as the poisonous effects of hydrogen sulfide on humans. The above-mentioned undesirable occurrences will be avoided by assembling in the laboratory using equipment composed of H_2S corrosion-resistant materials.

Tubing application

Various materials are utilized as a pipe in tubing application of lab set up depending on pressure, temperature, and highest concentration of the conveyed material. In our case, double walled stainless-steel tubing (Grade 316L) and Stainless steel (Grade 316L) can be used for highly toxic or corrosive gases in clean room application.

Before working with hydrogen sulfide, it is essential to consider the following information during the review of international safety regulations that are given in safety data sheet from hydrogen sulfide suppliers. The data sheet contains extensive information on how to handle H_2S.

First aid. A different approach is needed depending on the type of damage. A person who inhales hydrogen sulfide should be immediately taken to fresh air and placed in a comfortable position to breathe. If the patient is not breathing, artificial respiration should be used. If the gas comes into contact with human eyes, clean them thoroughly for at least 15 minutes.

Precaution for safe handling. Heat, heated surfaces, sparks, open flames, and other ignition sources should all be avoided. When handling cylinders, use leather safety gloves and safety shoes. Use only non-sparking tools and explosion-proof equipment.

Conditions for safe storage.

Only store where the temperature will not rise over 125°F (52°C). In storage and usage areas, post "No Smoking/No Open Flames" signage. Protect shipments from potential fire and/or explosion damage by separating them.

Exposure control

Corrosion-resistant equipment should be used. Use a local exhaust system that is explosion-proof. To achieve safe exposure levels, local exhaust and overall ventilation must be adequate. (GENERAL) MECHANICAL: Use only in a closed system if this is insufficient. Employ explosion-proof lights and equipment. While handling cylinders, use safety glasses; vapor-proof goggles and a face shield when changing cylinders or whenever product contact is likely.

H_2S disposal

What precautions can be taken with H_2S separation from a natural gas composition or mixture? According to the literature [132], H_2S can be disposed of in a variety of ways:

1. Burning or ventilation

2. Reacting H_2S to a harmless compound.

3. Conversion to elemental sulfur using the Claus method

In our case, since the amount of H_2S is low, it is preferable to convert it to another compound using chemicals such as NaOH [77], iron sponge.

CH_4 disposal

Natural gas can be burned after measuring the quantity of H_2S in the adsorbed gas since it is less harmful to burn.

Appendix B

Data logging

To obtain data from input and output analyzers, Arduino Nano as a microcontroller board was used to read analog pin input in volts [0-5 V] and We wrote the Arduino code for data logging from the analyzers been developed:

```
float SensorReading1;
float SensorReading2;
float ResistorValue = 250;   //reference resistor resistance
float Cmax1 = 1000;
float Cmax2 = 100;          //Max of process variable range
float Cmin = 0;             //Min of process variable range
float Vref = 5;             //Reference voltage for AnalogRead
//int NUM_AVG = 100;
void setup() {
Serial.begin(9600);
}
void loop() {
//Serial.print(millis());
//Serial.print(",");

//Read the voltage across the reference resistor
SensorReading1 = analogRead(A0);
SensorReading2 = analogRead(A1);
//for (int i = 0; i<NUM_AVG; i++);
//-40 for the range of 1000ppm, -17 for the range of 300/500ppm
//-40 for the range of 500/1000ppm, -12 for the range of 150/500ppm
//
    SensorReading1=(Cmax1-Cmin)*Vref/(1024*ResistorValue*(0.02-
    0.004))*(SensorReading1-1023*0.004*ResistorValue/Vref)-32;

    SensorReading2=(Cmax2-Cmin)*Vref/(1024*ResistorValue*(0.02-
    0.004))*(SensorReading2-1023*0.004*ResistorValue/Vref)-1;

Serial.print(SensorReading1);
Serial.print(",");
Serial.println(SensorReading2);
delay(1000);
}
```

Appendix C

EDS spectra of the samples

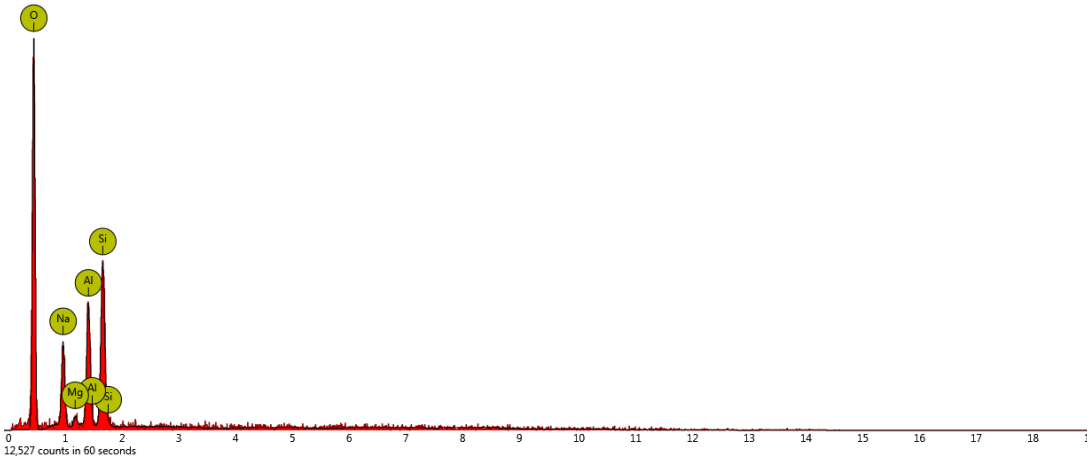

Disabled elements: B, Sb, Sn, Sr, Ti

a)

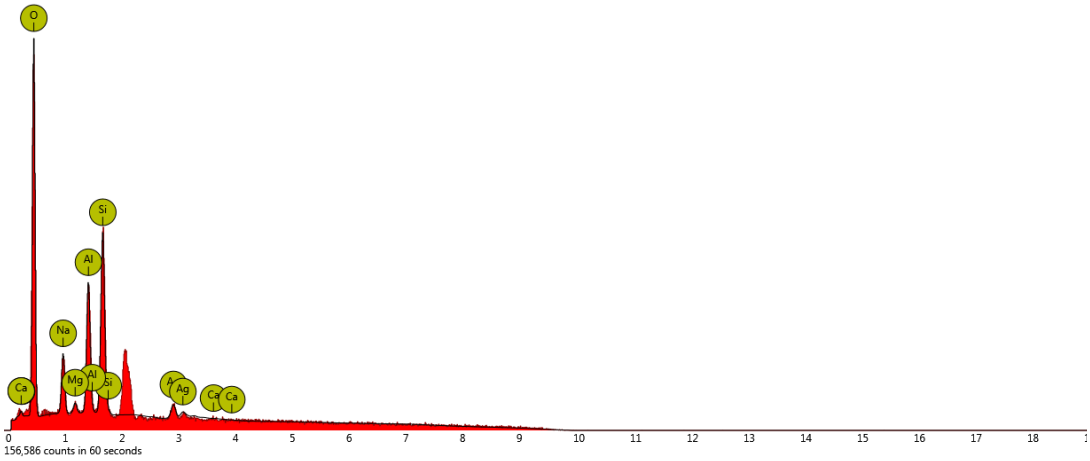

Disabled elements: Au, B, Hg, Nb, Pt, Zr

b)

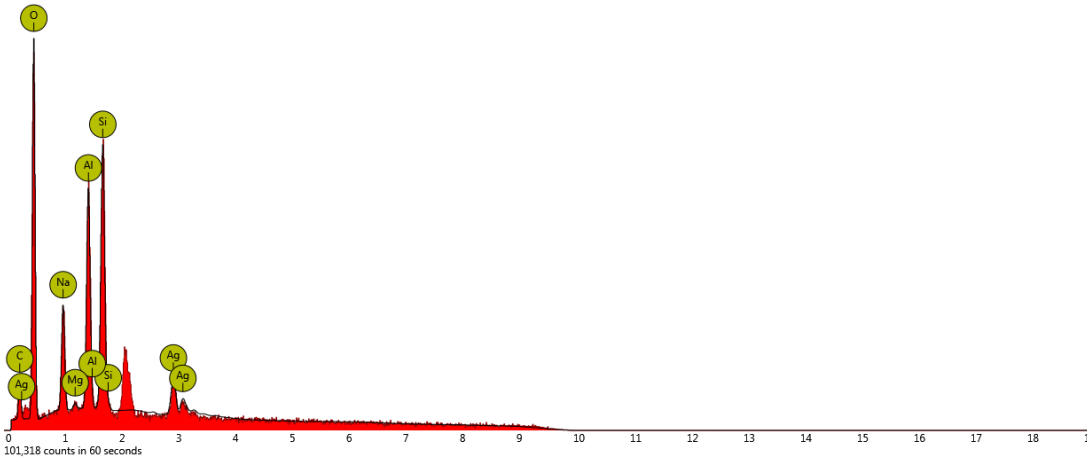

Disabled elements: Au, B, Hg, Nb, Pt, Sr, Zr

c)

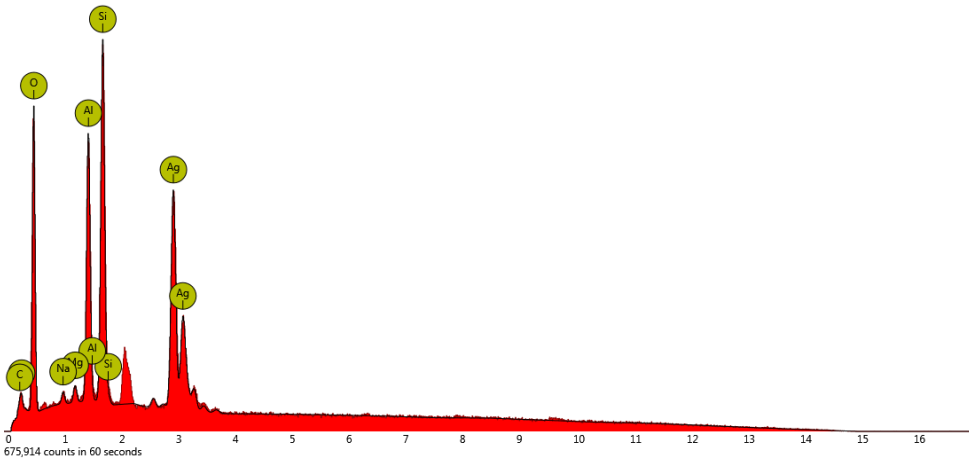

Disabled elements: B, Nb, Sr, Zr

d)

Figure 6-1. EDS spectra of 13X and AgI-13X, AgII-13X, and AgIII-13X

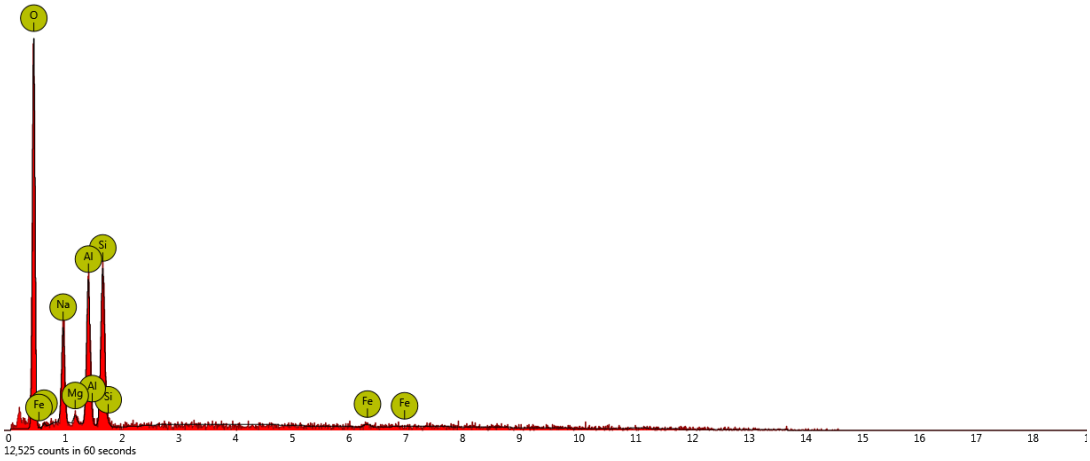

Disabled elements: B, C, K, Sb, V

a)

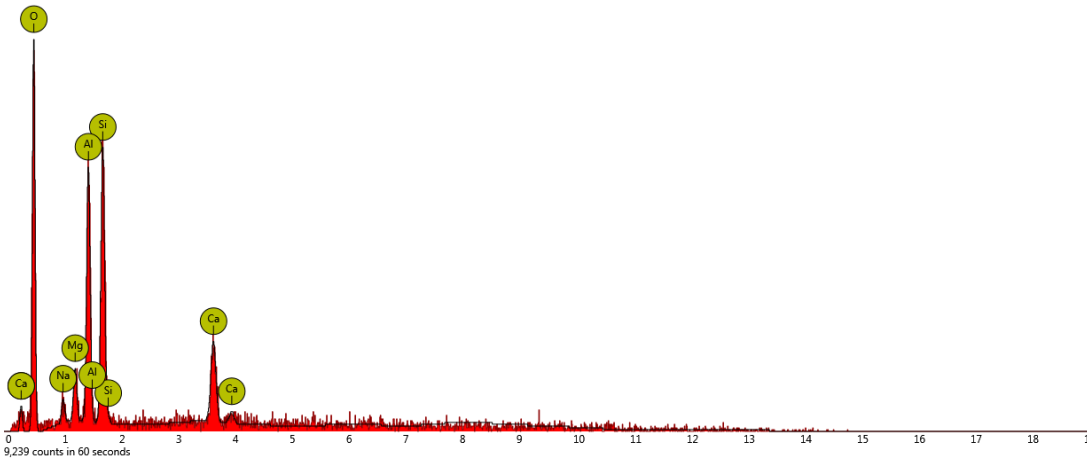

Disabled elements: B, Cs, Pm, Te

b)

Figure 6-2. EDS spectra of commercial a) 4A and b) 5A

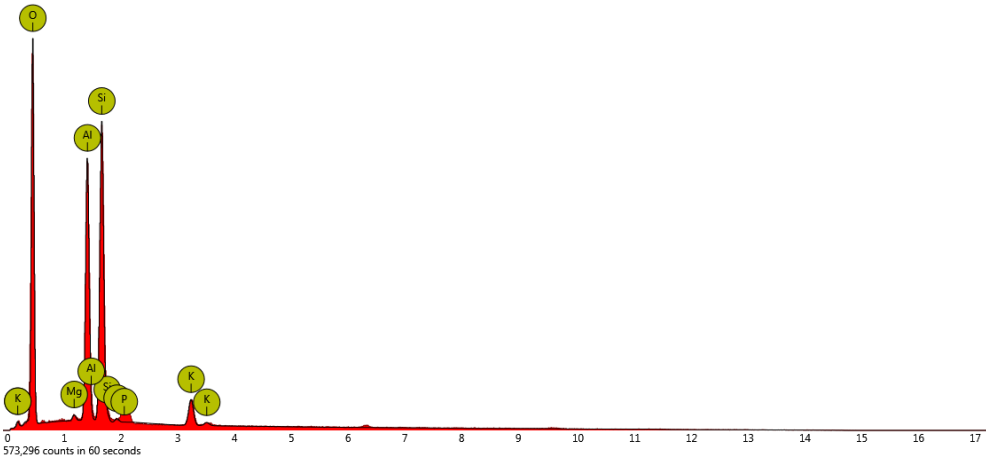

Disabled elements: Au, Nb, Re, Sr

a)

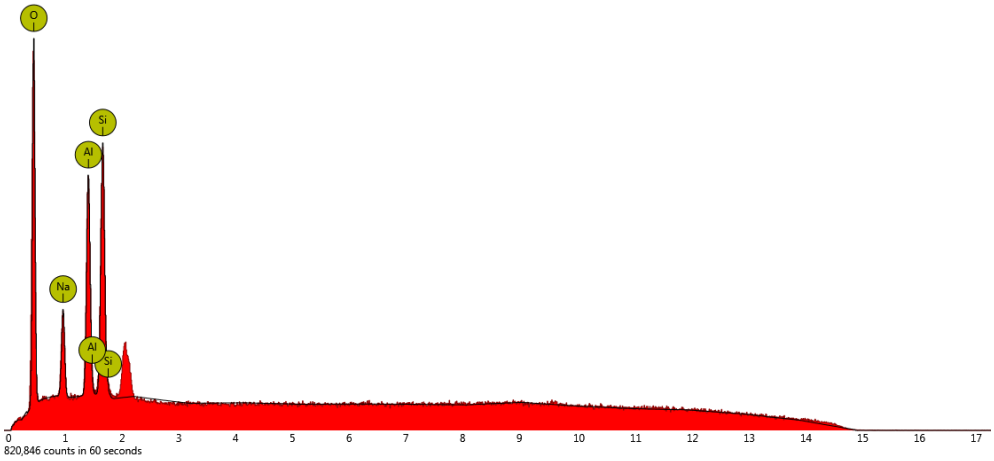

b)

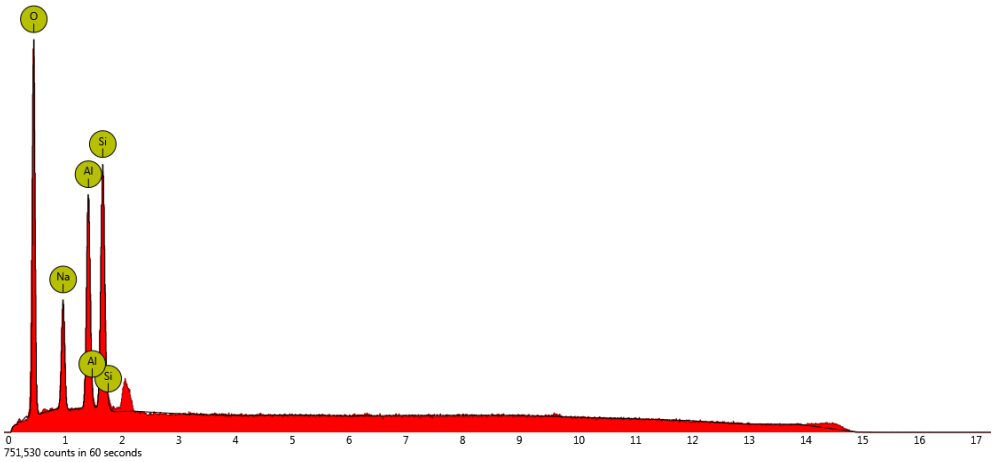

c)

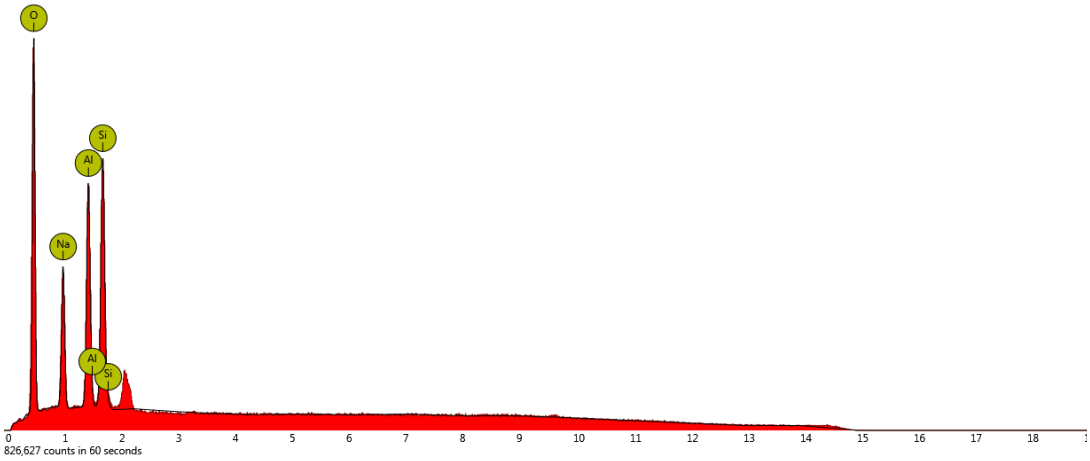

d)

Figure 6-3. EDS spectra of a) raw kaolin, b) 4A-I, c) 4A-II, d) 4A-III samples synthesizes by fusion/hydrothermal method e) 5A-III zeolite synthesized by ion-exchanging 4A-III.

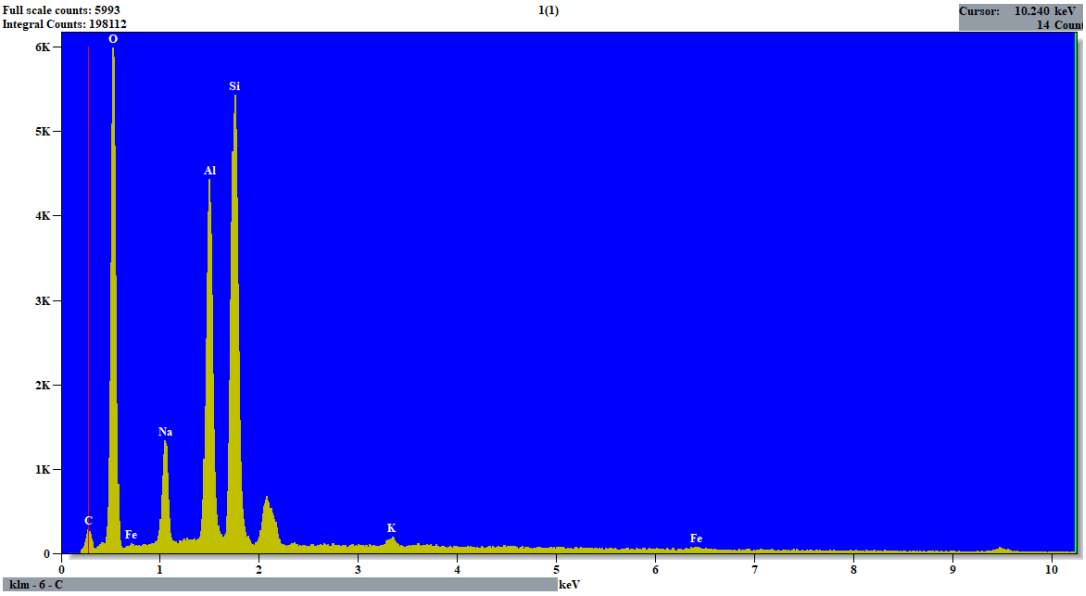
Full scale counts: 5993
Integral Counts: 198112
1(1)
Cursor: 10.240 keV
14 Coun
6K
5K
4K
3K
2K
1K
0
O
Si
Al
Na
C
Fe
K
Fe
0
1
2
3
4
5
6
7
8
9
10
klm - 6 - C
keV

a)

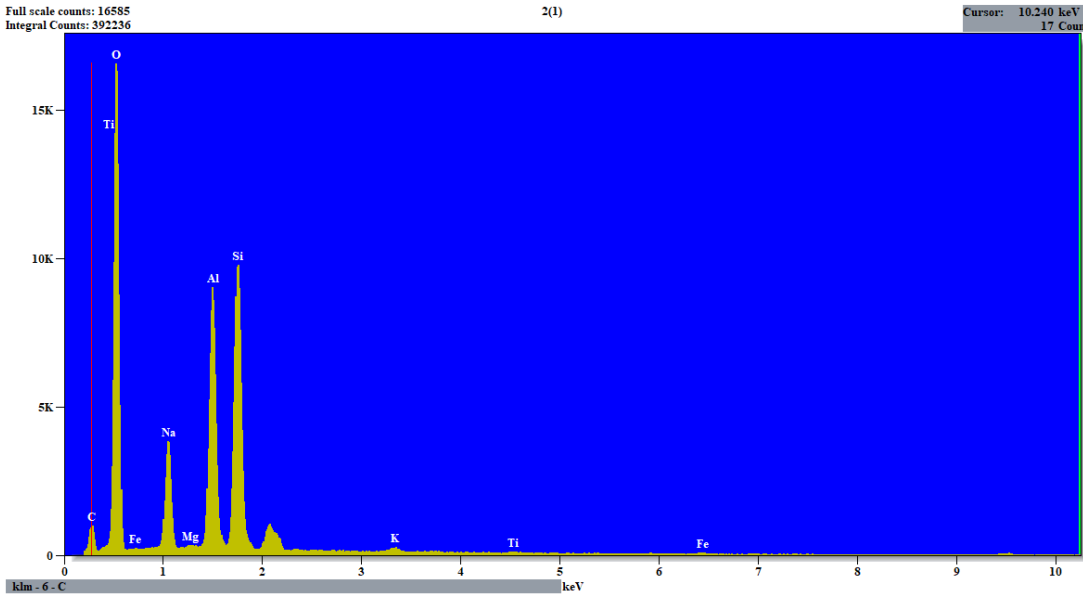
Full scale counts: 16585
Integral Counts: 392236
2(1)
Cursor: 10.240 keV
17 Coun
15K
10K
5K
0
O
Ti
Si
Al
Na
C
Fe
Mg
K
Ti
Fe
0
1
2
3
4
5
6
7
8
9
10
klm - 6 - C
keV

b)

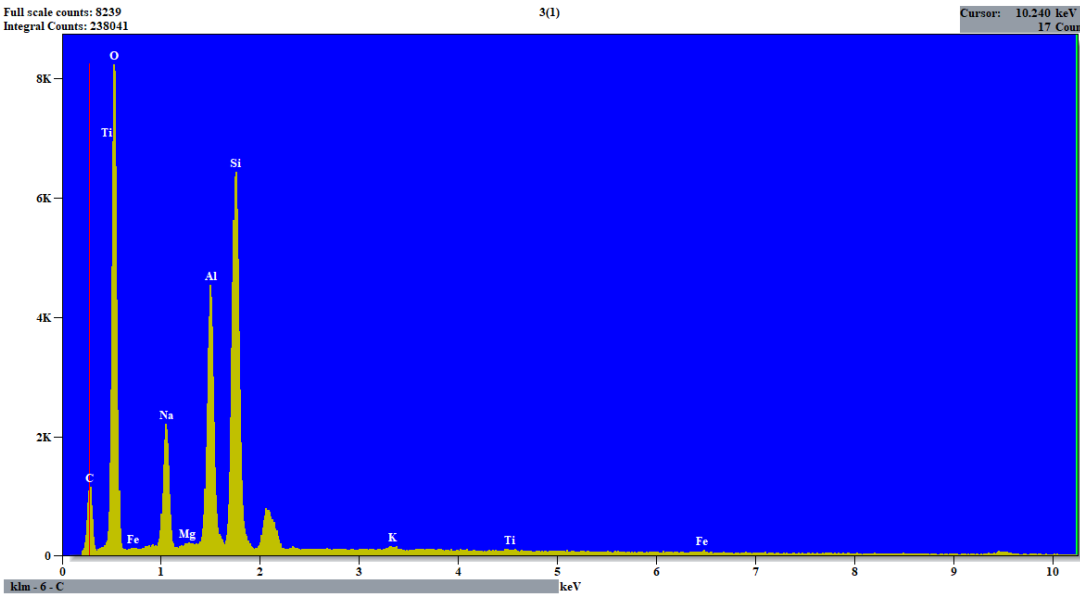

c)

Figure 6-4. EDS spectra of aS1, b) S2, c) S3 samples synthesizes by hydrothermal method

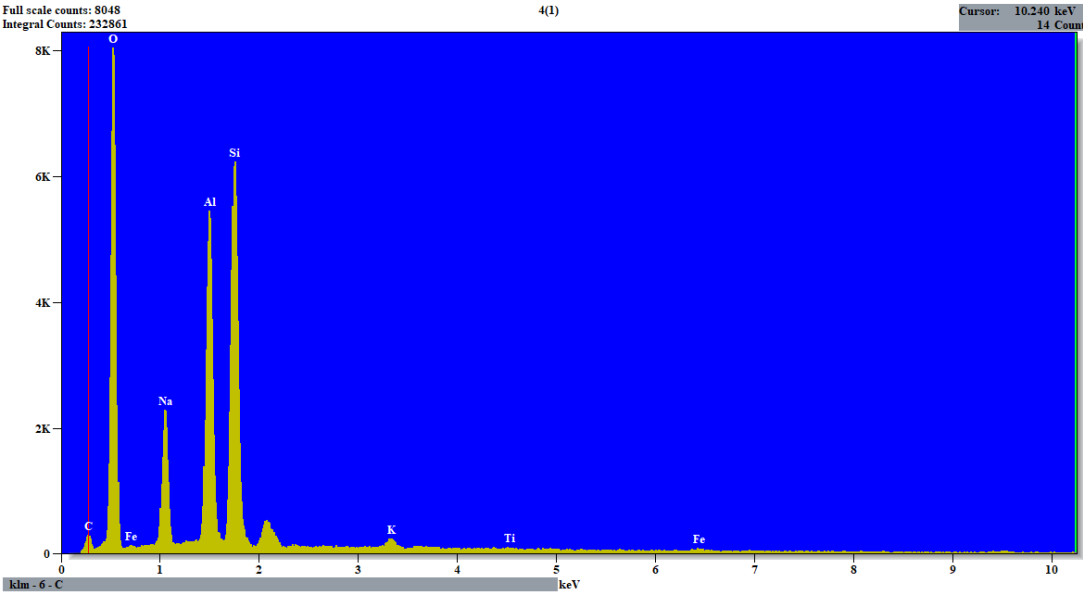

a)

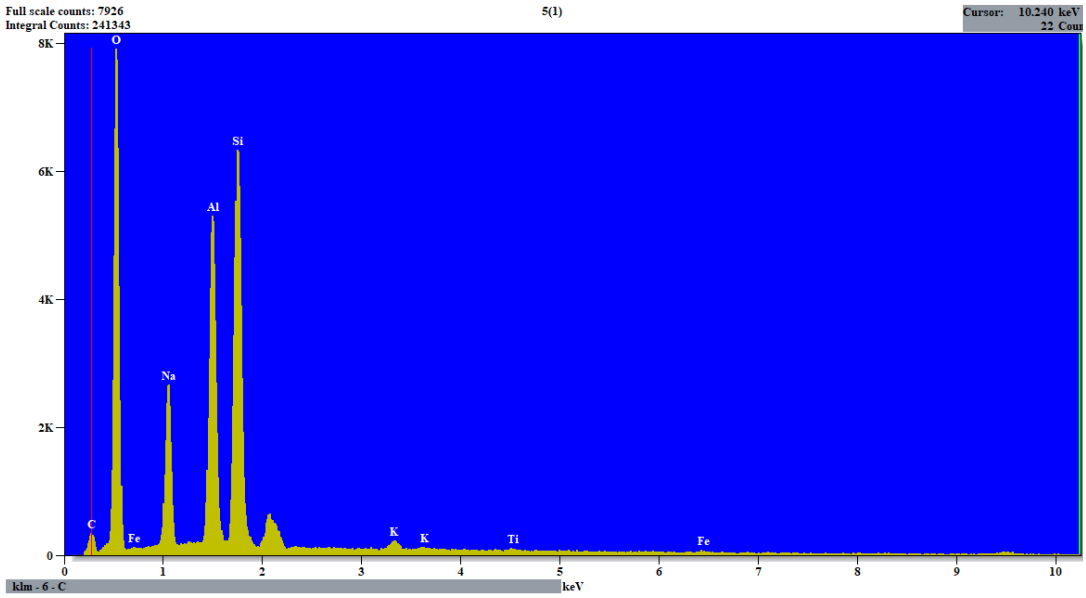

b)

Figure 6-5. EDS spectra of a) S4, b) S5 samples synthesizes by hydrothermal method

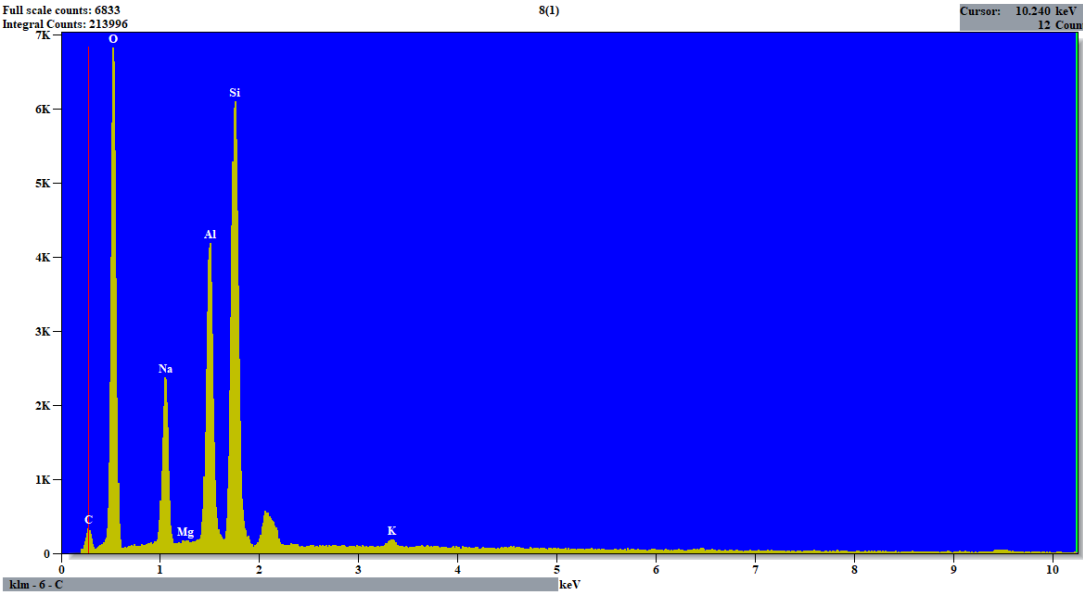

a)

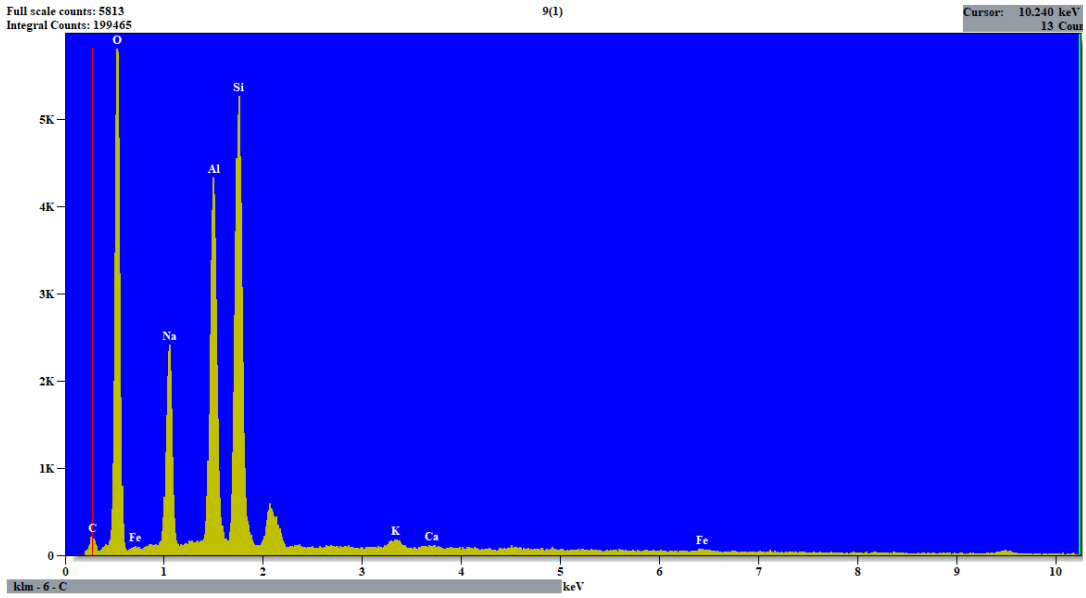

b)

Figure 6-6. EDS spectra of a) S8, b) S9 samples synthesizes by hydrothermal method

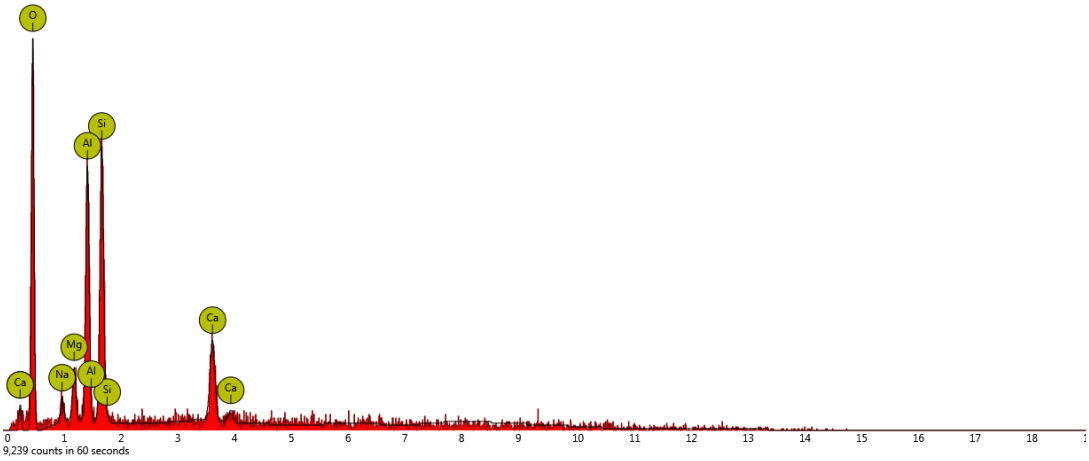

Disabled elements: B, Cs, Pm, Te

a)

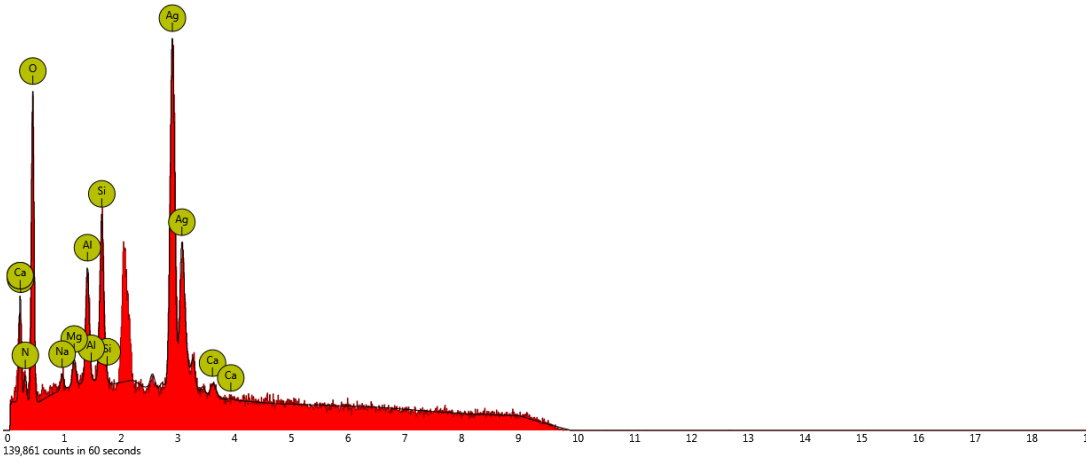

Disabled elements: Au, B, Br, Hg, Nb, Os, Pa, Pt, Sr, Zr

b)

Figure 6-7. EDS spectra of 5A and 5ANW